ROTATIONAL RAMAN SCATTERING INDUCED BY CH_4-CH_4, CH_4-Ar, AND CH_4-Xe INTERACTIONS

A Thesis

Submitted to

the Faculty of Graduate Studies

University of Manitoba

In Partial Fulfillment

of the Requirements for the Degree

Master of Science

by

Albert Raymond Penner

March 1983

ROTATIONAL RAMAN SCATTERING INDUCED BY CH_4-CH_4, CH_4-AR, AND CH_4-XE INTERACTIONS

BY

ALBERT RAYMOND PENNER

A thesis submitted to the Faculty of Graduate Studies of the University of Manitoba in partial fulfillment of the requirements of the degree of

MASTER OF SCIENCE

ACKNOWLEDGEMENTS

I am very grateful to my advisor, Dr. G. C. Tabisz, for his assistance and guidance throughout the course of this work. I would also like to thank Dr. N. Meinander for his much needed contributions.

A special thanks is given to Brad, Murray, and Vivek, who made the days much more enjoyable and to Barbara who was my biggest supporter.

ABSTRACT

The spectrum of light scattered, in the region from 0 cm^{-1} to 400 cm^{-1}, during CH_4-CH_4, CH_4-Ar, and CH_4-Xe collisions has been determined experimentally. These results are compared with theoretical spectra which are obtained from a model based on collision induced moments. Arising from these comparisons we arrived at a value of (.93±.06) $\AA^4$ for the dipole-quadrupole tensor of CH_4. We have also found that only the first few terms in the collision induced dipole expression contribute significantly to the spectrum of scattered light.

CONTENTS

List of Figures

List of Tables

CHAPTER 1

INTRODUCTION

Collision Induced Light Scattering (C.I.L.S.) is just what the name implies, the light scattered from two or more colliding molecules or atoms. Before we consider C.I.L.S. let us look first at the simple case of polarized light incident upon a single molecule or atom.

Polarized light incident upon an isotropic molecule will induce a dipole which will be in the same direction as the polarization of the incident light. The resulting scattered light will thus be polarized and as classical electrodynamics shows there will be no radiation scattered in the direction of the polarization of the incident light. The figure below gives the general features of the interaction.

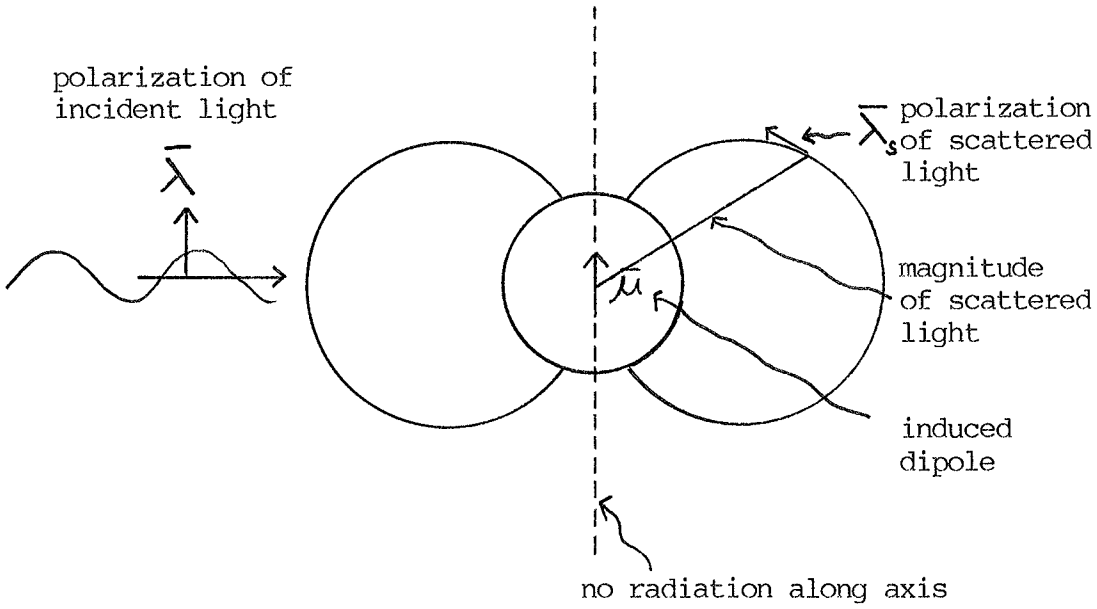

For the case of two interacting molecules (interacting will refer to the situation where the molecules are within ~30 Å of each other) there will be changes. The reason is that the induced dipole of one molecule will induce a dipole in the other and this first order induced dipole will in general have a component perpendicular to the original induced dipole (this is shown in the figure below). Thus some light will be scattered in the direction of the polarization of the

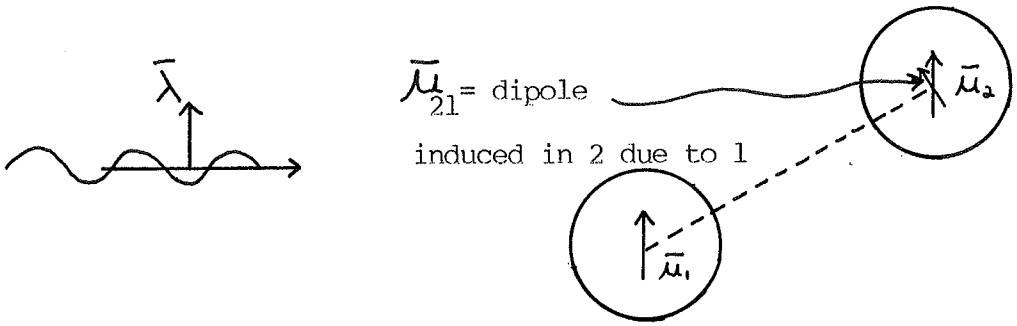

incident light. Observations along this direction will thus yield a spectrum of scattered light and the features of this spectrum will depend on both the polarizability constants of the molecules and on the mechanics of the interaction. This collision induced light scattering, based on the above dipole induced dipole (D.I.D.) model, has been fairly well studied[1]. Experimental results show that the intensity falls off roughly exponentially in good agreement with the theoretically derived spectra.

Experimental results[2] have also shown that in certain isotropic molecules (eg. CH_4, CF_4, SF_6, etc.) the spectrum has an intensity in excess of what is predicted by the D.I.D. model. This additional intensity is most noticeable in the region $> 100\ cm^{-1}$. It has been shown[3] that this excess tail can be accounted for by additional terms in the induced dipole, such as the dipole induced by the gradients of fields. These additional terms turn out to be responsible for induced

rotational transitions which extend to high frequencies and produce the far tails on the spectra.

The experiments, on which this thesis is based, are a continuation of the work of Shelton[4], specifically his work on the pure CH_4 spectra. He obtained a value for the dipole-quadrupole polarizability tensor for CH_4 and, by subtracting the spectrum due to the additional terms in the induced dipole expression, the pure translational spectrum. A major uncertainty with the results was whether the induced dipole expression could be terminated at a specific point and whether the anisotropic short range forces are important.

The purpose of this thesis is to reduce the uncertainties of the previous work. This was achieved by looking at CH_4-Ar and CH_4-Xe interactions in addition to the CH_4-CH_4 interaction. In the cases of CH_4-Ar and CH_4-Xe many of the terms, specifically those involving double transitions, in the total induced dipole expression are equal to zero. This allows one, by comparing the CH_4-CH_4 results with the CH_4-Ar and CH_4-Xe results, to make conclusions regarding the termination of the induced dipole expression. In addition to this a definitive value for the dipole-quadrupole tensor of CH_4 is obtained, accurate translational spectra for CH_4-CH_4, CH_4-Ar, and CH_4-Xe are found, and a general verification of the collision induced rotational scattering model is presented.

The following chapters of this thesis will present the theoretical derivation of the spectra, the experimental spectra obtained, and the resulting comparisons and conclusions.

CHAPTER 2

THEORY

2.1 Pair Polarizability Expression

The first two sections of this chapter follow the method presented by Buckingham and Tabisz[3].

The general expressions for the first few multipole moments of a molecule in a field $\bar{F}$ are (the hyperpolarizability terms have been neglected as their contributions to the CH_4 collision induced spectrum are insignificant[5])

$$\mu_\alpha = {}_o\mu_\alpha + \alpha_{\alpha\beta}F_\beta + \frac{1}{3}A_{\alpha\beta\gamma}F'_{\beta\gamma} + \frac{1}{15}E_{\alpha\beta\gamma\delta}F''_{\beta\gamma\delta} + \ldots$$

$$\Theta_{\alpha\beta} = {}_o\Theta_{\alpha\beta} + A_{\alpha\beta\gamma}F_\gamma + C_{\alpha\beta\gamma\delta}F'_{\gamma\delta} + \ldots \qquad (1)$$

$$\Omega_{\alpha\beta\gamma} = {}_o\Omega_{\alpha\beta\gamma} + E_{\alpha\beta\gamma\delta}F_\delta + \ldots$$

where the subscripts refer to the components of the tensor. The tensor $\tilde{\alpha}$ is called the dipole polarizability, the tensor $\tilde{A}$ is called the dipole-quadrupole polarizability*, and the tensor $\tilde{E}$ is called the dipole-octopole polarizability. As stated previously it is uncertain when the terms in these equations become insignificant. Theoretical calculations based on two metallic spheres have shown that one may have to consider several hundred terms[6]. However the application of these results to real atoms and molecules is in doubt.

Using the above expressions it is possible to derive the equation for the total dipole moment of a pair of interacting molecules in a uniform field (for the case of two noninteracting molecules one would have $\mu_\alpha^{(1)} + \mu_\alpha^{(2)} = {}_o\mu_\alpha^{(1)} + {}_o\mu_\alpha^{(2)} + \alpha_{\alpha\beta}^{(1)}F_\beta + \alpha_{\alpha\beta}^{(2)}F_\beta$). To start with, the

---

* for a more detailed description of the tensor $\tilde{A}$ see Appendix 2-A

field at one of the molecules due to the dipole at the other is given by the familiar expression

$$F_\alpha = \frac{(3R_\alpha R_\beta - R^2\delta_{\alpha\beta})}{R^5}\mu_\beta \qquad (2)$$

where $\bar{R}$ is the separation of the two molecules. This can be written as $F_\alpha = (\nabla_\alpha\nabla_\beta(\frac{1}{R}))\mu_\beta = T_{\alpha\beta}\mu_\beta$ where $\tilde{T}$ is a tensor whose components are given by $T_{\alpha\beta} = \nabla_\alpha\nabla_\beta(\frac{1}{R})$. The general tensor components for higher order expressions are given by

$$T_{\alpha\beta\gamma\cdots\nu} = \nabla_\alpha\nabla_\beta\nabla_\gamma\cdots\nabla_\nu(R^{-1}). \qquad (3)$$

As an example, while $T_{\alpha\beta}\mu_\beta^{(1)}$ is in the α component of the field at molecule 2 due to the dipole of molecule 1, $T_{\alpha\beta\gamma}\mu_\gamma^{(1)}$ is the $\alpha\beta$ component of the field gradient $(\partial F_\alpha/\partial\beta)$ at 2 due to the dipole of 1. Similar relationships hold for fields due to quadrupole and octopole moments.

With the use of these expressions for $\bar{F}$ and its gradients the total induced dipole of molecule 1 to first order is found to be given by

$$\mu_\alpha^{(1)} = {}_0\mu_\alpha^{(1)} + {}_0\mu_\alpha^{(1)}F + \alpha_{\alpha\beta}^{(1)}(T_{\beta\gamma}\mu_\gamma^{(2)} + \frac{1}{3}T_{\beta\gamma\delta}\Theta_{\gamma\delta}^{(2)} + \frac{1}{15}T_{\alpha\beta\gamma\delta}\Omega_{\beta\gamma\delta}^{(2)} + \ldots) + \frac{1}{3}A_{\alpha\beta\gamma}^{(1)}(-T_{\beta\gamma\delta}\mu_\delta^{(2)} - \frac{1}{3}T_{\beta\gamma\delta\epsilon}\Theta_{\delta\epsilon}^{(2)} + \ldots) \qquad (4)$$
$$+ \frac{1}{15}E_{\alpha\beta\gamma\delta}^{(1)}(T_{\beta\gamma\delta\epsilon}\mu_\epsilon^{(2)} + \frac{1}{3}T_{\beta\gamma\delta\epsilon\zeta}\Theta_{\epsilon\zeta}^{(2)} + \ldots) + \ldots$$

with a similar expression for molecule 2.

To continue it is necessary to specify the types of molecules being studied. For our purposes it is necessary to look at interactions between two tetrahedral molecules (CH_4-CH_4) and the interaction between a tetrahedral molecule and a spherically symmetric molecule (CH_4-Ar and CH_4-Xe).

Consider a molecule of tetrahedral symmetry. Table 2-1 [7]

TABLE 2-1

TERM IN DIPOLE MOMENT EXPRESSION	PHYSICAL PROPERTY REPRESENTS THE RELATION BETWEEN	# OF INDEPENDENT CONSTANTS TETRAHEDRAL SYM.	SPHERICAL SYM.
$\alpha_{\alpha\beta}F_{\beta}$	Vector and Vector	1	1
$\frac{1}{3} A_{\alpha\beta\gamma}F'_{\beta\gamma}$	Vector and Tensor	1	0
$\frac{1}{15} E_{\alpha\beta\gamma\delta}F''_{\beta\gamma\delta}$	Vector and Tensor	1	0

indicates the number of independent constants for the given physical property for molecules of tetrahedral and spherical symmetry. From this it is seen that for a tetrahedral molecule the tensors $\tilde{\alpha}$, $\tilde{A}$, and $\tilde{E}$ have only one independent constant each. With this knowledge and the fact that the tensors must have tetrahedral symmetry the structure of the three tensors are uniquely specified[8,9].

$$\alpha_{\alpha\beta} = \alpha \delta_{\alpha\beta}$$

$$A_{\alpha\beta\gamma} = A^*(i_\alpha j_\beta k_\gamma + i_\alpha j_\gamma k_\beta + i_\beta j_\gamma k_\alpha + i_\beta j_\alpha k_\gamma + i_\gamma j_\alpha k_\beta + i_\gamma j_\beta k_\alpha) \qquad (5)$$

$$E_{\alpha\beta\gamma\delta} = \frac{5}{2} E(i_\alpha i_\beta i_\gamma i_\delta + j_\alpha j_\beta j_\gamma j_\delta + k_\alpha k_\beta k_\gamma k_\delta - \frac{1}{5}(\delta_{\alpha\beta}\delta_{\gamma\delta} + \delta_{\alpha\gamma}\delta_{\beta\delta} + \delta_{\alpha\delta}\delta_{\beta\gamma}))$$

where $\bar{i}$, $\bar{j}$, $\bar{k}$, represent the unit vectors along the axes of the tetrahedron. Also for a tetrahedral molecule the first non-vanishing permanent multipole moment is the octopole moment so ${}_0\mu_\alpha = {}_0\Theta_{\alpha\beta} = 0$.

For a spherically symmetric molecule the tensors $\tilde{A}$ and $\tilde{E}$ vanish while the expression for the polarizability tensor $\tilde{\alpha}$ is the same as that for a tetrahedral molecule.

With these results an expression for the pair polarizability $\alpha^{(1,2)}_{\alpha\beta}$ $(= \partial/\partial F_\beta(\mu^{(1)}_\alpha + \mu^{(2)}_\alpha))$ for the tetrahedral - tetrahedral interaction and the tetrahedral-sphere interaction can be derived. For the tetrahedral-tetrahedral interaction one has

$$\begin{aligned}
\alpha_{\alpha\beta} = {} & (\alpha_1 + \alpha_2)\delta_{\alpha\beta} + 2\alpha_1\alpha_2 T_{\alpha\beta} + \frac{1}{3} T_{\alpha\gamma\delta}(\alpha_1 A^{(2)}_{\beta\gamma\delta} - \alpha_2 A^{(1)}_{\beta\gamma\delta}) \\
& + \frac{1}{3} T_{\beta\gamma\delta}(\alpha_1 A^{(2)}_{\alpha\gamma\delta} - \alpha_2 A^{(1)}_{\alpha\gamma\delta}) \\
& - \frac{1}{9} T_{\gamma\delta\epsilon\eta}(A^{(1)}_{\alpha\gamma\delta} A^{(2)}_{\beta\epsilon\eta} + A^{(2)}_{\alpha\gamma\delta} A^{(1)}_{\beta\epsilon\eta}) \qquad (6) \\
& + \frac{1}{15} T_{\alpha\gamma\delta\epsilon}(\alpha_2 E^{(1)}_{\gamma\delta\epsilon\beta} + \alpha_1 E^{(2)}_{\gamma\delta\epsilon\beta}) \\
& + \frac{1}{15} T_{\delta\epsilon\eta\beta}(\alpha_2 E^{(1)}_{\alpha\delta\epsilon\eta} + \alpha_1 E^{(2)}_{\alpha\delta\epsilon\eta})
\end{aligned}$$

---

* a theoretical determination of A is given in Appendix 2-A

+ double E term

while for the tetrahedral-sphere interaction (molecule 1 is the tetrahedron)

$$\alpha_{\alpha\beta} = (\alpha_1+\alpha_2)\delta_{\alpha\beta} + 2\alpha_1\alpha_2 T_{\alpha\beta} + \frac{1}{3} T_{\alpha\gamma\delta}(-\alpha_2 A^{(1)}_{\beta\gamma\delta}) + \frac{1}{3} T_{\beta\gamma\delta}(-\alpha_2 A^{(1)}_{\alpha\gamma\delta}) + \frac{1}{15} T_{\alpha\gamma\delta\epsilon}(\alpha_2 E^{(1)}_{\gamma\delta\epsilon\beta}) + \frac{1}{15} T_{\delta\epsilon\eta\beta}(\alpha_2 E^{(1)}_{\alpha\delta\epsilon\eta}) + \ldots \quad . \tag{7}$$

For both these expressions $\tilde{A}$ and $\tilde{E}$ are given by equation (5).

In the derivation of these pair polarizability equations we have neglected the effect of the short-range interactions, i.e. electron overlap. These forces can be taken into account by including additional terms in the expressions for F_α , $F'_{\alpha\beta}$, and the higher order derivatives. However as the contributions that these short-range forces make to the force expressions are not very well known we have only attempted to take them into account in the D.I.D. term (see section 2-3). Birnbaum and Sutter[10] have studied the contribution that short-range anisotropic overlap makes to the collision-induced absorption spectrum of SF_6. This anisotropic force will induce rotational transitions as do the higher order terms in equation (7). Their results show that the major part of the absorption can be attributed to the short-range overlap. As stated in Chapter 1 one of the aims of this experiment is to find out if this anisotropic overlap contribution can be neglected (i.e. whether or not equation (7), with a correction for the D.I.D. term, is adequate).

From the above expressions for the pair polarizability, and knowledge of the orbits of the interacting molecules, the spectrum of light emitted by the two molecules can be found.

2.2 Contribution of the Various Terms to the Spectrum

The contributions of each of the terms in the pair polarizability expression to the total intensity of the scattered light can be obtained from the classical expression for the zeroth moment[11],

$$\phi^{(o)} = C(\tau)_{\tau=o} \propto \lambda_{si}\lambda_j\lambda_{sk}\lambda_l \langle \alpha_{ij}\alpha_{kl} \rangle \tag{8}$$

where $\langle\ \rangle$ represents an average over all orientations of the two molecules and of the intermolecular separation $\bar{R}$. The vectors $\bar{\lambda}_s$ and $\bar{\lambda}$ represent the polarization of the scattered and incident light respectively. In our experimental setup the electric field was polarized along the Z-axis and incident along the X-axis while observations were made in the Z direction. Therefore the expression of interest to us is

$$\phi_z^{(o)} \propto \langle \alpha_{xz}^2 \rangle + \langle \alpha_{yz}^2 \rangle . \tag{9}$$

For the symmetric molecules we are studying $\langle \alpha_{xz}^2 \rangle = \langle \alpha_{yz}^2 \rangle$ thereby giving the result that the intensity of the light scattered in the Z direction is proportional to $\langle \alpha_{xz}^2 \rangle$.

The relative contribution of each of the terms of the pair polarizability for the tetrahedral-tetrahedral interaction (equation (6)) is therefore given by the following expression (the cross terms average to zero),

$$\langle \alpha_{xz}^2 \rangle = \langle (2\alpha_1\alpha_2 T_{xz})^2 \rangle + \langle (\tfrac{1}{3} T_{x\gamma\delta}(\alpha_1 A^{(2)}_{z\gamma\delta} - \alpha_2 A^{(1)}_{z\gamma\delta}))^2 \rangle$$

$$+ \langle (\tfrac{1}{3} T_{z\gamma\delta}(\alpha_1 A^{(2)}_{x\gamma\delta} - \alpha_2 A^{(1)}_{x\gamma\delta}))^2 \rangle \tag{10}$$

$$+ \text{double A term} + \alpha E \text{ terms} + \text{double E term} + \ldots$$

The first term is just

$$4\alpha_1^2\alpha_2^2 \langle (T_{xz})^2 \rangle = 4\alpha_1^2\alpha_2^2 \left\langle \frac{9\, x^2 z^2}{R^{10}} \right\rangle = \frac{12}{5}\alpha_1^2\alpha_2^2\, \overline{R^{-6}}$$

By similar averaging for the other terms, the relative contributions of each of the terms of the pair polarizability to the spectrum are found to be

$$2\alpha_1\alpha_2 T_{\alpha\beta} \longrightarrow \frac{12}{5}\alpha_1^2\alpha_2^2\,\overline{R^{-6}}$$

$$\left.\begin{aligned}&\frac{1}{3}T_{\alpha\gamma\delta}(\alpha_1 A^{(2)}_{\beta\gamma\delta} - \alpha_2 A^{(1)}_{\beta\gamma\delta})\\ &+\frac{1}{3}T_{\beta\gamma\delta}(\alpha_1 A^{(2)}_{\alpha\gamma\delta} - \alpha_2 A^{(1)}_{\alpha\gamma\delta})\end{aligned}\right\} \longrightarrow \frac{48}{35}\left[(\alpha_1 A_2)^2 + (\alpha_2 A_1^2\right]\,\overline{R^{-8}}$$

$$\text{double A term} \longrightarrow \frac{62912}{4725}(A_1A_2)^2\,\overline{R^{-10}} \qquad (11)$$

$$\alpha E \text{ terms} \longrightarrow \frac{11}{9}\left[(\alpha_1 E_2)^2 + (\alpha_2 E_1)^2\right]\,\overline{R^{-10}}$$

$$\text{double E term} \longrightarrow 12^*(E_1E_2)^2\,\overline{R^{-12}}$$

To find $\overline{R^{-n}}$ one needs to average over g(R), the radial distribution function for the two molecules. To first order $\overline{R^{-n}}$ is given by

$$\overline{R^{-n}} \propto \int_0^\infty R^{-n}\; e^{-\phi(r)/kT}\; R^2\, dR \qquad (12)$$

where $\phi(r)$ is the intermolecular potential. For the tetrahedron-sphere interaction the above expressions hold with $A_2=E_2=0$.

As the intensity contribution of the various terms is now known, it remains to calculate the spectral lineshapes resulting from the individual terms in the pair polarizability expressions.

---

* the factor 12 is an estimate[4]

2.3 D.I.D. Spectrum

The first term $2\alpha_1\alpha_2 T_{\alpha\beta}$ represents the dipole induced in one molecule due to the induced dipole in the other. To repeat, $T_{\alpha\beta}\mu_\beta^{(2)}$ is the α component of the field at molecule 1 due to a dipole at molecule 2. Therefore the induced dipole for molecule 1 due to this term is $\alpha_1 T_{\alpha\beta}\mu_\beta^{(2)}$. To first order $\mu_\beta^{(2)}=\alpha_2 F_\beta$ giving $\mu_\alpha^{(1)}=\alpha_1\alpha_2 T_{\alpha\beta}F_\beta$. With a similar expression for μ_2 one obtains the first term of the pair polarizability. This term is thus called the first order D.I.D. (dipole induced dipole) contribution. As stated before the D.I.D. term has been well studied and so only a summary of the calculation of the resulting line shape will be presented.

First of all it is necessary to rewrite the expression as

$$2\alpha_1\alpha_2 T_{\alpha\beta} = \frac{6\alpha_1\alpha_2}{R^3}(u_\alpha u_\beta - \frac{1}{3}\delta_{\alpha\beta}) \qquad (13)$$

where $\bar{u}$ specifies the orientation of the intermolecular axis of the pair. The term $6\alpha_1\alpha_2/R^3$ is called the polarizability anisotropy, $\beta(r)$, and it is this expression we shall now discuss in greater detail.

In the above D.I.D. expression we have only considered the dipole induced in one molecule by the dipole in the other. If we consider higher order expressions, i.e. the dipole induced in molecule 1 due to the dipole in molecule 2 induced by molecule 1 and so on, one has additional terms the first of which is shown in the equation below.

$$\beta(R) = \frac{6\alpha_1\alpha_2}{R^3} + \frac{3\alpha_1\alpha_2^2 + 3\alpha_1^2\alpha_2}{R^6} + \mathcal{O}(R^{-9}) + \ldots \qquad (14)$$

This classical expression for $\beta(R)$ neglects several significant effects. The first one being electron overlap[10,12,13]. Electron overlap between two molecules will occur for small values of R. The result will

be to reduce the pair polarizability, the reason being that the asymmetry of the molecular pair will decrease as the electron clouds begin to overlap. Another effect which is ignored in this classical derivation is electron density fluctuations. Quantum mechanical calculations show that the effect of electron density fluctuation is to introduce additional terms in $\beta(R)$. (This mechanism is analogous to the London dispersion term which adds to the interatomic potential).

All these corrections - higher order induced dipole terms, electron overlap and electron density fluctuations - can be approximated by the following expression

$$\beta(R)= \frac{6\alpha_1\alpha_2}{R^3} + K \frac{(3\alpha_1\alpha_2^2+ 3\alpha_1^2\alpha_2)}{R^6} - f(\alpha) e^{-R/Ro} \qquad (15)$$

where K and Ro are constants and $f(\alpha)$ is a function of α which we will take to be $L\alpha_1\alpha_2$ where L is a constant. This functional form has been fitted to several different noble gas spectra. The values we used to calculate the theoretical spectra come from the krypton results of Barocchi et al[14]. The reason krypton was used stems from the similarities of the intermolecular potential and the polarizability of krypton and methane[15]. Using their results one finds K=2.91, L=33.62 Å^{-3} and Ro = .530 Å. Thus the equation to be used is

$$\beta(R)= \frac{6\alpha_1\alpha_2}{R^3} + (2.91) \frac{(3\alpha_1\alpha_2^2+ 3\alpha_1^2\alpha_2)}{R^6} - (33.62)\alpha_1\alpha_2 e^{-R/.530} \qquad (16)$$

With the above expression for $\beta(R)$ one may proceed along several different lines to determine the resulting classical spectrum. Due to the availability of a computer program[16] the path chosen was that of Fromhold[17]. Starting from the classical electrodynamic expression for the power radiated per unit solid angle due to an accelerating

charge e (as given below)

$$\frac{dP}{d\Omega} = \left(\frac{e^2}{4\pi c^3}\right)\left\{\bar{\lambda}_s \cdot [\ \hat{n} \times (\ \hat{n} \times \vec{a}\ )]\right\}^2 \qquad (17)$$

it can be shown that the resulting spectrum for a molecular pair with impact parameter b and relative speed s is given by

$$dI(\nu) \propto s[(1.5)\left\{\int_0^\infty \beta(r(t))\cos[2\Phi(t)+2\pi\nu t]\,dt\right\}^2 \qquad (18)$$
$$+[\int_0^\infty \beta(r(t))\cos(2\pi\nu t)\,dt]^2 + (1.5)\left\{\int_0^\infty \beta(r(t))\cos[2\Phi(t)-2\pi\nu t]\,dt\right\}^2]$$

where r(t) and $\Phi(t)$ are the polar coordinates for the trajectory of the collision. This expression has to be integrated over all values of the impact parameter and averaged over the Maxwell speed distribution to find the total spectrum. Reliable results are only expected in the region $> 20\ cm^{-1}$.

In order to calculate r(t) and $\Phi(t)$ it is of course necessary to specify the intermolecular potentials. As stated previously the CH_4-CH_4 potential is very similar to the Kr-Kr potential[15]. Thus for the CH_4-CH_4 and CH_4-Xe interactions we have used the potentials which have been determined for Kr-Kr[18] and Kr-Xe[19]. As an accurate potential for CH_4-Ar[20] was found in literature it was used instead of Kr-Ar.

The forms of the potentials used are shown below with X=R/Rmin, where Rmin is the position of the potential minimum*. These expressions are plotted on Figure 2-1.

CH_4-CH_4 potential
$$U(R) = \epsilon\left\{Ae^{-\alpha x} - \left(\frac{C6}{x^6} + \frac{C8}{x^8} + \frac{C10}{x^{10}}\right)F(x)\right\}$$
$$\text{where } F(x) = e^{[-(\frac{1.28}{x}-1)^2]} \qquad x<1.28 \qquad (19)$$
$$= 1 \qquad x\geq 1.28$$

CH_4-Ar potential
$$U(R) = \epsilon\begin{cases} e^{2\beta(1-x)} - 2e^{\beta(1-x)} & x\leq 1.10 \\ \sum_{i=0}^{3} B_i\,(x-1.10)^i & 1.10 < x < 1.40 \\ -C6/x^6 - C8/x^8 & x\geq 1.40 \end{cases} \qquad (20)$$

---

* Table 2-2 lists some of the parameters of the three interactions.

CH_4-Xe potential

$$U(R)=\epsilon\left[\left\{\sum_{i=0}^{5}A_i(x-1)^i\right\}e^{12.5(1-x)} - \sum_{j=0}^{3}C_{2j+6}/(.01+x^{2j+6})\right] \qquad (21)$$

Several resulting trajectories for the CH_4-Ar interaction are shown on figure 2-2. The resulting spectra for CH_4-CH_4, CH_4-Ar, and CH_4-Xe are shown on figures 2-3 to 2-5. On these figures the translational spectra for both the one term $\beta(R)$, the simple D.I.D. model, and the fully corrected expression are given. The spectra which were calculated using the first term were used to find the relative proportions of the various other terms, using equation (11), in the pair polarizability expression. After the various proportions have been assigned the one term translational spectrum is replaced by the translational spectrum which was obtained using the corrected expression for $\beta(R)$.

TABLE 2-2

	Interaction		
	CH_4-CH_4	CH_4-Ar	CH_4-Xe
Potential minimum (Å)	4.012	3.88	4.1786
Potential depth (meV)	17.3	14.4	19.8
α (Å^3)	2.642-2.642	2.642-1.679	2.642-4.22
Mass (a.u.)	16.03-16.03	16.03-39.96	16.03-131.30
Reduced mass (a.u.)	8.02	11.44	14.29

2.4 Rotational Spectra

The spectrum due to the remaining terms in the pair polarizability expression may be calculated classically as was done for the D.I.D. term. However, as will be seen, these terms induce rotational transitions and thus the proper way to proceed is quantum mechanically.

The probability that a molecule will make a transition from rotational state J_1 to J_1' under the influence of E.M. radiation is given by [22]

$$\frac{d\sigma}{d\Omega} = k^4 \left| \langle J_1' \left| \lambda_i \alpha_{ij} \lambda_{sj} \right| J_1 \rangle \right|^2 \tag{22}$$

where $\bar{\lambda}$ is the original polarization of the radiation, $\bar{\lambda}_s$ is the polarization of the scattered radiation, and α_{ij} is the dipole polarizability tensor for the molecule.

For the case of two interacting molecules, with the scattering geometry previously defined, the probability of molecule 1 making a transition from J_1 to J_1' and molecule 2 making a transition from J_2 to J_2' is proportional to

$$\left| \langle J_1', J_2' | \alpha_{xz}^{(1,2)} | J_1, J_2 \rangle \right|^2 \tag{23}$$

where $\alpha_{xz}^{(1,2)}$ is the xz component of the pair polarizability tensor. This is averaged over all orientations of the individual molecules and all orientations of the intermolecular vector.

To evaluate this matrix element we will write it in spherical tensor form. For the rotational states we use the normalized symmetric top wavefunction [23]

$$\sqrt{\frac{2J+1}{8\pi^2}} \; D_{mk}^{J*}(\Omega) \tag{24}$$

where $D_{mk}^{J}(\Omega)$ is the Wigner rotation matrix. The quantum number J

represents the angular momentum of the molecule while m and k represent the projection of the angular momentum vector on the space fixed z axis and the molecule fixed z axis respectively. Thus the probability that a molecule in state J, m, k has Euler angles between α_1 and α_2, β_1 and β_2, γ_1 and γ_2, is given by

$$\int_{\gamma_1}^{\gamma_2}\int_{\beta_1}^{\beta_2}\int_{\alpha_1}^{\alpha_2} \left(\frac{2J+1}{8\pi^2}\right) D^{J}_{mk}(\Omega)\, D^{J*}_{mk}(\Omega)\, d\Omega \quad . \tag{25}$$

It remains now to write the pair polarizability tensor in spherical tensor form. The same argument that led to an expression for $\tilde{A}$ and $\tilde{E}$ in terms of cartesian coordinates, one independent variable and Td symmetry, leads to expressions in spherical tensor form [24,25]. The results are

$$A_{\alpha\beta\gamma} \rightarrow A_{3m} \propto A(D^{3*}_{m2}(\Omega) - D^{3*}_{m-2}(\Omega)) \tag{26}$$

$$E_{\alpha\beta\gamma\delta} \rightarrow E_{4m} \propto E\left(\left(\frac{14}{5}\right)^{\frac{1}{2}} D^{4*}_{mo}(\Omega) + D^{4*}_{m4}(\Omega) + D^{4*}_{m-4}(\Omega)\right).$$

The probability of a rotational transition is found by substituting equation (6) into the expression for the transition probability. As the tensors $\tilde{T}$ do not depend on the individual molecular orientations they may be brought out of the matrix element. This gives the following expressions,

$$\begin{aligned} &4\alpha_1^2\alpha_2^2 \,|T_{\alpha\beta}|^2 \,|\langle J_1', J_2' | J_1, J_2\rangle|^2 \\ &+ \tfrac{1}{9}\,|T_{\alpha\gamma\delta}|^2\alpha_1^2\,|\langle J_1', J_2' | A^{(2)}_{\beta\gamma\delta} | J_1, J_2\rangle|^2 \\ &+ \tfrac{1}{9}\,|T_{\alpha\gamma\delta}|^2\alpha_2^2\,|\langle J_1', J_2' | A^{(1)}_{\beta\gamma\delta} | J_1, J_2\rangle|^2 \\ &+ \ldots \quad . \end{aligned} \tag{27}$$

Evaluating the various matrix elements[24], by converting to spherical tensors with the use of equations (24) and (26), one obtains the following inequalities.

$$|\langle J_1', J_2' | J_1, J_2\rangle|^2 \neq 0 \quad \text{for } J_1 = J_1',\ J_2 = J_2' \quad . \tag{28}$$

Thus the D.I.D. term does not induce any rotational transitions.

$$|\langle J_1', J_2' | A_{3m} | J_1 J_2 \rangle|^2 \neq 0 \quad \text{for} \quad \Delta J_i = 0$$
$$\Delta J_j = 0, \pm 1, \pm 2, \pm 3 \tag{29}$$
$$J_j + J_j' \geq 3 \quad .$$

Thus the αA terms induce rotational transitions in one or the other molecule.

$$|\langle J_1', J_2' | A_{3m} A_{3m'} | J_1, J_2 \rangle|^2 \neq 0 \qquad \text{for} \quad \Delta J_i = 0, \pm 1, \pm 2, \pm 3$$
$$\Delta J_j = 0, \pm 1, \pm 2, \pm 3$$
$$J_i + J_i' \geq 3 \tag{30}$$
$$J_j + J_j' \geq 3 \quad .$$

Thus the A^2 terms induce rotational transitions in both molecules.

$$|\langle J_1', J_2' | E_{4m} | J_1, J_2 \rangle|^2 \neq 0 \qquad \text{for} \quad \Delta J_i = 0$$
$$\Delta J_j = 0, \pm 1, \pm 2, \pm 3, \pm 4 \tag{31}$$
$$J_j + J_j' \geq 4 \quad .$$

So like the αA terms the αE terms induce transitions in one or the other molecule.

$$|\langle J_1', J_2' | E_{4m} E_{4m'} | J_1, J_2 \rangle|^2 \neq 0 \qquad \text{for} \quad \Delta J_i = 0, \pm 1, \pm 2, \pm 3, \pm 4$$
$$\Delta J_j = 0, \pm 1, \pm 2, \pm 3, \pm 4$$
$$J_i + J_i' \geq 4 \tag{32}$$
$$J_j + J_j' \geq 4 \quad .$$

So the E^2 term like the A^2 term induces transitions in both molecules.

Now we may go back to the problem of finding the line shapes for the various terms in (11). It is known which rotational transitions correspond to which terms. We also know[3] that the relative intensity of the individual transitions can be found by the following expression involving thermal weights

$$\Gamma(J_1', J_2', J_1, J_2) = \omega_r^4 \, (2J_1'+1)(2J_2'+1)(2J_1+1)(2J_2+1)$$

$$\times \exp\ -[J_1(J_1+1)\ B_1+J_2(J_2+1)B_2)]^{hc}/kT \qquad (33)$$

where the position of the line is given by*

$$\omega_r=\omega_o-[J_1'(J_1'+1)-J_1(J_1+1)]\ B_1-[J_2'(J_2'+1)-J_2(J_2+1)]\ B_2 \qquad (34)$$

with ω_o being the frequency of the incident light and B_i the rotational constant for a given molecule. With this information it is a simple process to find the rotational line spectrum due to each term. Of course the calculation of the lineshapes still remains.

Posch[26] has done theoretical calculations on the lineshapes of the rotational lines. His results show that the broadening of the lines depends on the R^{-n} part of the terms in the pair polarizability expression (see equation (11)) with broadening increasing with increasing n. This also follows from a simple argument based on the uncertainty principle $\Delta E \Delta t \leq h$. Consider the first two terms of the pair polarizability expression; the D.I.D. term has a R^{-6} dependence while the αA term has a R^{-8} dependence. The αA term is a stronger function of R than the D.I.D. term and as such the majority of the light scattered due to the αA term will occur over a smaller range of R than with the D.I.D. term. It thus follows that the length of time over which scattering takes place is greater for the D.I.D. term than for the αA term. From the uncertainty principle one has that the longer the scattering time the smaller the energy spread of the scattered light. So the spectral widths corresponding to the αA rotational lines will be

---

* This is using the first order approximation for a rigid rotor. Taking into account centrifugal distortion the rotational levels would be given by $E= J(J+1)\ B - J^2(J+1)^2D$. However for our purposes the first term will do.

larger than the corresponding translational (D.I.D.) line width. Taking the broadening of the lines to have roughly the form $e^{-(\omega-\omega_r)/\omega^*}$ one can obtain from Posch's results the approximate linear relationship $\omega^*=Kn$ with K being a constant.

The experimental data for pure CH_4 can be approximated by the expression $I(o)e^{-\omega/15.5\ cm^{-1}}$ in the region where the D.I.D. term dominates ($< 150\ cm^{-1}$). So for CH_4 we obtain $K \approx (15.5\ cm^{-1})/6 \approx 2.6 cm^{-1}$. The broadening of the rotational lines was thus taken to be of the form $e^{-(\omega-\omega_r)/\omega^*}$ where for the αA transitions $\omega^*=(2.6cm^{-1})(8)$, for double A transition and αE transitions $\omega^*= (2.6cm^{-1})(10)$, and for double E transitions $\omega^*=(2.6cm^{-1})(12)$.

In addition to the dependence of the broadening on R^{-n}, Posch's expression gives a $1/\sqrt{\mu}$ dependence where $\sqrt{\mu}$ is the reduced mass of the molecular pair. This dependence can be simply derived by the following argument. For a given temperature the molecular velocities are inversely proportional to $\sqrt{\mu}$. Therefore the collision time is proportional to $\sqrt{\mu}$. From the uncertainty principle the bandwidth of the resulting spectrum is inversely proportional to the collision time and thus inversely proportional to $\sqrt{\mu}$. Following from this the broadening constants for CH_4-Ar will be taken as $\omega^*\sqrt{\frac{\mu_{CH_4-CH_4}}{\mu_{CH_4-Ar}}}$ where ω^* is the corresponding value for a given CH_4-CH_4 transition. Similarly this procedure was applied to CH_4-Xe spectrum.

The resulting spectra for several different values of A and E are given on figures 2-6 and 2-7. The relative total intensities of the spectra in these figures are given by equation (11).

2.5 Construction of Theoretical Spectra

The following is a summary of the procedure used to produce a theoretical spectrum.

1. The translational spectrum using $\beta = 6\alpha^2/r^3$ is obtained using the method given by Fromhold.
2. Rotational spectra corresponding to the additional terms in the pair polarizability expression are generated (we considered the first 40 rotational states of CH_4). This is performed with the use of expressions (33) and (34) to find the relative intensity and position for the various transitions and then broadening them accordingly.
3. The total intensity of the various rotation spectra are then normalized so as to agree with equation (11).
4. The D.I.D. spectrum calculated using $\beta = 6\alpha^2/r^3$ is then replaced by the more accurate spectrum using
$$\beta = \frac{6\alpha^2}{r^3} + (2.91)\ 6\alpha^3/r^6 - (33.62)\alpha^2\ e^{-r/.530}$$
5. This corrected translational spectrum is added to the rotational spectra to give the total spectrum.

This procedure is indicated in figure 2-8.

The total spectrum for CH_4-CH_4, CH_4-Ar, and CH_4-Xe, for a given A and E are shown on figure 2-9. The dependence of the CH_4-CH_4 spectrum on A and E is given on figures 2-10 and 2-11.

FIGURE 2-1

The intermolecular potentials for the CH_4-CH_4, CH_4-Ar, and CH_4-Xe interactions.

The scale is in units of meV.

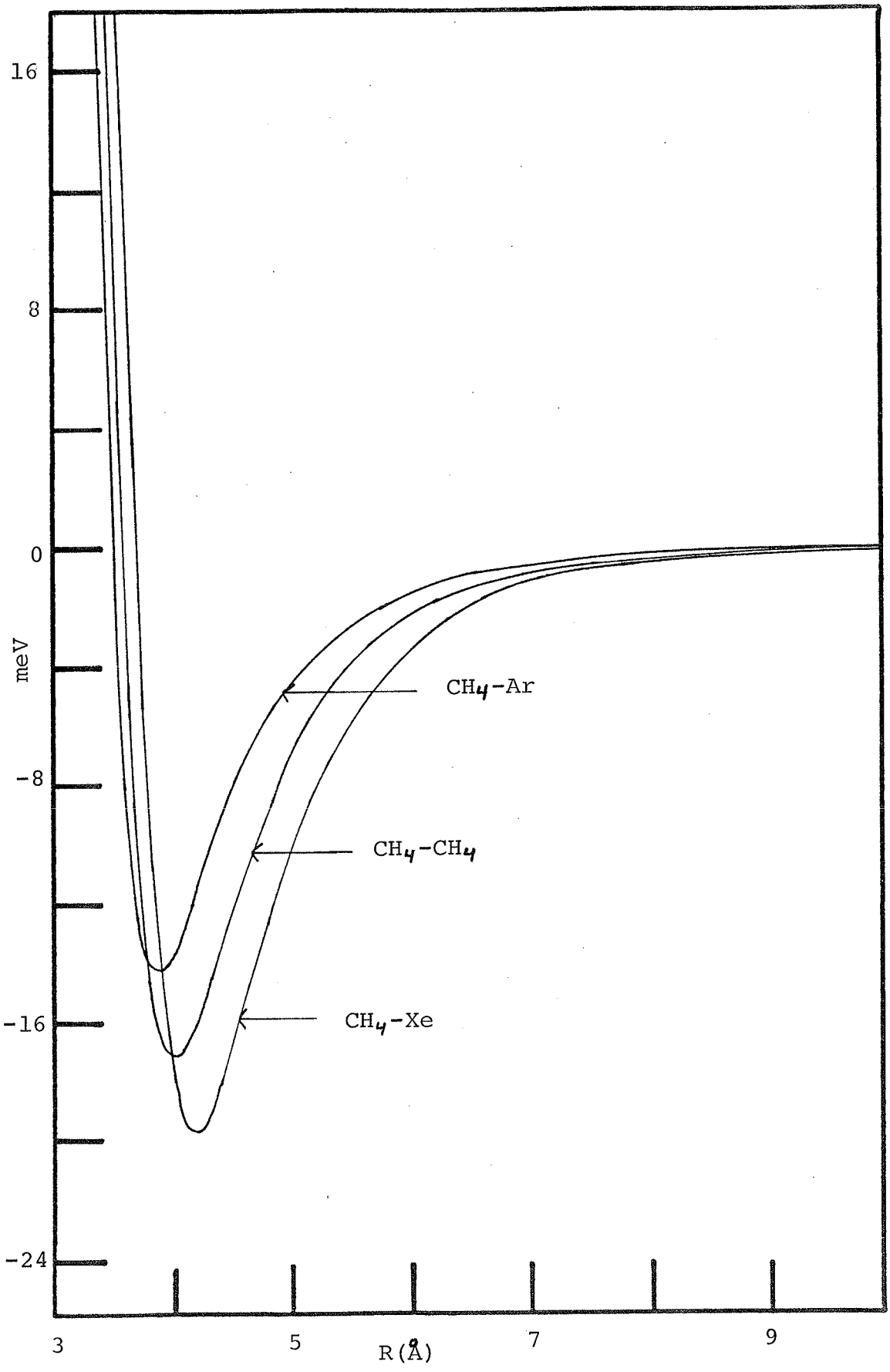
16
8
0
-8
-16
-24
meV
3
5
7
9
R(Å)
CH_4-Ar
CH_4-CH_4
CH_4-Xe

FIGURE 2-2

The orbits of molecules which have an impact parameter $\gtrsim 10$ Å are not significantly affected by the other molecule. For impact parameters ≤ 4 Å direct collisions take place. In the calculation of the translational spectrum impact parameters up to 30 Å were considered.

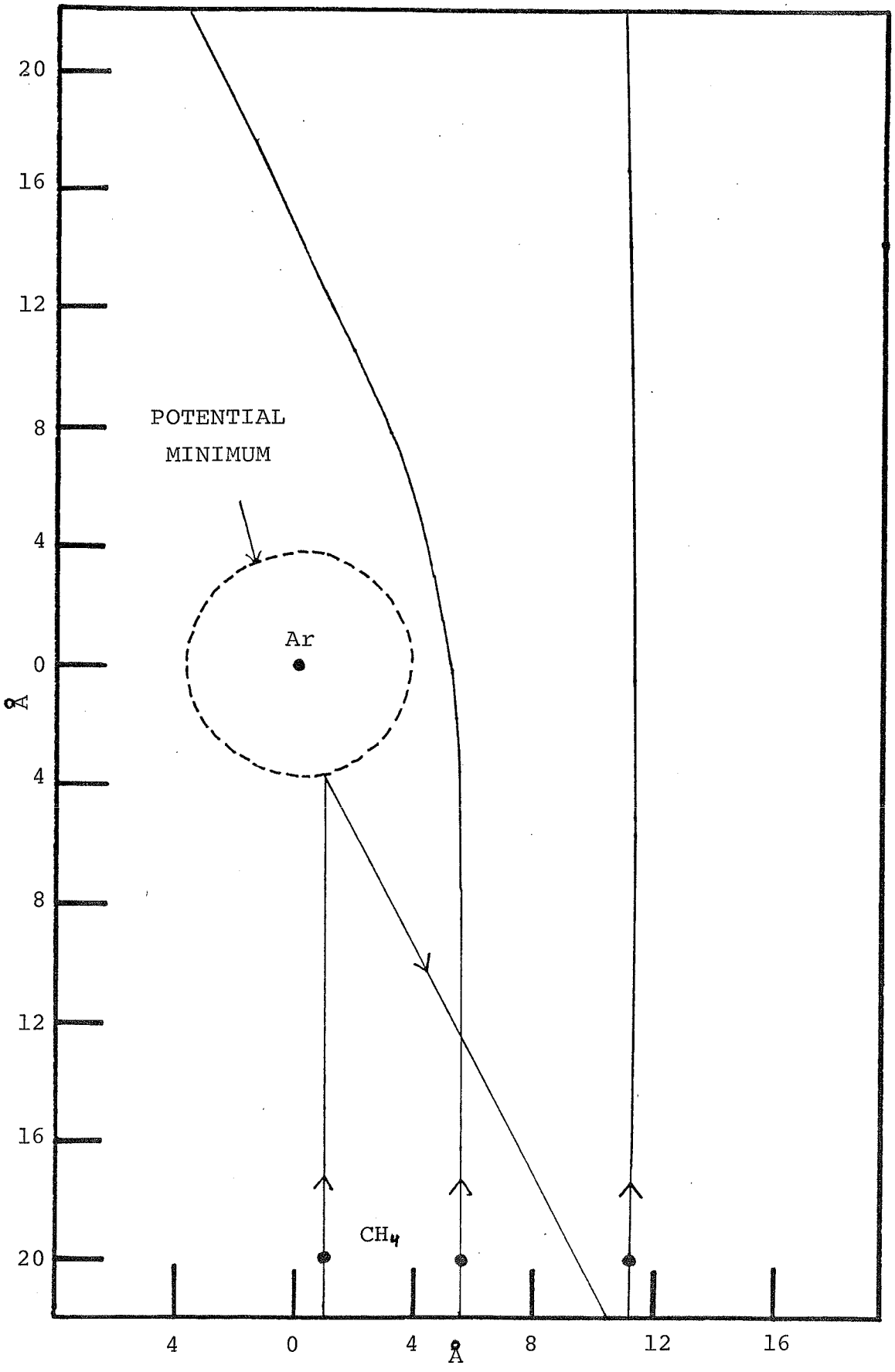
20
16
12
8
4
0
4
8
12
16
20
Å
POTENTIAL
MINIMUM
Ar
CH4
4
0
4
8
12
16
Å

FIGURES 2-3 TO 2-5

The following three figures show the translational spectrum for CH_4-CH_4, CH_4-Ar, and CH_4-Xe for both the one term D.I.D. term and the full corrected term.

The intensity scale is given in units of cm^6 (see reference (21)).

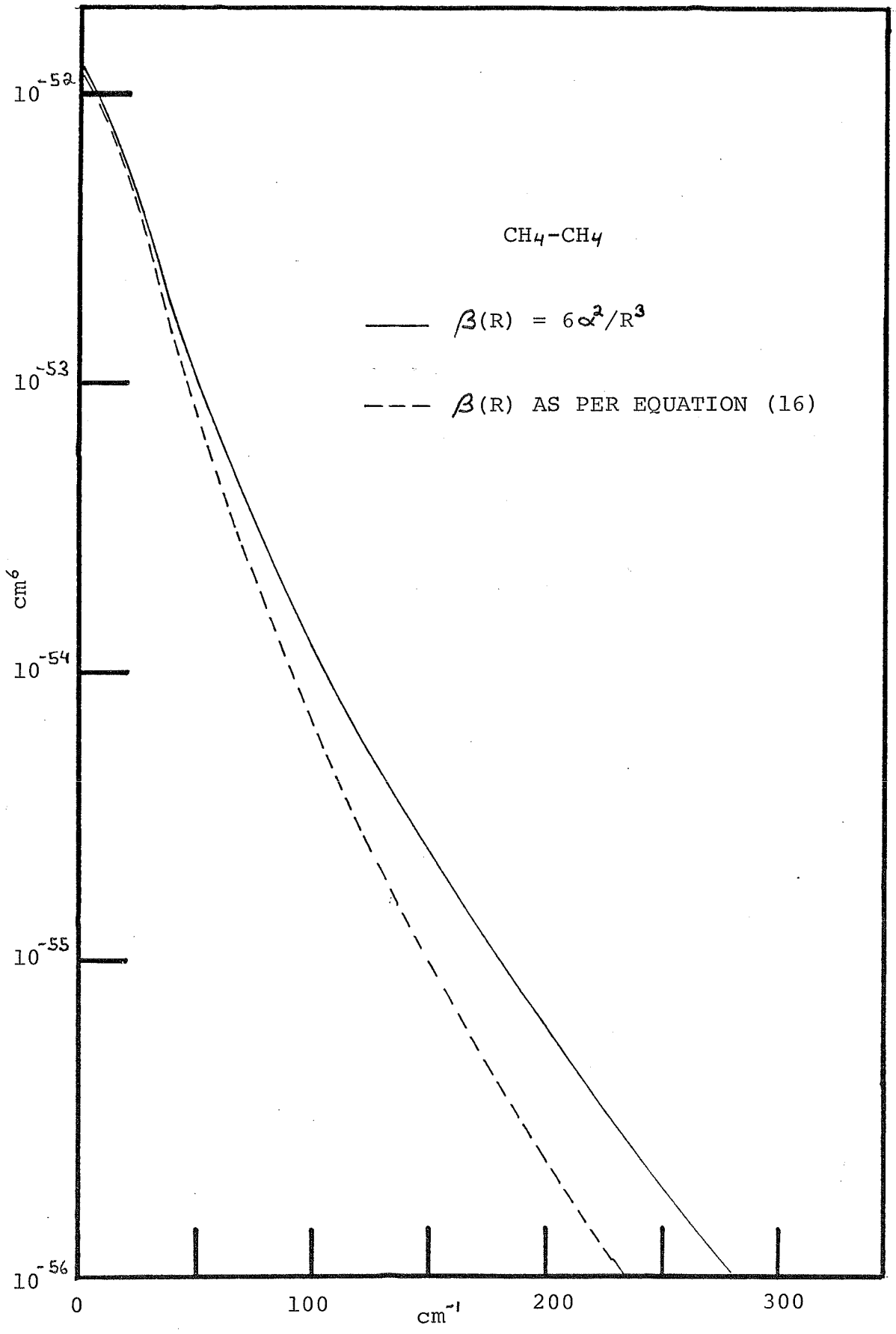
CH_4-CH_4
$\beta(R) = 6\alpha^2/R^3$
$\beta(R)$ AS PER EQUATION (16)
10^{-52}
10^{-53}
10^{-54}
10^{-55}
10^{-56}
cm^6
0
100
200
300
cm^{-1}

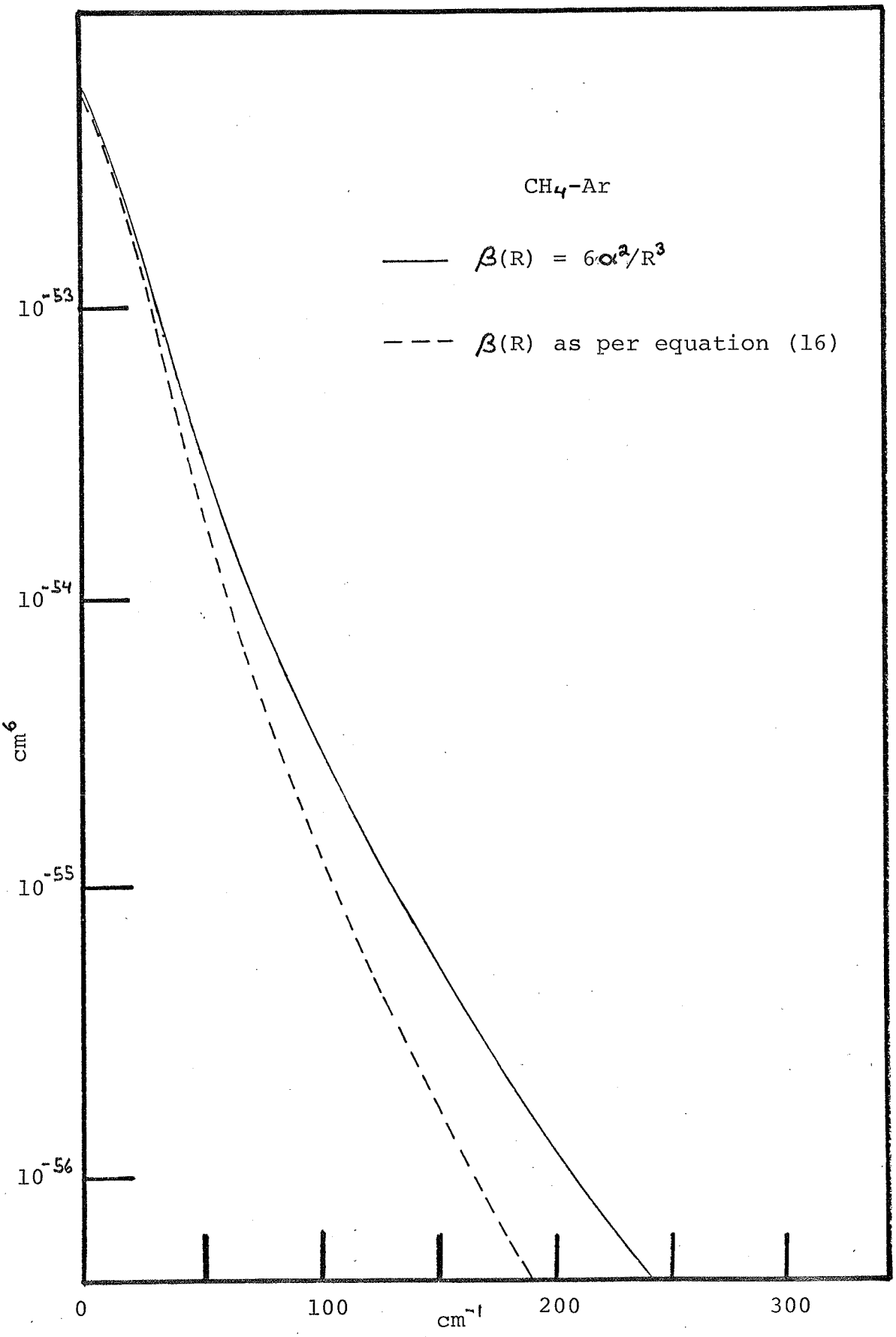
CH_4-Ar
$\beta(R) = 6\alpha^2/R^3$
$\beta(R)$ as per equation (16)
10^{-53}
10^{-54}
10^{-55}
10^{-56}
cm^6
0
100
200
300
cm^{-1}

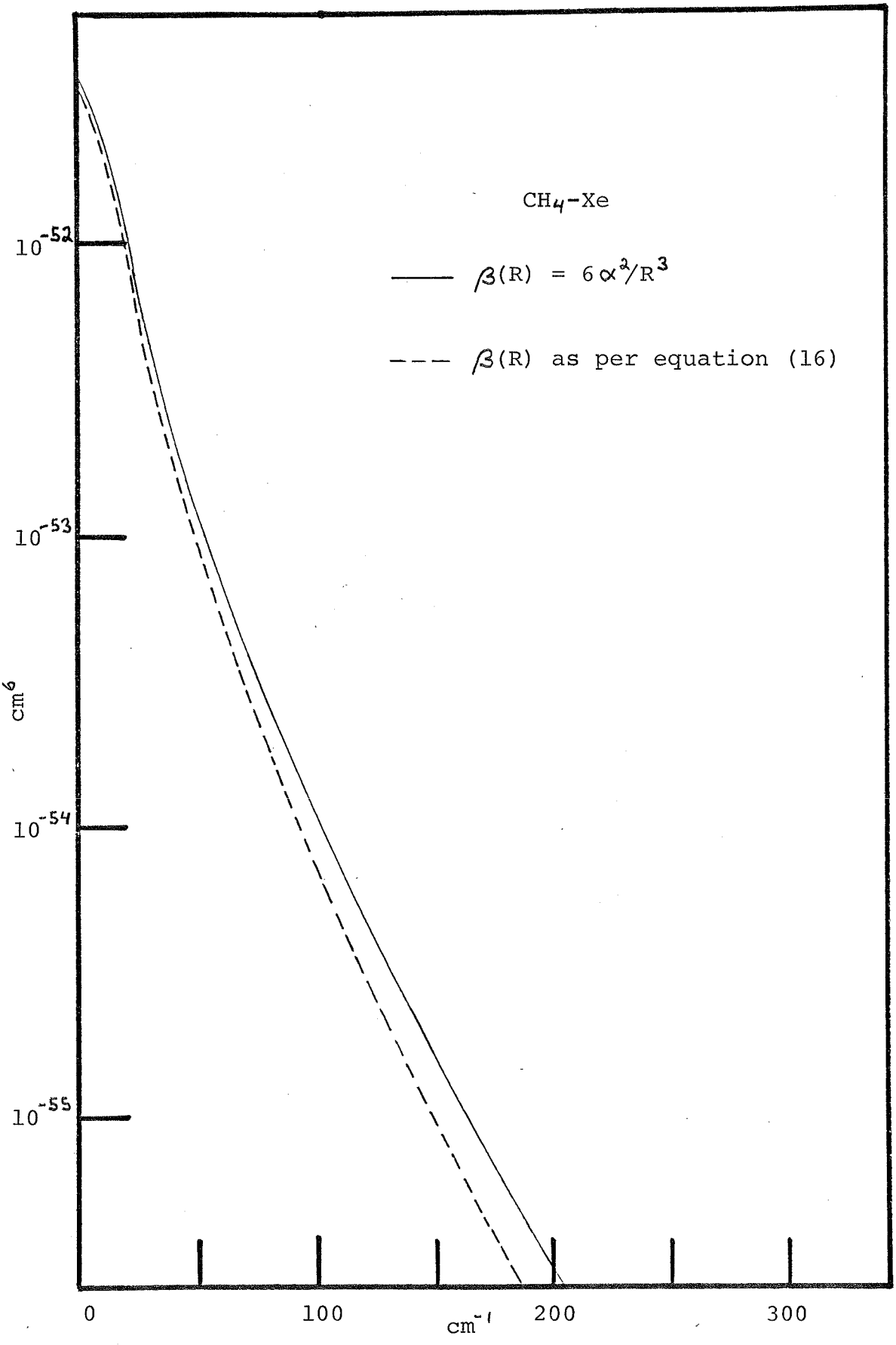
CH_4-Xe
$\beta(R) = 6\alpha^2/R^3$
$\beta(R)$ as per equation (16)
10^{-52}
10^{-53}
10^{-54}
10^{-55}
cm^6
0
100
200
300
cm^{-1}

FIGURES 2-6 AND 2-7

The relative contributions of the rotational terms. The term involving single A dominates in the region $< 500\ cm^{-1}$. From figure 2-7 it can be seen that the relative importance of the terms involving double transitions increases with increasing values of A and E.

The values of 1 $\mathring{A}^4$ for |A| and 1 $\mathring{A}^5$ for |E| are theoretical values as determined in Appendix 2-A.

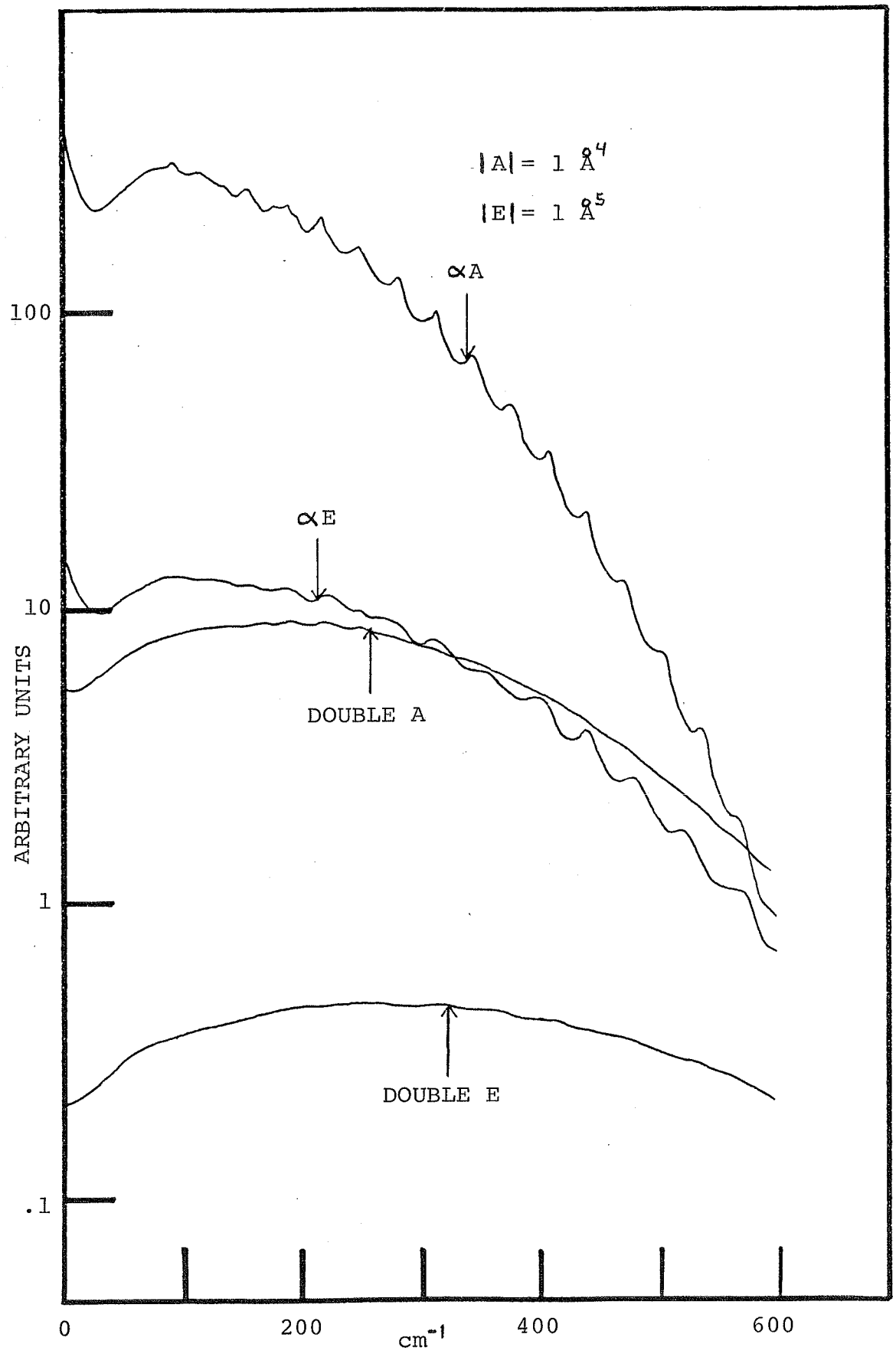
|A| = 1 Å^4
|E| = 1 Å^5
∝A
∝E
DOUBLE A
DOUBLE E
100
10
1
.1
ARBITRARY UNITS
0
200
400
600
cm^-1

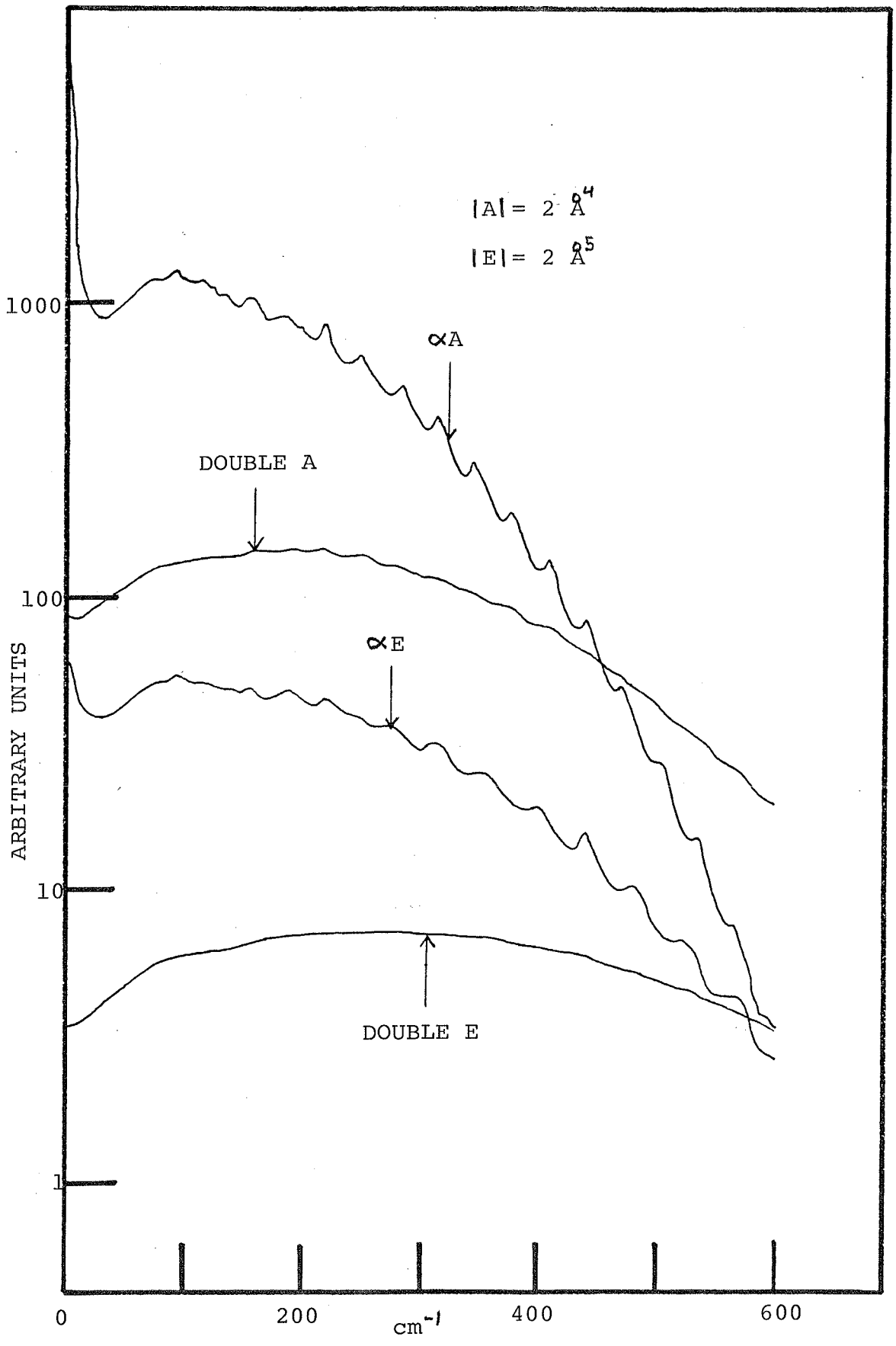
|A| = 2 Å^4
|E| = 2 Å^5
1000
100
10
1
ARBITRARY UNITS
∝A
DOUBLE A
∝E
DOUBLE E
0
200
400
600
cm^-1

FIGURE 2-8

The total rotational spectrum, the translational spectrum, and the total resulting spectrum for CH_4-CH_4. The translational term dominates in the region $\lesssim 125$ cm^{-1} while the spectrum is almost completely rotational in the region $\gtrsim 200$ cm^{-1}.

The intensity scale is given in units of cm^6.

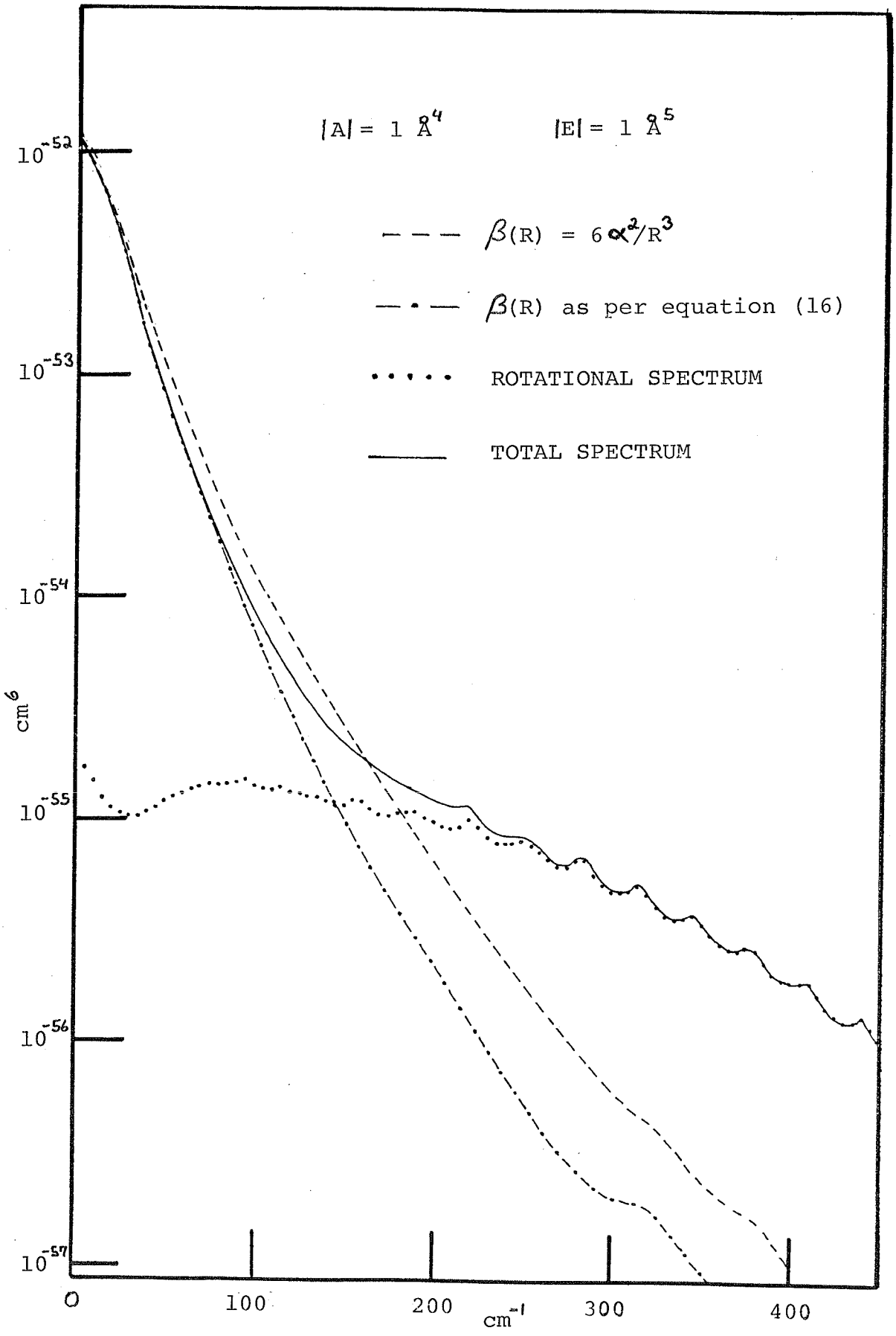
|A| = 1 Å⁴
|E| = 1 Å⁵
β(R) = 6α²/R³
β(R) as per equation (16)
ROTATIONAL SPECTRUM
TOTAL SPECTRUM
10⁻⁵²
10⁻⁵³
10⁻⁵⁴
10⁻⁵⁵
10⁻⁵⁶
10⁻⁵⁷
cm⁶
0
100
200
300
400
cm⁻¹

FIGURE 2-9

The total spectrum for CH_4-CH_4, CH_4-Ar, and CH_4-Xe for $|A| = 1$ Å^4 and $|E| = 1$ Å^5. The rotational structure increases as the reduced mass of the system increases.

The intensity scale is given in units of cm^6.

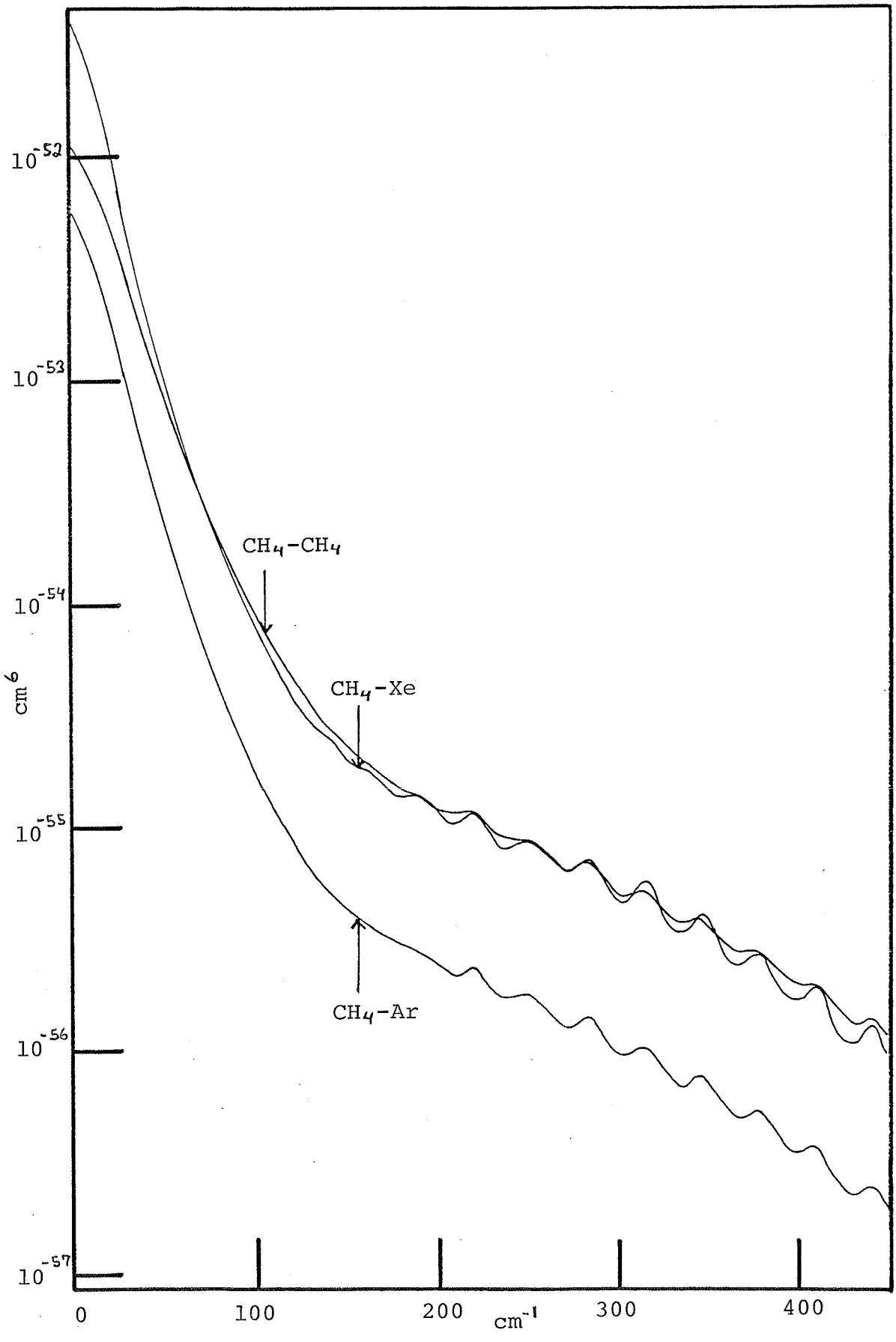
10^{-52}
10^{-53}
10^{-54}
10^{-55}
10^{-56}
10^{-57}
cm^6
CH_4-CH_4
CH_4-Xe
CH_4-Ar
0
100
200
300
400
cm^{-1}

FIGURE 2-10

The dependence of the total CH_4-CH_4 spectrum on the magnitude of A. |E| is equal to 1 $Å^5$ for all three spectra given. As is expected the importance of the rotational spectrum increases for increasing A.

The intensity scale is given in units of cm^6.

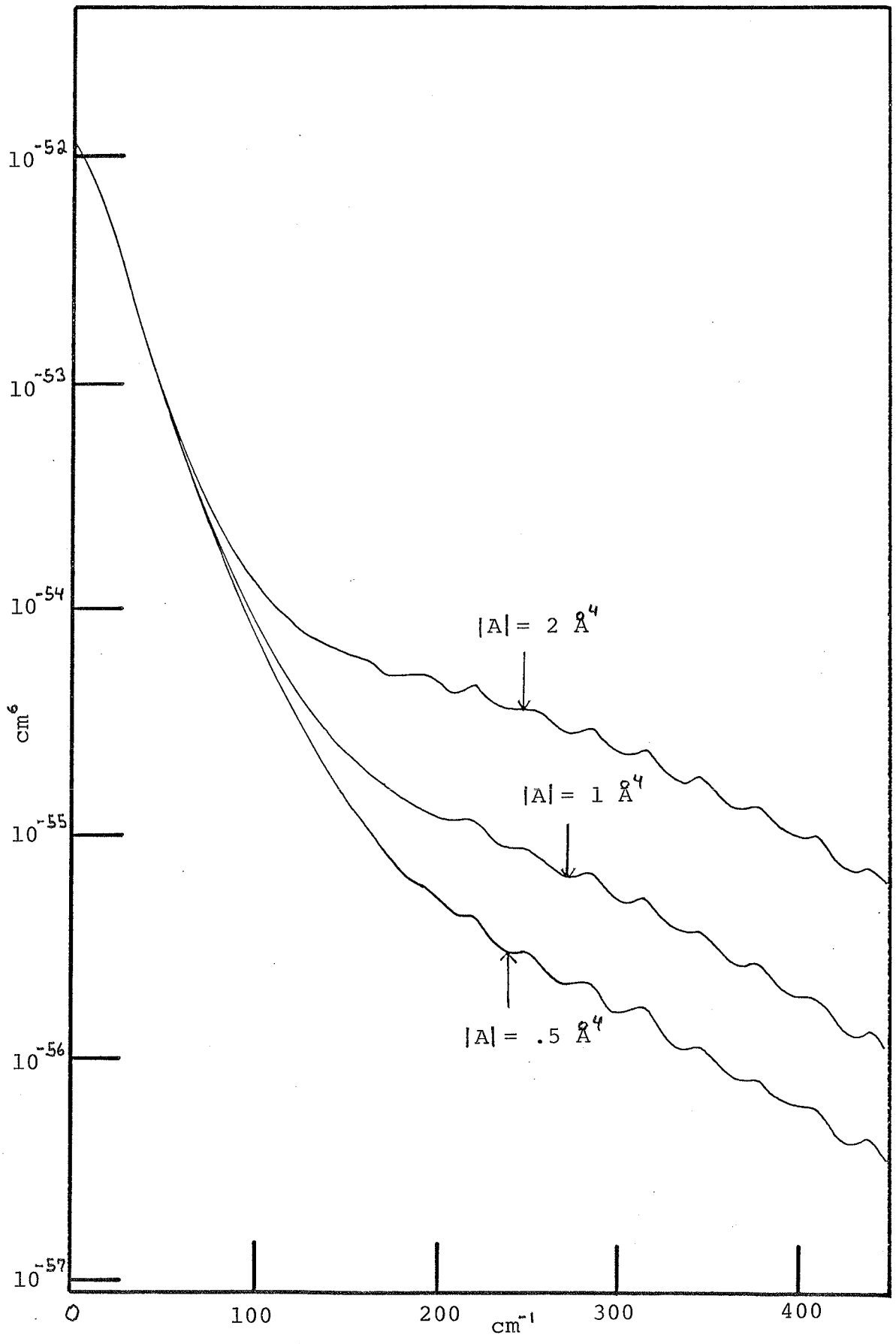
10^{-52}
10^{-53}
10^{-54}
10^{-55}
10^{-56}
10^{-57}
cm^6
|A| = 2 Å^4
|A| = 1 Å^4
|A| = .5 Å^4
0
100
200
300
400
cm^{-1}

FIGURE 2-11

The dependence of the total CH_4-CH_4 spectrum on the magnitude of E. |A| is equal to 1 $Å^4$ for all three spectra given. The spectrum is only weakly dependent on the value of E.

The intensity scale is given in units of cm^6.

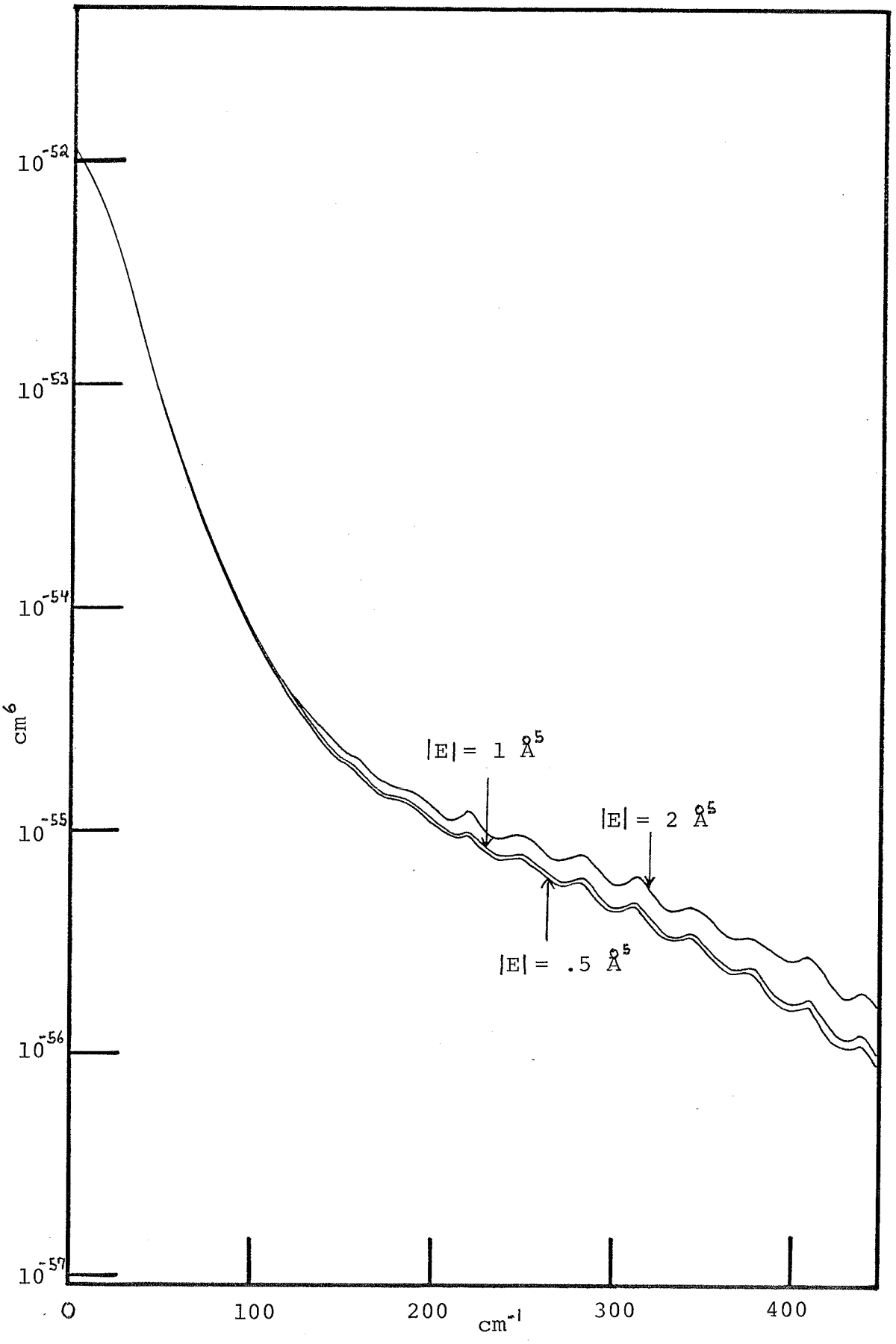
10^{-52}
10^{-53}
10^{-54}
10^{-55}
10^{-56}
10^{-57}
cm^6
|E| = 1 Å^5
|E| = 2 Å^5
|E| = .5 Å^5
0
100
200
300
400
cm^{-1}

APPENDIX 2-A

Dipole - Quadrupole Polarizability Tensor

The following discussion[27,5] gives insight into the physical meaning of the dipole-quadrupole polarizability tensor. An approximate value for A is also obtained.

The CH_4 molecule consists of a centrally located carbon atom with four hydrogen atoms arranged tetrahedrally at a distance Ro from its centre.

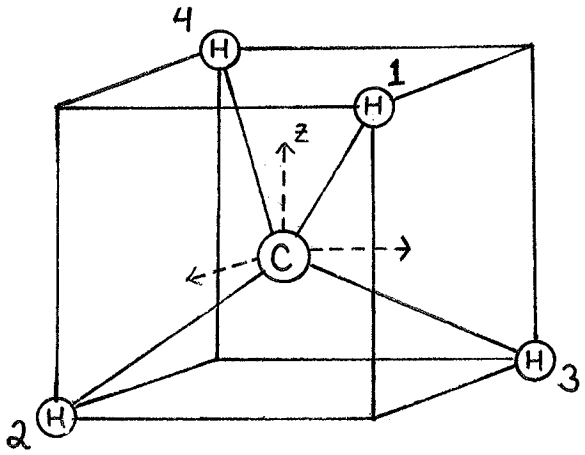

Consider hydrogen atom 1 with $\hat{n}$ representing the direction along the bond.

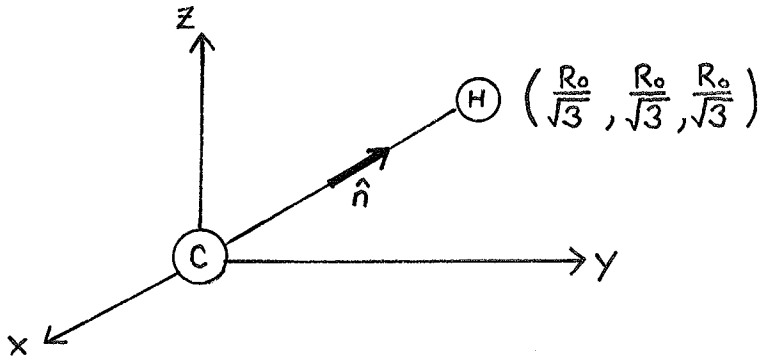

The dipole induced in this CH pair by an external field $\bar{F}$ is given by

$$\bar{\mu} = \alpha_{,,}(\bar{F}.\hat{n})\ \hat{n} + \alpha_{\perp}((\hat{n}x\bar{F})\ x\hat{n})$$

where $\alpha_{,,}$ is the polarizability of the CH group along the bond and $\alpha_{\perp}$

is the polarizability of the CH group perpendicular to the bond. This can be written as

$$\bar{\mu}^{(1)} = \tilde{\alpha}^{(1)} \bar{F}$$

where the components of $\tilde{\alpha}^{(1)}$ are given by $\alpha^{(1)}_{\alpha\beta} = \alpha_\perp \delta_{\alpha\beta} + (\alpha_{,,} - \alpha_\perp)\, n^{(1)}_\alpha n^{(1)}_\beta$. (The superscript refers to hydrogen atom 1). This expression holds for each of the four CH groups, so in general

$$\alpha^{(i)}_{\alpha\beta} = \alpha_\perp \delta_{\alpha\beta} + (\alpha_{,,} - \alpha_\perp) n^{(i)}_\alpha n^{(i)}_\beta$$

where $\hat{n}^{(i)}$ is the unit vector from the centre outward along the bond to the i th hydrogen atom.

Consider this model being placed in a field Fy which is dependent on x i.e. there exists a field gradient $F'xy$. If the field at H atom 1 and 2 is $F^{o}y$ the field at atoms 3 and 4 will be $F^{o}y - F'xy \frac{2Ro}{\sqrt{3}}$. By the symmetry of the molecule the net dipole of the four CH groups will be along the Z axis and will be given by the following equation.

$$\begin{aligned}
\mu_Z &= \alpha_{zy}\, Fy \\
&= (\alpha_{,,} - \alpha_\perp)\, (n_z^{(1)} n_y^{(1)} + n_z^{(2)} n_z^{(2)})\, F^{o}y \\
&+ (\alpha_{,,} - \alpha_\perp)\, (n_z^{(3)} n_y^{(3)} + n_z^{(4)} n_z^{(4)})(F^{o}y - F'xy \frac{2Ro}{\sqrt{3}}) \\
&= (\alpha_{,,} - \alpha_\perp)\, \frac{4Ro}{3\sqrt{3}}\, F'xy
\end{aligned}$$

Equating this to the third term in equation (1) one has

$$A = Azxy = (\alpha_{,,} - \alpha_\perp)\, \frac{4Ro}{\sqrt{3}}$$

Similarly for E one finds that for a tetrahedral molecule

$$E = \frac{-8}{3} (\alpha_{,,} - \alpha_\perp) Ro^2.$$

The polarizability difference $(\alpha_{,,} - \alpha_\perp)$ has been determined to be $0.39\ \text{Å}^3$ [28] while Ro for methane is 1.09 Å. Substituting these values into the above expressions for A and E one obtains the following theoretical values

$|A| = .98\ \text{Å}^4$

$|E| = 1.24\ \text{Å}^5$.

For the theoretical spectra generated in Chapter 2 the value of A was taken to be 1 Å^4 while that of E was 1 Å^5.

APPENDIX 2-B

Program Used to Construct Theoretical Spectra

The computer program used to generate the theoretical spectra is given here. It consists of a main program and six subroutines whose purpose is outlined below.

MAIN - calls the six subroutines and then weights the various nomalized spectra according to equations (11).

RAVGCC- calculates $\overline{R^{-n}}$ according to equation (12)

ASPEC- calculates the spectrum due to the αA term and normalizes it.

ESPEC- calculates the spectrum due to αE term and normalizes it.

DASPEC- calculates the spectrum due to the double A term and normalizes it.

DESPEC- calculates the spectrum due to the double E term and normalizes it.

TRANS- takes the values of the translational spectrum, calculated by Fromholds translational program, and normalizes it.

MAIN

```
      REAL ANINT(600),ENINT(600),DANINT(600),DENINT(600)
      REAL CCA(600),CCE(600),CCAA(600),CCEE(600),CCSPEC(600)
      REAL CIS(600),CCCIS(600)
      REAL RAVCC(12)
      REAL I(600)
      INTEGER SEP
      CALL RAVGCC(RAVCC)
      READ 5,8,WLINE
    5 FORMAT(' ',2F15.5)
      READ 6,CH4ALP,A,E
    6 FORMAT(' ',3F15.5)
      PRINT 16,CH4ALP,A,E
   16 FORMAT(' ',3F15.5)
      READ 7,ARGALP
    7 FORMAT(' ',F15.5)
      PRINT 17,ARGALP
   17 FORMAT(' ',F15.5)
      READ 8,ADECAY,EDECAY,DADECY,DEDECY
    8 FORMAT(' ',4F15.5)
      PRINT 18,ADECAY,EDECAY,DADECY,DEDECY
   18 FORMAT(' ',4F15.5)
      READ 9,NUM,SEP
    9 FORMAT(' ',2I3)
      PRINT 19,NUM,SEP
   19 FORMAT(' ',2I3)
      J=(NUM-1)*SEP+1
      DO 20 K=1,J,SEP
      READ 21,I(K)
   21 FORMAT(' ',F15.5)
      PRINT 22,I(K)
   22 FORMAT(' ',F15.5)
   20 CONTINUE
      CALL TRANS(NUM,SEP,1,CIS)
      CALL ASPEC(8,WLINE,ADECAY,ANINT)
      CALL ESPEC(8,WLINE,EDECAY,ENINT)
      CALL DASPEC(8,WLINE,DADECY,DANINT)
      CALL DESPEC(8,WLINE,DEDECY,DENINT)
      DO 500 L=1,600
      CCCIS(L)=(12./5.)*(CH4ALP*CH4ALP)**(2)*RAVCC(6)*CIS(L)
      CCA(L)=(48./35.)*2.*(CH4ALP*A)**(2)*RAVCC(8)*ANINT(L)
      CCE(L)=(11./9.)*2.*(CH4ALP*E)**(2)*RAVCC(10)*ENINT(L)
      CCAA(L)=(62912./4725.)*A**(4)*RAVCC(10)*DANINT(L)
      CCEE(L)=(12.)*E**(4)*RAVCC(12)*DENINT(L)
      CCSPEC(L)=CCA(L)+CCE(L)+CCAA(L)+CCEE(L)
      PRINT 11,L,CCCIS(L),CCA(L),CCE(L),CCAA(L),CCEE(L),CCSPEC(L)
   11 FORMAT(' ',I5,F12.5,5X,5F12.5)
  500 CONTINUE
      STOP
      END
```

RAVGCC

```
      SUBROUTINE RAVGCC(RAVCC)
      REAL DISCC(3000),VCC(3000),RAVCC(12),K
      INTEGER R
      EXT=2.7183
      K=8.63E-02
      TEMP=295.
      FM=83.80
      EPS=2.7597E-21
      RVMIN=4.012
      D=1.28
      A=0.1215312E8
      ALPHA=16.496763
      C6=1.1561739
      C8=0.5414923
      C10=0.2839735
      GAMMA=2.4
      RM=RVMIN
      DO 20 NN=6,12
      N=-NN
      RAVCC(NN)=0.
      DO 10 R=300,3000
      RR=R/100.
      X=RR/RM
      F=1.
      IF(X.GE.D) GO TO 99
      XZZ=(D/X-1.)**2
      IF(XZZ.GT.174.)XZZ=174.
      F=EXT**(-XZZ)
   99 ZZZ=ALPHA*X
      IF(ZZZ.GT.174.)ZZZ=174.
      VA=EPS*(A*X**GAMMA/ EXT**(ZZZ)-F*(C6/X**6+C8/X**8+C10/X**10))
      VCC(R)=VA/1.6E-22
      DR=R/10.
      I=INT(DR)
      DD=DR-I
      IF(DD.NE.0.) GO TO 7
      IF(NN.NE.6) GO TO 7
      T=I/10.
      PRINT 25,T,VCC(R)
   25 FORMAT(' ',F5.1,F15.5)
    7 BOLTZ=EXT**(-VCC(R)/(K*TEMP))
      DISCC(R)=RR
      DSUM=(RR**(N+2))*BOLTZ*.01
      RAVCC(NN)=RAVCC(NN)+DSUM
   10 CONTINUE
      PRINT 15,NN,RAVCC(NN)
   15 FORMAT(' ',I5,E12.5)
   20 CONTINUE
      RETURN
      END
```

ASPEC

```
      SUBROUTINE ASPEC(B,WLINE,ADECAY,ANINT)
      INTEGER DELTAJ,WN
      REAL INTEN(400),RPOS(400),TINTEN(600),ANINT(600)
      EXP=2.7183
      SUM=0.
      I=1
      N=0
      DO 10 IJ=1,41
      J=IJ-1
      DO 10 IJP=1,41
      JP=IJP-1
      DELTAJ=JP-J
      JSUM=J+JP
      IF(DELTAJ.LT.0) GO TO 10
      IF(DELTAJ.GT.3) GO TO 10
      IF(JSUM.LT.3) GO TO 10
      RELPOS=(JP*(JP+1)-J*(J+1))*B
      POS=(WLINE-RELPOS)/WLINE
      RPOS(I)=RELPOS
      IF(J.EQ.0) GO TO 8
      BC=J*(J+1)*8*0.004886
      BOLTZ=EXP**BC
      GO TO 9
    8 BOLTZ=1.
    9 INTEN(I)=POS**(4.0)*(2*J+1)*(2*JP+1)/BOLTZ
      I=I+1
      N=N+1
   10 CONTINUE
      PRINT 13,N
   13 FORMAT(' ',I5)
      DO 20 WN=1,600
      TINTEN(WN)=0
      DO 30 K=1,N
      PART=INTEN(K)/EXP**(ABS(WN-RPOS(K))/ADECAY)
   30 TINTEN(WN)=TINTEN(WN)+PART
      SUM=SUM+TINTEN(WN)*(1.+EXP**(-.004886*WN))
   20 CONTINUE
      DO 40 L=1,600
      ANINT(L)=TINTEN(L)/SUM*10000.
   40 CONTINUE
      RETURN
      END
```

ESPEC

```
      SUBROUTINE ESPEC(B,WLINE,EDECAY,ENINT)
      INTEGER DELTAJ,WN
      REAL INTEN(400),RPOS(400),TINTEN(600),ENINT(600)
      EXP=2.7183
      SUM=0.
      I=1
      N=0
      DO 10 IJ=1,41
      J=IJ-1
      DO 10 IJP=1,41
      JP=IJP-1
      DELTAJ=JP-J
      JSUM=J+JP
      IF(DELTAJ.LT.0) GO TO 10
      IF(DELTAJ.GT.4) GO TO 10
      IF(JSUM.LT.4) GO TO 10
      RELPOS=(JP*(JP+1)-J*(J+1))*B
      POS=(WLINE-RELPOS)/WLINE
      RPOS(I)=RELPOS
      IF(J.EQ.0) GO TO 8
      BC=J*(J+1)*B*0.004886
      BOLTZ=EXP**BC
      GO TO 9
    8 BOLTZ=1.
    9 INTEN(I)=POS**(4.0)*(2*J+1)*(2*JP+1)/BOLTZ
      I=I+1
      N=N+1
   10 CONTINUE
      PRINT 13,N
   13 FORMAT(' ',I5)
      DO 20 WN=1,600
      TINTEN(WN)=0
      DO 30 K=1,N
      PART=INTEN(K)/EXP**(ABS(WN-RPOS(K))/EDECAY)
   30 TINTEN(WN)=TINTEN(WN)+PART
      SUM=SUM+TINTEN(WN)*(1.+EXP**(-.004886*WN))
   20 CONTINUE
      DO 40 L=1,600
      ENINT(L)=TINTEN(L)/SUM*10000.
   40 CONTINUE
      RETURN
      END
```

DASPEC

```
      SUBROUTINE DASPEC(B,WLINE,DADECY,DANINT)
      INTEGER DELTAJ,DELTJ2,WN
      REAL INTEN(10000),RPOS(10000),TINTEN(600),DANINT(600)
      EXP=2.7183
      SUM=0.
      I=1
      N=0
      DO 10 IJ=1,16
      J=IJ-1
      DO 10 IJP=1,16
      JP=IJP-1
      DELTAJ=JP-J
      JSUM=J+JP
      IF(DELTAJ.LT.0) GO TO 10
      IF(DELTAJ.GT.3) GO TO 10
      IF(JSUM.LT.3) GO TO 10
      DO 10 IJ2=1,16
      J2=IJ2-1
      DO 10 IJP2=1,16
      JP2=IJP2-1
      DELTJ2=JP2-J2
      J2SUM=J2+JP2
      IF(DELTJ2.GT.3) GO TO 10
      IF(DELTJ2.LT.-3) GO TO 10
      IF(J2SUM.LT.3) GO TO 10
      RELPOS=(JP*(JP+1)-J*(J+1))*B+(JP2*(JP2+1)-J2*(J2+1))*B
      IF(RELPOS.LT.0.) GO TO 10
      POS=(WLINE-RELPOS)/WLINE
      RPOS(I)=RELPOS
      BC=(J*(J+1)+J2*(J2+1))*B*0.004886
      IF(BC.EQ.0.) GO TO 8
      IF(BC.GT.10.) GO TO 11
      BOLTZ=EXP**BC
      GO TO 9
    8 BOLTZ=1.
    9 INTEN(I)=POS**(4.0)*(2*J+1)*(2*JP+1)*(2*J2+1)*(2*JP2+1)/BOLTZ
      GO TO 12
   11 INTEN(I)=0.
   12 I=I+1
      N=N+1
   10 CONTINUE
      PRINT 13,N
   13 FORMAT(' ',I5)
      DO 20 WN=1,600
      TINTEN(WN)=0
      DO 30 K=1,N
      Q=ABS(WN-RPOS(K))/DADECY
      IF(Q.GT.10.) GO TO 30
      PART=INTEN(K)/EXP**(ABS(WN-RPOS(K))/DADECY)
      TINTEN(WN)=TINTEN(WN)+PART
   30 CONTINUE
      SUM=SUM+TINTEN(WN)*(1.+EXP**(-.004886*WN))
   20 CONTINUE
      DO 40 L=1,600
      DANINT(L)=TINTEN(L)/SUM*10000.
   40 CONTINUE
      RETURN
      END
```

DESPEC

```
      SUBROUTINE DESPEC(B,WLINE,DEDECY,DENINT)
      INTEGER DELTAJ,DELTJ2,WN
      REAL INTEN(15000),RPOS(15000),TINTEN(600),DENINT(600)
      EXP=2.7183
      SUM=0.
      I=1
      N=0
      DO 10 IJ=1,16
      J=IJ-1
      DO 10 IJP=1,16
      JP=IJP-1
      DELTAJ=JP-J
      JSUM=J+JP
      IF(DELTAJ.GT.4) GO TO 10
      IF(DELTAJ.LT.0) GO TO 10
      IF(JSUM.LT.4) GO TO 10
      DO 10 IJ2=1,16
      J2=IJ2-1
      DO 10 IJP2=1,16
      JP2=IJP2-1
      DELTJ2=JP2-J2
      J2SUM=J2+JP2
      IF(DELTJ2.GT.4) GO TO 10
      IF(DELTJ2.LT.-4) GO TO 10
      IF(J2SUM.LT.4) GO TO 10
      RELPOS=(JP*(JP+1)-J*(J+1))*B+(JP2*(JP2+1)-J2*(J2+1))*B
      IF(RELPOS.LT.0.) GO TO 10
      POS=(WLINE-RELPOS)/WLINE
      RPOS(I)=RELPOS
      BC=(J*(J+1)+J2*(J2+1))*B*0.004886
      IF(BC.EQ.0.) GO TO 8
      IF(BC.GT.10.) GO TO 11
      BOLTZ=EXP**BC
      GO TO 9
    8 BOLTZ=1.
    9 INTEN(I)=POS**(4.0)*(2*J+1)*(2*JP+1)*(2*J2+1)*(2*JP2+1)/BOLTZ
      GO TO 12
   11 INTEN(I)=0.
   12 I=I+1
      N=N+1
   10 CONTINUE
      PRINT 13,N
   13 FORMAT(' ',I5)
      DO 20 WN=1,600
      TINTEN(WN)=0
      DO 30 K=1,N
      Q=ABS(WN-RPOS(K))/DEDECY
      IF(Q.GT.10.) GO TO 30
      PART=INTEN(K)/EXP**(ABS(WN-RPOS(K))/DEDECY)
      TINTEN(WN)=TINTEN(WN)+PART
   30 CONTINUE
      SUM=SUM+TINTEN(WN)*(1.+EXP**(-.004886*WN))
   20 CONTINUE
      DO 40 L=1,600
      DENINT(L)=TINTEN(L)/SUM*10000.
   40 CONTINUE
      RETURN
      END
```

TRANS

```
      SUBROUTINE TRANS(NUM,SEP,I,CIS)
      INTEGER SEP
      REAL I(600),CIS(600)
      EXP=2.7183
      J=(NUM-1)*SEP+1
      DO 100 L=1,600
  100 CIS(L)=0.
      SUM=-I(1)*(1.+EXP**(-.004886))
      L=0
      DO 10 K=1,J,SEP
      L=L+1
      F=2
      Z=L/2.
      N=INT(Z)
      DIFF=Z-N
      IF(DIFF.EQ.0.)F=F*2
      SUM=SUM+F*I(K)*(1.+EXP**(-.004886*K))
   10 CONTINUE
      SUM=SUM*SEP/3.
      DO 20 N=1,J,SEP
      CIS(N)=I(N)/SUM*10000
   20 CONTINUE
      RETURN
      END
```

CHAPTER 3

EXPERIMENT

3.1 Equipment

As stated in the previous chapter, the experiment is set up so as to permit observation of the depolarized component of scattered light from CH_4-CH_4, CH_4-Ar, and CH_4-Xe mixtures. The equipment layout is shown on figure 3-1 and a general explanation of the various components will now be given[4, 29].

1) Due to the size of the laser it was necessary to mount it on a separate table. Instability due to the separate mounting was not noticed as both tables were sufficiently massive so as to completely damp out any associated vibrations.
2) The laser light is provided by a 6 W argon ion laser built by Coherent Radiation. This tube was later replaced by a 8 W tube. The laser line chosen was 5145 Å which provided an average of 1 W power for a laser current of 28 amperes. The laser was equipped with a light regulator which kept the laser output constant during a run.
3) Three prism reflectors are used to direct the laser beam towards the cell.
4) A half-wave plate, followed by a Nicol prism which removes any undesired components after the beam has passed through the half-wave plate, is used to give the required polarization.
5) The beam is reflected upwards by the prism and then focused by a lens placed just below the cell.
6) The cell is essentially a solid block of stainless steel which

FIGURE 3-1

The equipment layout as described in Section 3-1.

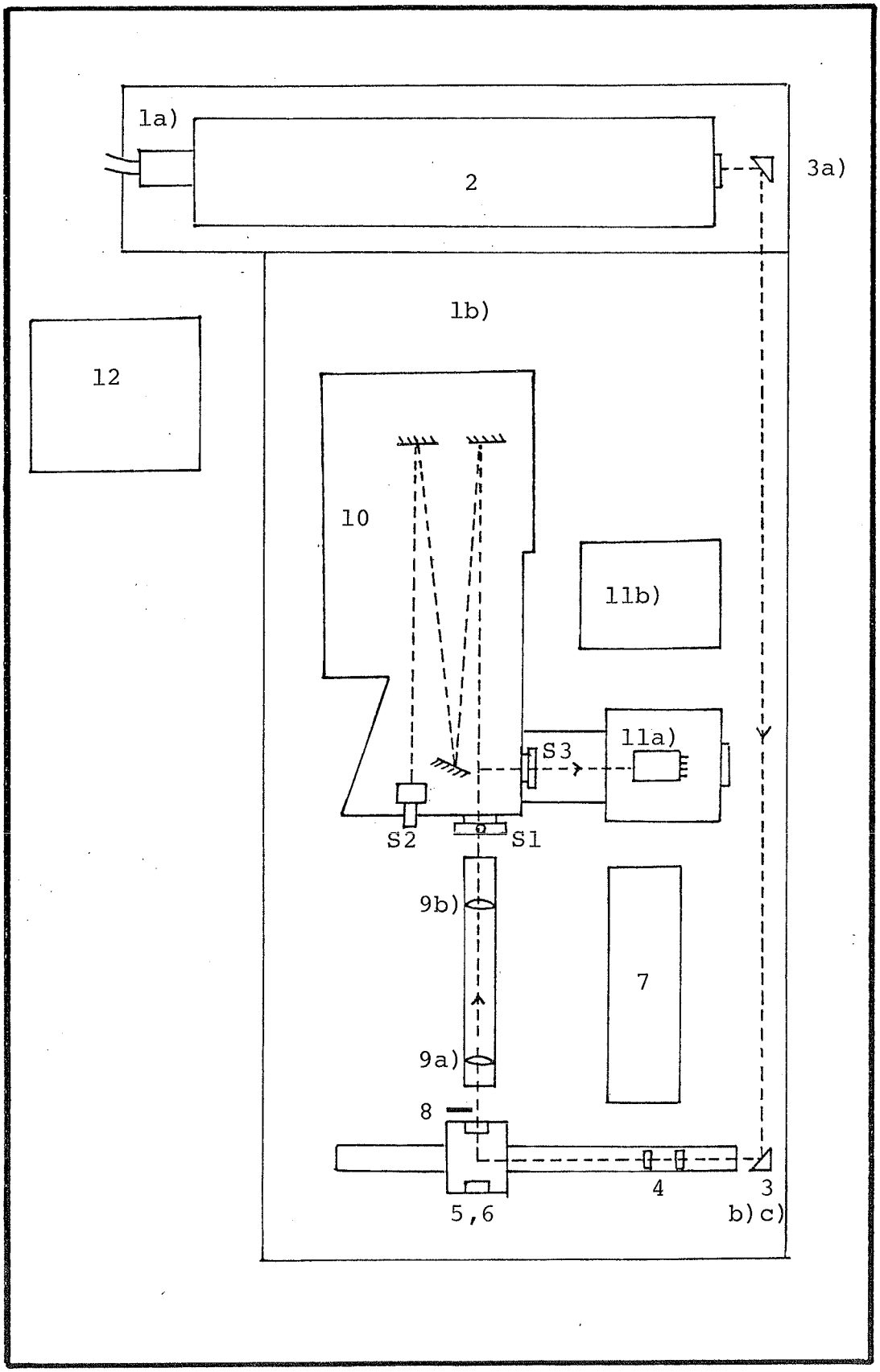
1a)
2
3a)
1b)
12
10
11b)
11a)
S3
S2
S1
9b)
7
9a)
8
4
3
5,6
b) c)

has been crossbored with 1 inch diameter holes. The cell has a volume of 32.3 cm^3 [30].

7) The cell-filling equipment is contained in this area. Included is a 0-3000 p.s.i. gauge.

8) A shutter was placed after the cell so a constant check of background during a run can be made.

9) Two lenses comprise the collection optics which image the source region onto the entrance slit of the spectrometer. Lens 9 b) was regularly adjusted to keep the image focused.

10) The spectrum is scanned by a tandem Czerny-Turner monochromator built by Jarrell-Ash.

11) The light emerging from the double monochromator is focused on to the photocathode of a RCA C31034 photomultiplier tube, which is mounted in a refrigerated housing (11a). The refrigerator compressor, condenser, and temperature controller are mounted at (11b).

12) The electronics are mounted in this region. They include an amplifier and signal channel analyzer for processing the pulses from the photomultiplier tube and a multi-channel scalar from which the spectra are obtained.

There are several controls which must be set before an experimental run is made. The four major ones are as follows:

1) The three slits of the spectrometer (S1→S3 in the figure) are set according to the spectral resolution wanted. Observation of the theoretical spectra indicate that no features of < 3 cm^{-1} width are to be expected. Thus the slits were set to a width

of 0.090 mm which corresponds to a spectral width of ~2.7 cm^{-1} (for the laser wavelength of 5145 Å).

2) The spectrometers camera mirror needs to be set. This was done by maximizing the intensity observed while at a given point in the spectrum. The actual setting was found to be dependent on temperature (changes in temperature of one degree or more required realignment of the camera mirror). For this reason two thermostat controlled baseboard heaters were placed on either side of the spectrometer to help stabilize the temperature.

3) The collector lenses needed to be aligned regularly. This adjustment was done, as with the camera mirror, by maximizing the intensity observed.

4) The power output of the laser was regularly checked and adjustments to the prism were necessary to keep the power output at a maximum and constant.

3.2 Gas Samples

The gas samples used in the experimental runs were CH_4, Ar, and Xe. These were taken directly from supply cylinders. The purities of the three were given as 99.97, 99.999, and 99.995 percent respectively and no further purification was necessary (dust filters were present).

The methane pressures used ranged from approximately 10 to 25 atmospheres. The pressures of the added argon gas, for the CH_4-Ar spectra, were in the range of 50 to 100 atmospheres while the pressures of the added xenon gas, for the CH_4-Xe spectra, were in the range 5 to 35 atmospheres. The maximum pressures used for both Ar and Xe were

determined by the corresponding bottle pressure of the gases.

While a first impression may lead to an opinion that very high gas pressures are wanted so as to increase the intensity of the scattered light, further analysis shows that complications enter. These complications arise from the fact that although the theoretical spectra were derived from 2-body collisions in an actual gas 3-body and higher multibody collisions take place. It has been shown that the translational spectrum may be represented by a power series expansion in density[31,32]

$$I(\omega) = I^{(2)}(\omega)\rho^2 + I^{(3)}(\omega)\rho^3 + I^{(4)}(\omega)\rho^4 + \ldots \qquad (35)$$

where the leading term is the 2-body contribution, $I^{(3)}(\omega)\rho^3$ is the 3-body correlation contribution and so on for higher body collisons.

Previous work on the 3-body contribution [2,33,34] has shown that at the CH_4 densities used the contribution is of the order of 10%. However this excess intensity only appears at low frequency shifts which is not surprising as only two bodies can overlap strongly and the third member of the triplet must be relatively distant. Long time processes are therefore probed and as a result the 3-body spectrum should appear at low frequencies.

The actual contribution that the 3-body collisions make to our spectra at high frequencies, greater than $\sim$150 cm^{-1}, can best be determined by comparing the various runs of a given mixture, done for different number densities. As can be seen in figures 3-6 to 3-8, which have been normalized with respect to the number of 2-body collisions, there are no number-density related trends. This leads one to conclude that the 3-body contribution at high frequencies is negligible at the pressures being used.

As will be seen in section (3-5) the number density, or at least the relative number density, of the gases in the cell is necessary if comparisons are to be made between the various spectra. As the pressure is known this can be found by the gas law $\rho = P/kT$ for ideal gases. The gases CH_4 and Ar behave nearly ideally at the pressures used[35] and thus the above expression was adequate. Xe does not behave ideally however. The number density-pressure characteristics for Xe has been determined experimentally[36] and it is this result that is used (the method of determination of the number density of the Xe in the CH_4-Xe mixtures is given in Appendix 3-A).

3.3 Individual Spectra

It took approximately 150 hours of running time to obtain a spectrum when no equipment problems arose. The exact running time was of course dependent on the intensity of the scattered light which itself is dependent on the given mixture. One also needed to balance the requirements of a larger number of counts with the stability of the system at a given time. Each spectra consists of approximately half a dozen uninterrupted runs covering from 50 cm^{-1} to 100 cm^{-1} of the spectrum. An example of the raw data obtained from a run is given on figure 3-2. The method of fitting the various regions of the spectrum together is shown on figure 3-3.

Since each spectrum takes an extended time to complete, the stability of the system is extremely important. To make sure that there was not any loss in intensity, reference points on each spectrum (20 cm^{-1}, 50 cm^{-1}, or 100 cm^{-1}) were checked before and after each run.

The fact that we wish to compare the intensities of the various

spectra required stability over a period of months. Cross checks were thus necessary and resulted in scaling some of the resulting data so as to give results consistent with each other (this was especially necessary as the laser tube was replaced half way through the experiment). The reference used for the cross checks was pure CH_4 at a pressure of 16.7 atmospheres.

The spectral response function of the spectrometer was found to be nearly constant over a range of several hundred wavenumbers (the hydrogen rotational lines at shifts of 355 cm^{-1} and 587 cm^{-1} were used for this measurement)*. As such the corresponding corrections to the spectra were not necessary.

3.4 Spectra for Gas Mixtures

To find the spectrum due to collisions between two different molecules, in our case CH_4-Ar and CH_4-Xe, three different spectra need to be taken. In the case of CH_4-Ar, a CH_4-CH_4 spectrum, an Ar-Ar spectrum, and the total spectrum when Ar is mixed with CH_4, are needed. To find the spectrum of the colliding CH_4 and Ar molecules it is then necessary to subtract the single gas spectra, at the same number densities that they have in the mixture, from the total spectrum.

The actual experimental results for one of the CH_4-Ar runs are shown on figure 3-4. For this run a CH_4 spectrum was taken at a

---

* Previous measurements [4] which extend out to 200 cm^{-1}, with respect to the laser line, give a slope for the spectral response function of approximately 1.5% per 100 cm^{-1}. This is small compared with the other errors associated with the spectra.

pressure of 16.7 atmospheres. Then Ar was added to give a total pressure of 157.6 atmospheres. After this spectrum was taken, all that remained was an Ar spectrum at a pressure of 140.9 atmospheres. In actual fact an Ar spectrum which was taken at a lower pressure and then scaled up to correspond to the necessary pressure was used. In the case of CH_4-Xe special care was needed, as Xe does not behave like an ideal gas,to take a Xe spectrum which corresponds to the same number density that was in the CH_4-Xe mixture. Results for one of the CH_4-Xe runs are shown on figure 3-5.

The error associated with the resulting spectra for CH_4-Ar and CH_4-Xe will turn out to be larger than that associated with the CH_4-CH_4 spectra, or any other single gas spectra. This is simply due to the fact that to obtain the spectrum for the CH_4-Ar and CH_4-Xe collisions one needs to take the difference between one spectrum and two others which leads to a compounding of errors. Also an error in the alignment of the spectra of the order of 1 cm^{-1}, because the positions of the spectra obtained have an accuracy of approximately 1 cm^{-1}, will result in increased error especially in the region nearest the laser line. For these reasons the values obtained from the CH_4-CH_4 spectra will be more accurate than those obtained from the CH_4-Ar or CH_4-Xe spectra.

3.5 Normalization and Normalized Experimental Results

To make a comparison between the spectra it is necessary to normalize the data. There are several ways to do this. One way would be to normalize the spectra with respect to the number of collisions taking place per second so that the resulting spectra are indicative of

the scattering per collision.

Consider the pure methane spectrum first. The number of collisions per second that take place in a volume V_s (the volume of the cell that is seen by the spectrometer) is given by

$$(\rho_{CH_4} V_s) \quad \frac{1}{\tau} \tag{36}$$

where ρ_{CH_4} is the number density of the methane molecules and τ is the collision time. The collision frequency is given by the expression[38]

$$\frac{1}{\tau} = 4\sqrt{\frac{2}{\pi}}\,\sigma_{tot}\,\bar{v}\,\rho_{CH_4} \tag{37}$$

where σ_{tot} is the cross section of the collisions and $\bar{v}$ is the average velocity of the colliding molecules. Substituting (37) into (36) and dividing by a factor of two since each collision is counted twice, once for molecule 1 and once for molecule 2, one has the final result for pure CH_4,

$$\#\text{of collisions in } V_s \text{ in 1 second} = 4\sqrt{\frac{2}{\pi}}\,\sigma_{tot}\sqrt{\frac{kT}{\mu}}\,V_s\,\rho_{CH_4}^2/2. \tag{38}$$

The expressions for the CH_4-Ar and CH_4-Xe mixtures are similar except that each collision is counted only once so the factor 2 disappears.

$$\#\text{ of collisions between } CH_4 \text{ and Ar molecules in } V_s \text{ in 1 sec.} = 4\sqrt{\frac{2}{\pi}}\,\sigma_{tot}\sqrt{\frac{kT}{\mu}}\,V_s\,\rho_{CH_4}\rho_{Ar} \tag{39}$$

$$\#\text{ of collisions between } CH_4 \text{ and Xe molecules in } V_s \text{ in 1 sec.} = 4\sqrt{\frac{2}{\pi}}\,\sigma_{tot}\sqrt{\frac{kT}{\mu}}\,V_s\,\rho_{CH_4}\rho_{Xe} \tag{40}$$

Dividing the experimental results by these factors will give the scattering per collision.

Another way to normalize the data would be to normalize with respect to the number of molecular pairs. This is the way the theoretical results are presented and thus the way we normalized the

experimental spectra. The normalization factors are as follows,

CH_4-CH_4 mixture # of pairs $= \rho_{CH_4}^2/2$ (41)

CH_4-Ar mixture # of pairs $= \rho_{CH_4}\rho_{Ar}$ (42)

CH_4-Xe mixture # of pairs $= \rho_{CH_4}\rho_{Xe}$ (43)

By dividing the experimental data by these factors results are obtained which are directly proportional to the scattering per molecular pair. Results are shown on figures 3-6 to 3-8.

3.6 Final Experimental Results

With the normalized results given on figures 3-6 to 3-8 we can make comparisons between the different mixtures. However if we want to make direct comparisons with the theoretical results and want to obtain some numbers we need to do more work.

The theoretical results are given in terms of the cross section per unit bandwidth multiplied by the cell volume[21]. To put our experimental results into this form would require detailed knowledge of the geometry of the collection of the scattered light.* Fortunately the spectra of pure monoatomic gases have been fairly well studied and experimental results for Ar in units of cm^6 are fairly abundant. The results that we used were those of Barocchi et al[39]. So to obtain results in units of cm^6 we compared our Ar results with those of Barocchi et al. From this we obtained a scaling factor of $(6.25 \pm 5\%) \times 10^{-3}$ cm^6/(our units). Thus our experimental spectra, figures 3-6 to 3-8, were

* Appendix 3-B gives the relationship between the units used on figures 3-6 to 3-8, which for simplicity we will call our units, and the units of cross section per unit bandwidth multiplied by the cell volume (cm^6).

multiplied by this scaling factor.

To obtain single spectra for the various mixtures,the multiple runs for a given mixture were averaged. The final results in units of cm^6 are shown on figures 3-9 to 3-11. The error bars shown on these figures are the resultant of both the error due to the spread of the runs, which includes the statistical $\sqrt{N}$ error,and the errors involved in the normalization and scaling.

As the experimental spectra are now in the same units as the theoretical spectra we are in a position to begin analysis.

FIGURE 3-2

An example of the raw data obtained for pure CH_4. As is seen every second channel contains background. The resulting data points are obtained by subtracting the background count from the corresponding total counts at a given wave number. The total time spent in each channel, for this example, was 640 seconds.

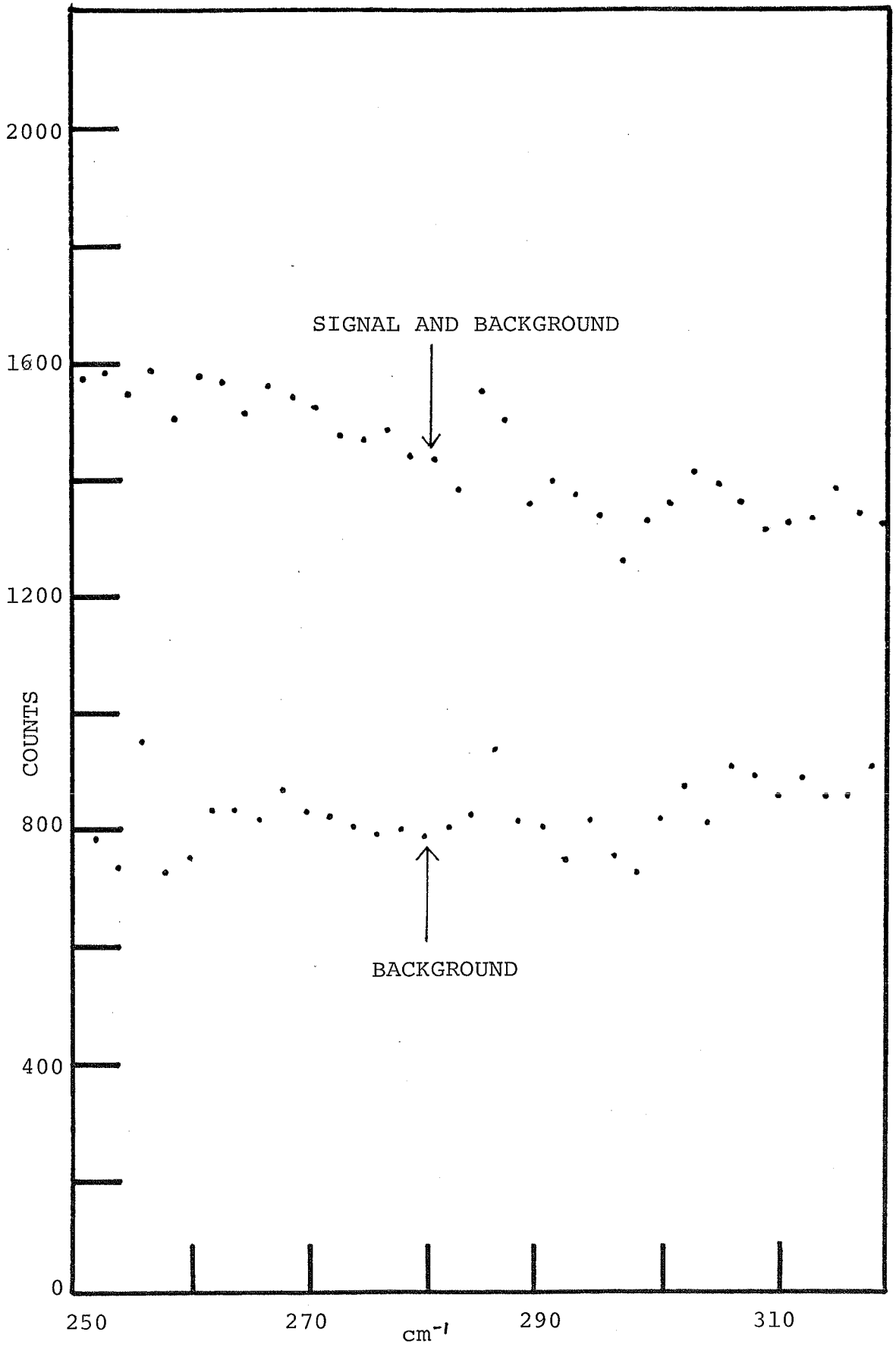
2000
1600
1200
800
400
0
COUNTS
SIGNAL AND BACKGROUND
BACKGROUND
250
270
290
310
cm-1

FIGURE 3-3

An example of how the separate runs were combined to give a total spectrum. The rule of thumb used was that if the overlapping portion of 2 runs gave different counts/sec. the one that gave the lower counts was scaled up to correspond to the one which gave the higher counts. In the majority of cases the runs agreed with each other and no scaling up was necessary.

The intensity scale is given in units of counts/(second . watt of laser power).

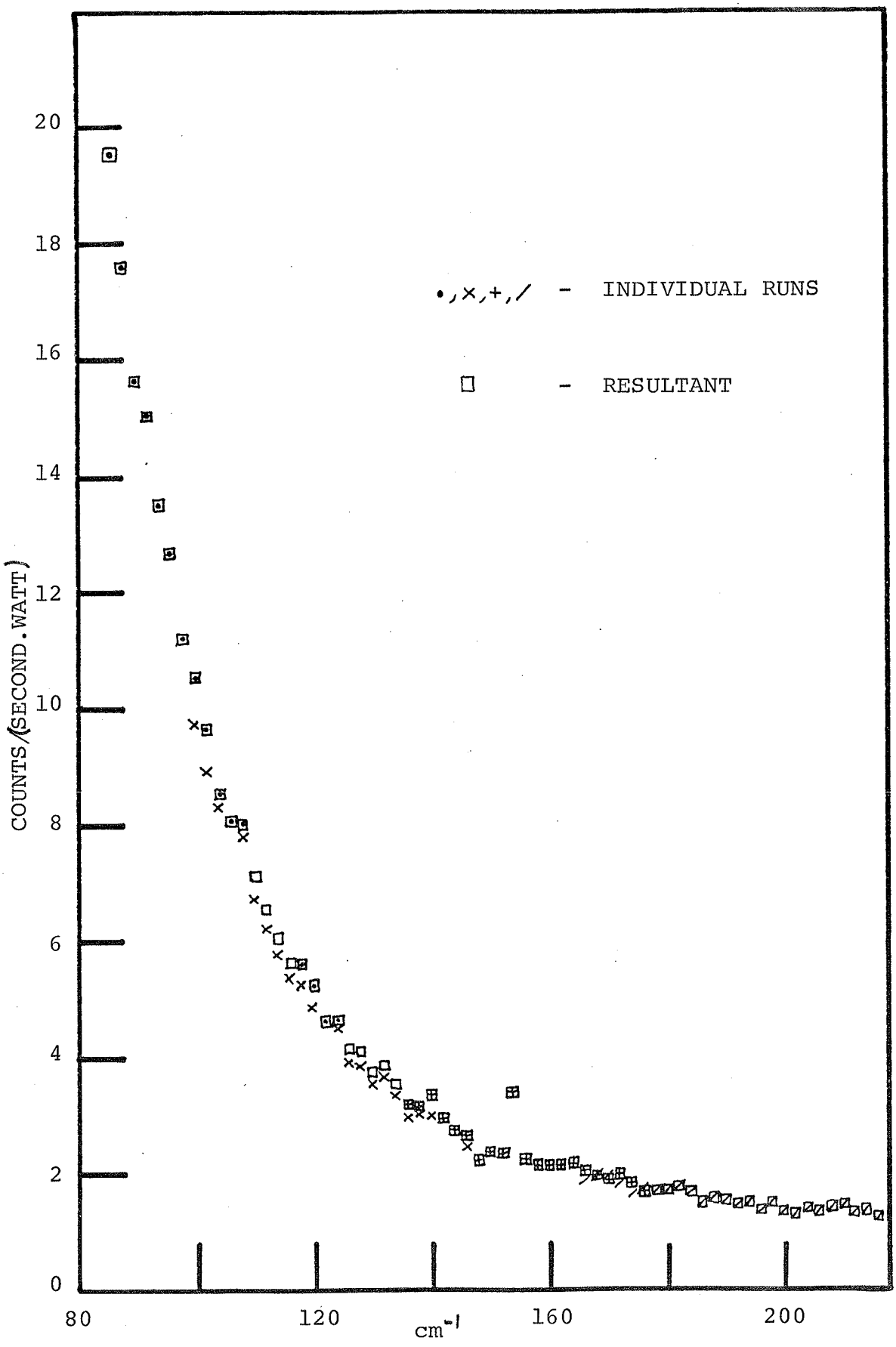
20
18
16
14
12
10
8
6
4
2
0
COUNTS/(SECOND·WATT)
•,×,+,/ - INDIVIDUAL RUNS
□ - RESULTANT
80
120
160
200
cm⁻¹

FIGURE 3-4

The experimental results for one of the CH_4-Ar runs (and one of the CH_4-CH_4 runs). Argon was added to CH_4, which was in the cell at a pressure of 16.7 atmospheres to give a total pressure of 157.6 atmospheres. The CH_4 spectrum and an Ar spectrum, with argon at a pressure of 140.9 atmospheres, were then subtracted resulting in the CH_4-Ar spectrum.

The intensity scale is given in counts/(second. watt of laser power).

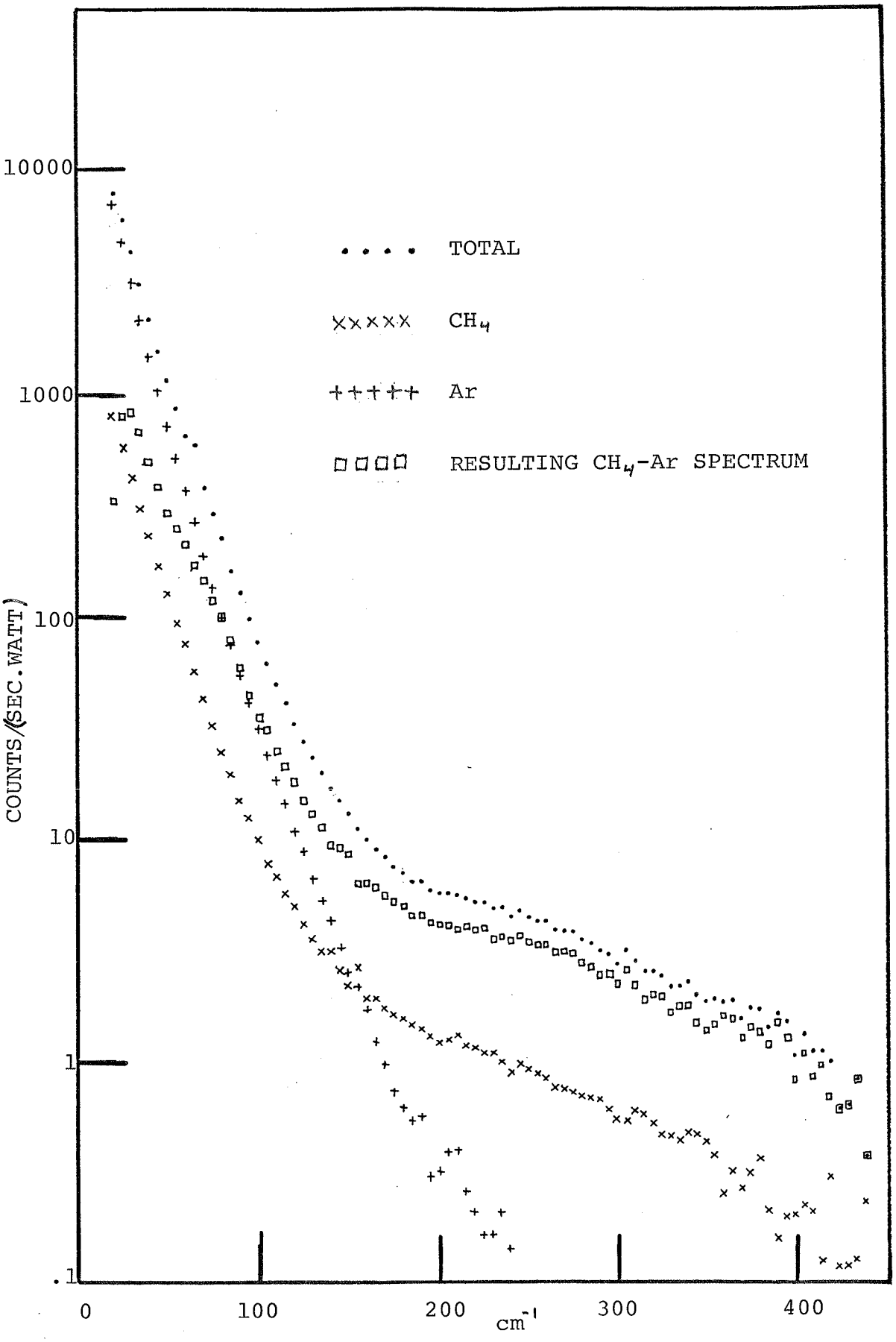
10000
1000
100
10
1
.1
COUNTS/(SEC.WATT)
0
100
200
300
400
cm⁻¹
TOTAL
CH4
Ar
RESULTING CH4-Ar SPECTRUM

FIGURE 3-5

The experimental results for one of the CH_4-Xe runs. Xenon was added to CH_4, which was in the cell at a pressure of 9.17 atmospheres, to give a Xe number density of .64 moles/l which corresponds to a pressure of 13.5 atmospheres.

Due to a poor pure Xe run (air got into the cell) only the first few data points could be used. To complete the Xe-Xe spectrum out to a 100 cm^{-1} the results of Zoppi et al[37] were used (these results were normalized so as to agree with our first few experimental points).

The intensity scale is given in counts/(second. watt of laser power).

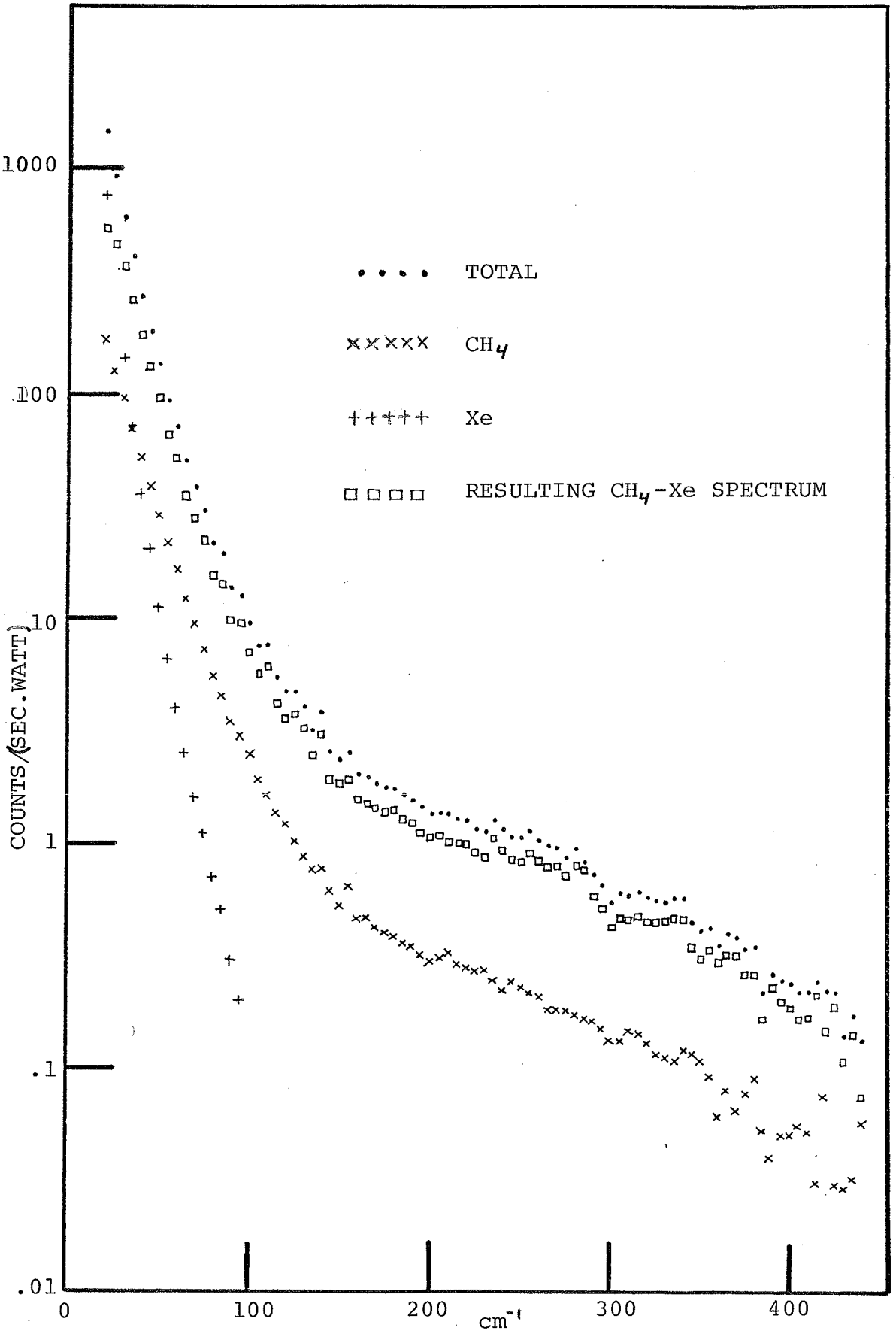
1000
100
10
1
.1
.01
COUNTS/(SEC.WATT)
0
100
200
300
400
cm⁻¹
TOTAL
CH4
Xe
RESULTING CH4-Xe SPECTRUM

FIGURE 3-6

The experimental results for CH_4-CH_4 after being normalized with respect to the number of molecular pairs.

$$C = \frac{\rho_{CH_4}^2}{2}$$

RUN	ρ_{CH_4} ($^{moles}/_{l}$)
•	.69
X	1.11
O	1.44

The intensity scale is in units of counts/(second.watt.C^2).

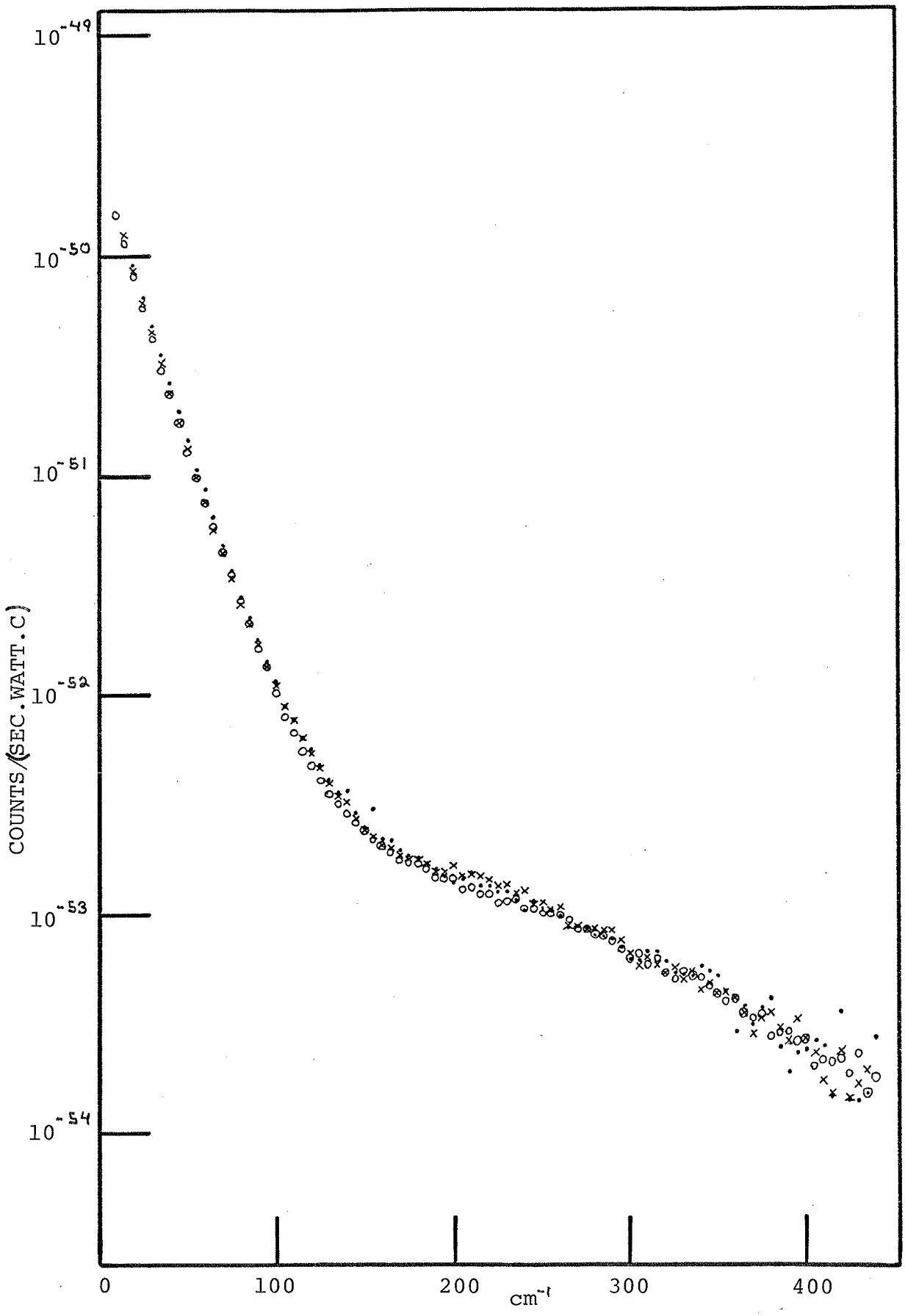
10^-49
10^-50
10^-51
10^-52
10^-53
10^-54
COUNTS/(SEC.WATT.C)
0
100
200
300
400
cm^-1

FIGURE 3-7

The experimental results for CH_4-Ar after being normalized with respect to the number of molecular pairs.

$$C = \rho_{CH_4} \rho_{Ar}$$

RUN	ρ_{CH_4} ($^{moles}/_{l}$)	ρ_{Ar} ($^{moles}/_{l}$)
X	.69	5.90
.	1.11	2.69
O	1.44	2.36

The intensity scale is in units of counts/(second.watt.C) .

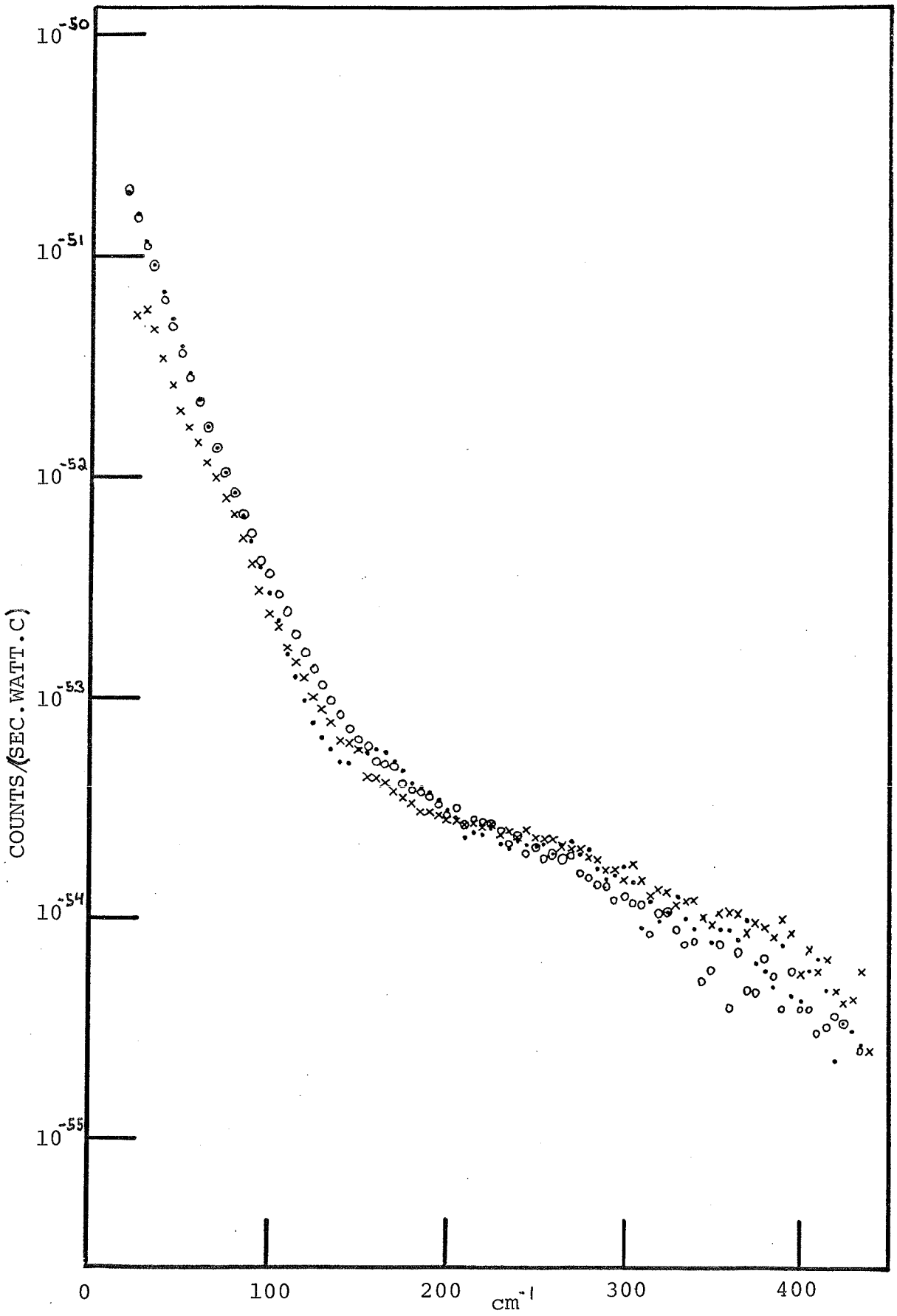
10^-50
10^-51
10^-52
10^-53
10^-54
10^-55
COUNTS/(SEC.WATT.C)
0
100
200
300
400
cm^-1

FIGURE 3-8

The experimental results for CH_4-Xe after being normalized with respect to the number of molecular pairs.

$$C = \rho_{CH_4} \rho_{Xe}$$

RUN	ρ_{CH_4} (moles 1)	ρ_{Xe} (moles/1)
X	.69	.24
O	.38	.64
.	.38	1.25
+	.38	1.67

The intensity scale is in units of counts/(second.watt.C) .

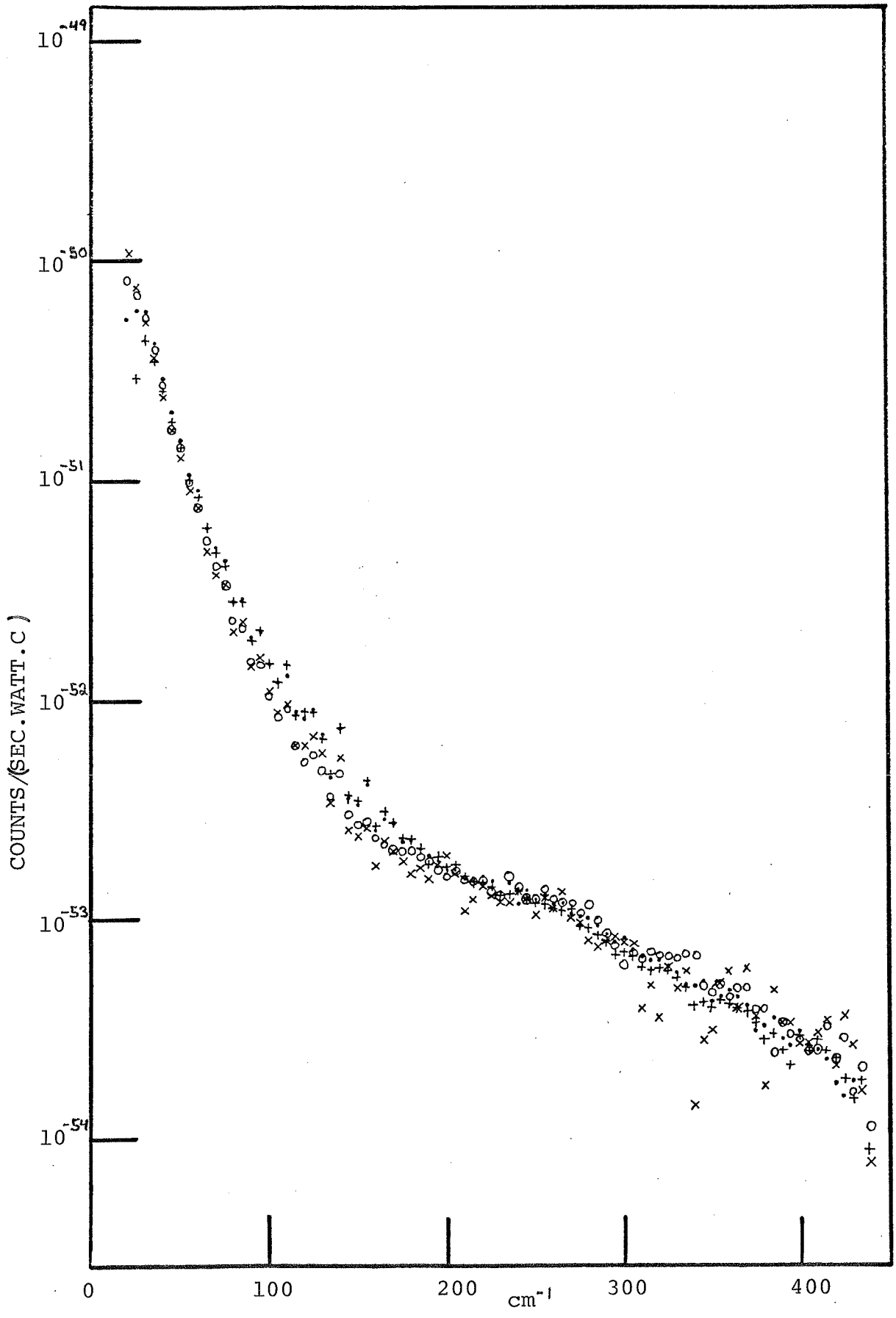
10^-49
10^-50
10^-51
10^-52
10^-53
10^-54
COUNTS/(SEC.WATT.C)
0
100
200
300
400
cm^-1

FIGURES 3-9 to 3-11

The final experimental spectra for CH_4-CH_4, CH_4-Ar, and CH_4-Xe. These spectra are the averages of the runs shown on figures 3-6 to 3-8 after they have been multiplied by 6.25×10^{-3} so as to express results in units of cm^6. The error bars associated with the CH_4-CH_4 spectrum are much smaller than those associated with either the CH_4-Ar spectrum or CH_4-Xe spectrum.

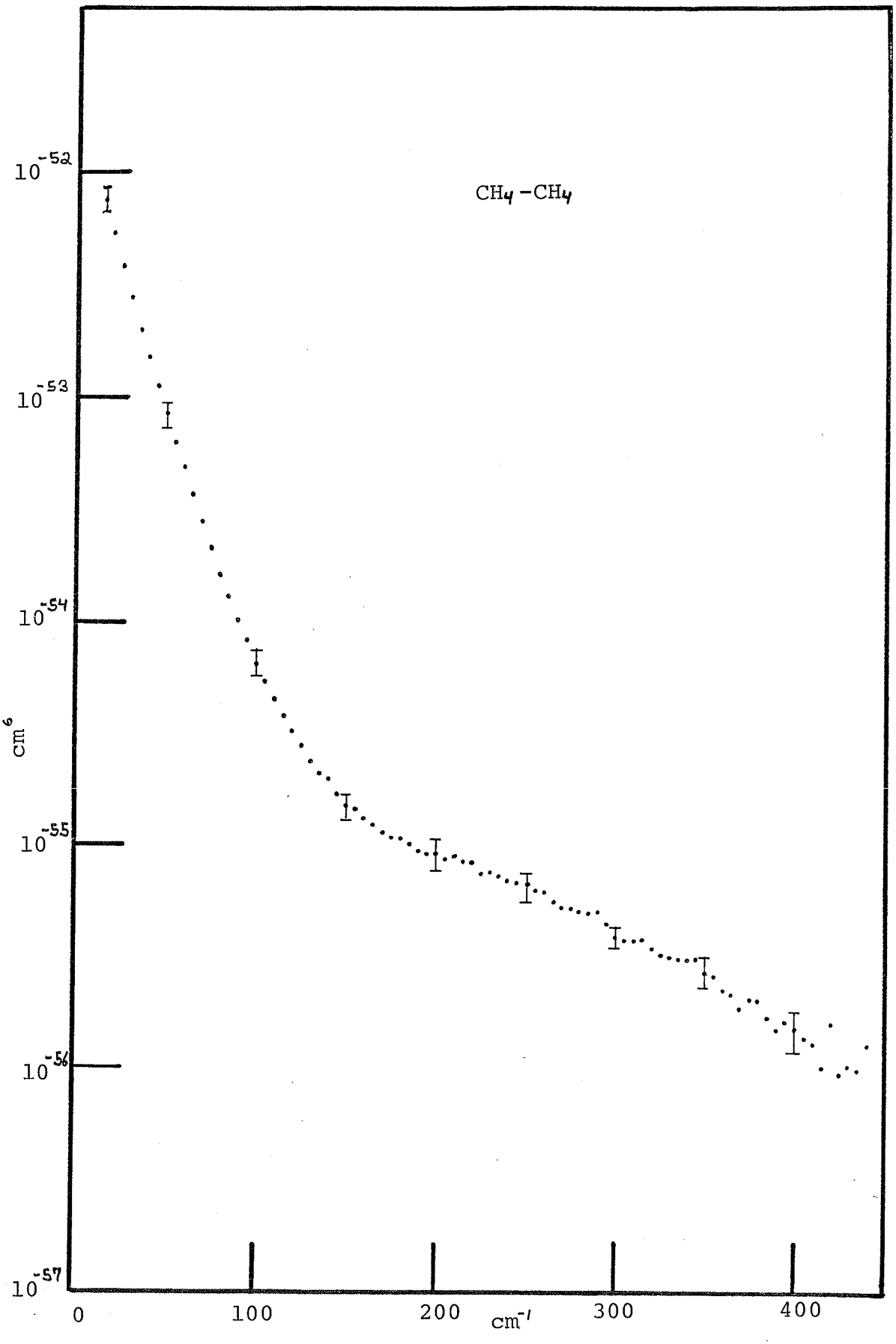
$CH_4 - CH_4$
10^{-52}
10^{-53}
10^{-54}
10^{-55}
10^{-56}
10^{-57}
cm^6
0
100
200
300
400
cm^{-1}

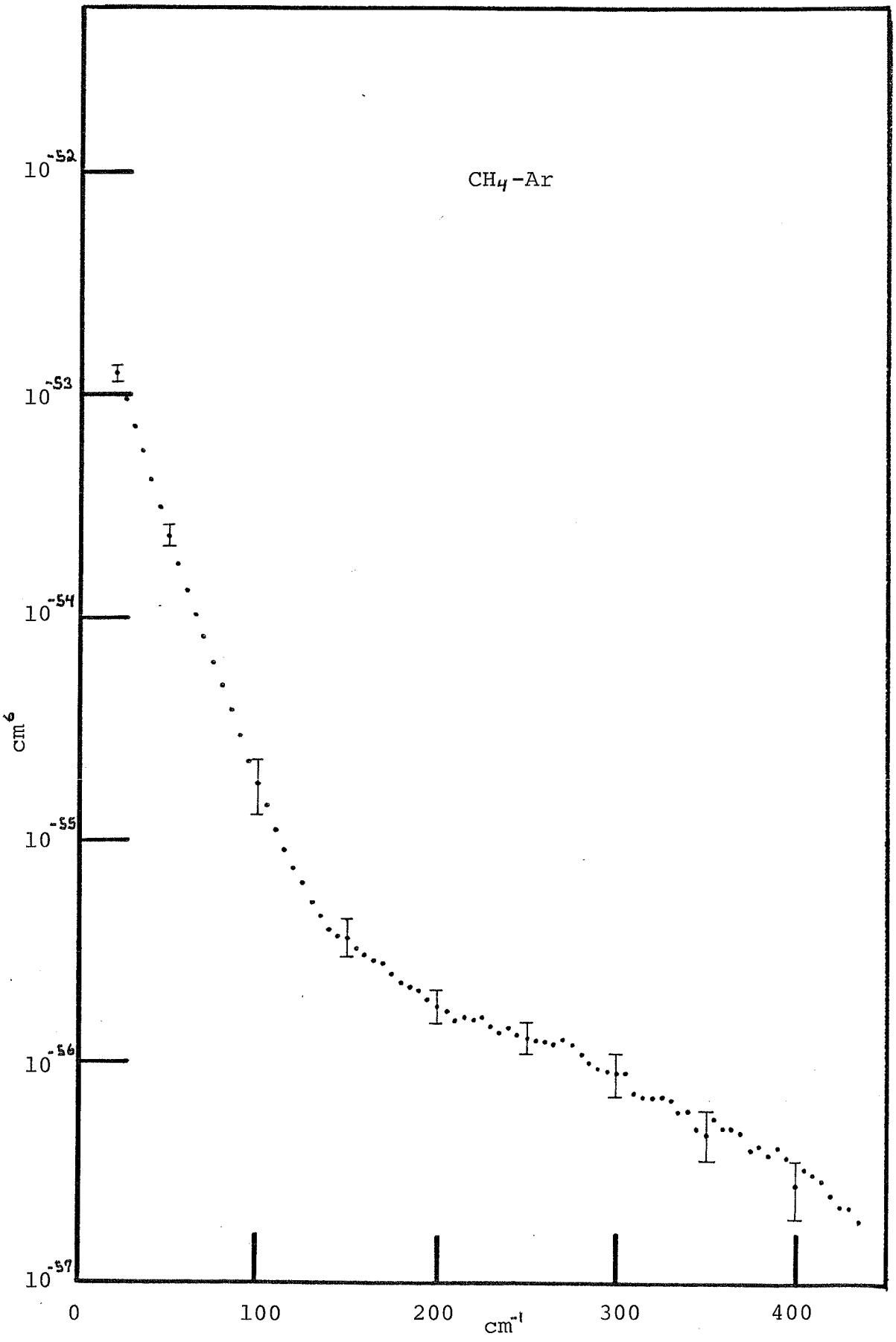
CH4-Ar
10^-52
10^-53
10^-54
10^-55
10^-56
10^-57
cm^6
0
100
200
300
400
cm^-1

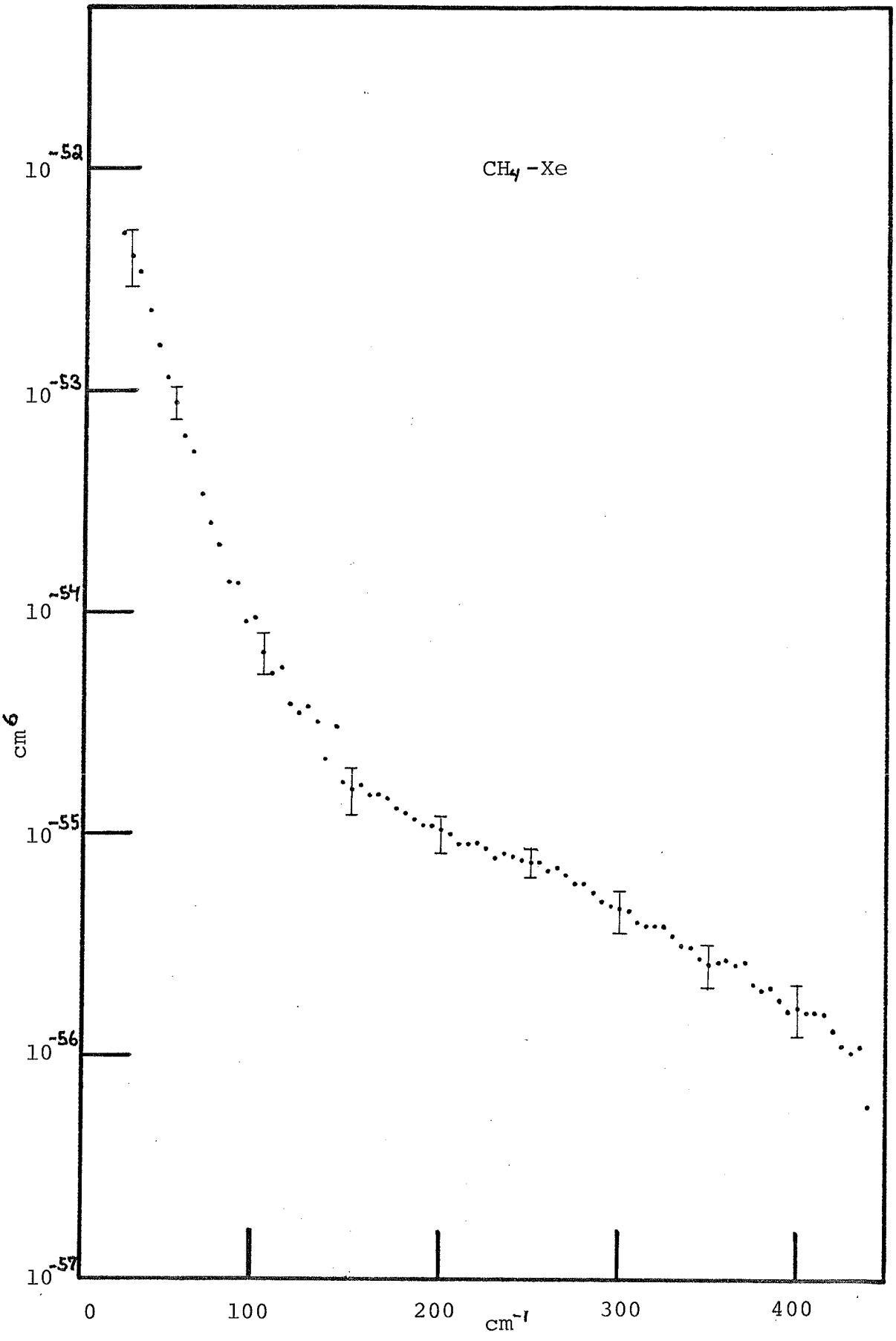
CH_4 -Xe
10^{-52}
10^{-53}
10^{-54}
10^{-55}
10^{-56}
10^{-57}
cm^6
0
100
200
300
400
cm^{-1}

APPENDIX 3-A

Number Density Determination for Xenon

The experimentally determined pressure-density characteristics of Xe gas at 25^{O} C is shown on figure 3-12.

The method used to determine the number density of the Xe gas in the CH_4-Xe mixture was dependent on the cell filling apparatus. A rough schematic of the apparatus is shown below.

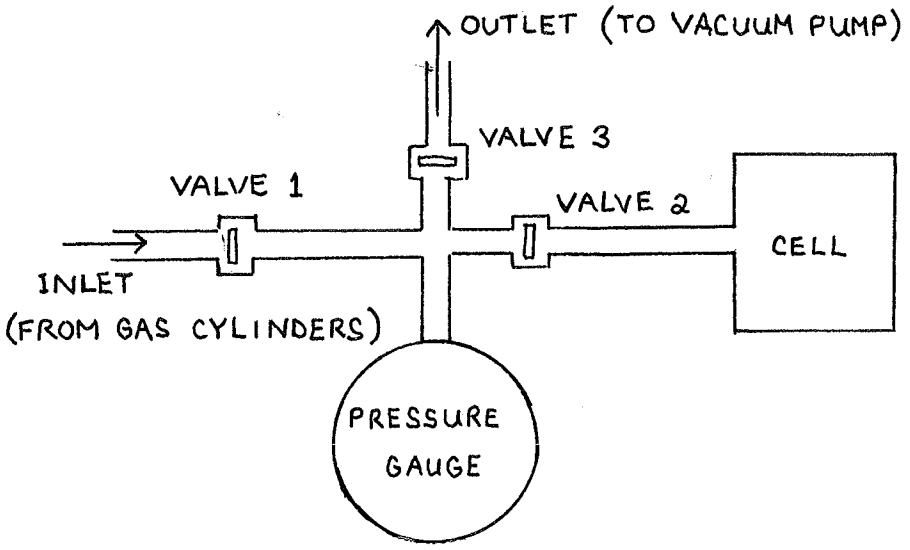

At the start CH_4, at a pressure of X atmospheres, is in the cell. Valve 2 is closed and the region before valve 2 is then evacuated by opening up valve 3 to the vacuum pump. Valve 3 is then closed and Xe is allowed in through valve 1. The pressure of the Xe in the tubing before the cell is taken (P_{xe1}). Valve 2 is then opened and closed quickly allowing some of the Xe gas to enter into the cell and mix with the CH_4. The pressure of the Xe gas in the region between valves 1 and 2 is thus reduced (P_{xe2}). With the above data, P_{xe1} and P_{xe2}, the

FIGURE 3-12

The pressure-density characteristics of Xe gas at $25^{o}C$ [36] along with the straight line characteristic of an ideal gas.

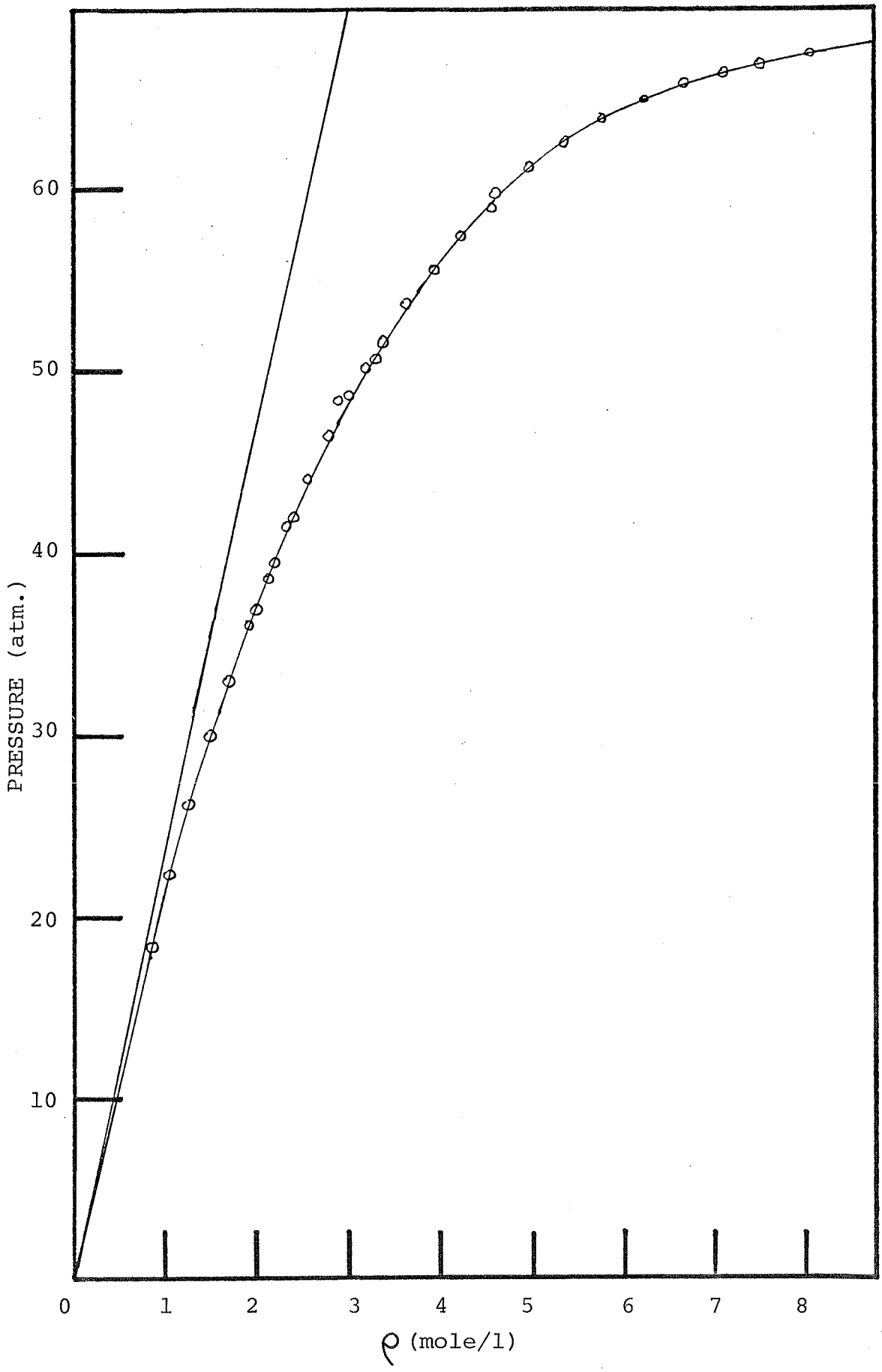
PRESSURE (atm.)
60
50
40
30
20
10
0
1
2
3
4
5
6
7
8
ρ (mole/l)

APPENDIX 3-B

Comparison of Units

This discussion derives the relationship between the units used on figures 3-6 to 3-8 and the standard units of cross section multiplied by the volume of the cell.

The scattering cross section is defined by the following equation

$$\frac{d^2\sigma}{d\Omega d\lambda^{-1}} = \frac{1}{I}\frac{d^2N}{d\Omega d\lambda^{-1}}$$

where I is the incident intensity (photons/second.cm^2) and $d^2N/d\Omega\, d\lambda^{-1}$ is equal to the scattered photons per second per unit bandwidth which pass through a unit solid angle of the detector. The number of molecular pairs observed by the detector, in the case of a pure gas, is given by

$$\#\text{ of pairs observed} = \frac{1}{2}(nV)^2\frac{Vs}{V}$$

where n is the number density of the gas, V is the volume of the cell, and Vs is the volume of the cell which is focused into the detector. From these two equations one finds that

$$\frac{\text{photons}}{\text{sec.cm}^{-1}}\ \text{at detector} = \left[I\int \frac{d^2\sigma}{d\Omega d\lambda^{-1}} d\Omega \right]\left[\frac{1}{2}(nV)^2\frac{Vs}{V} \right]$$

$$\cong \frac{1}{2}n^2\left[I\, V_s\Omega \right]\left(\frac{d^2\sigma}{d\Omega d\lambda^{-1}}\cdot V\right)$$

$$= \frac{1}{2}n^2 P\left[\frac{V_s\Omega}{h\nu_L A}\right]\left(\frac{d^2\sigma}{d\Omega d\lambda^{-1}}\cdot V\right)$$

where P is the laser power, ν_L is the frequency of the laser light, A is the cross sectional area of the laser beam, and Ω is the solid angle the detector subtends with respect to the scattering volume. This can be rewritten so as to give the relationship between the units used on

figures 3-6 to 3-8 and the standard units. This is done below

$$\left(\frac{d^2\sigma}{d\Omega d\lambda^{-1}} V \right) = \left(\frac{h\nu_L A\gamma}{Vs\Omega} \right) \quad \left(\frac{\text{counts}}{\text{sec.cm}^{-1}\text{.watt.C}} \right)$$

where γ is the ratio of the photons incident upon the detector to the counts collected and C is as previously defined equal to $\frac{1}{2} n^2$ for a pure gas and equal to $n_1 n_2$ for a mixture. Thus a factor $\left(\frac{h\nu_L A\gamma}{V_s \Omega}\right)$ represents the difference between our units and the standard units. As stated in section 3-6 we compared Barocchi et al Ar results with our own to find this factor.

CHAPTER 4

FINAL RESULTS AND CONCLUSIONS

4.1 Calculation of |A| for the Spectra

Looking back on the derivation of the theoretical spectra in Chapter 2 one sees that in the region $>150\ cm^{-1}$ the αA term dominates (at least for values of |A| of the order 1 $Å^4$) while the terms involving E are nearly negligible. Thus in calculating the A value which will give the best fit for the various spectra the value of E was kept constant at 1 $Å^5$.

The determination of |A| from the spectra proceeded as follows. For the data points corresponding to 200 cm^{-1}, 250 cm^{-1}, 300 cm^{-1}, 350 cm^{-1}, and 400 cm^{-1} the |A| value which corresponds to the maximum of the error bar and the minimum of the error bar was calculated. This was done with the use of figure 2-8 for CH_4-CH_4, and similar spectra for CH_4-Ar, and CH_4-Xe. As the αA terms dominates in the region one just needs to take the square root of the ratio of the theoretical figures at the above points to the experimental maximum and minimum points to find the corresponding A value (i.e. the intensity of the spectrum in this region is proportional to $(\alpha A)^2$ (see equation (11) and figure 2-6)). These maximum and minimum values were then averaged to give the maximum and minimum of the average |A| for the spectrum. The average of these two values were then taken to fix |A| while the average deviation from the minimum and maximum value is taken as the associated error. The values of |A| that were so calculated are given in the table below. The experimental results along with the various theoretical spectra for these values of |A| are presented on figures 4-1 to 4-3. Before we compare the

features of the experimental and theoretical spectra we will study the value of |A| more closely.

TABLE 4-1

Mixture	$\|A\|$ Å^4
CH_4-CH_4	.89 ± .07
CH_4-Ar	.90 ± .10
CH_4-Xe	1.02 ± .10

4.2 Final A

Using the values of |A| in the table one can calculate a best value. Assuming the errors in the three values are independent (in fact ~25% of the given errors are due to the scaling factor and thus are dependent) one may use the following formula[40]

$$|A| = \sum_{i=1}^{3}(1/\Delta Ai)^2 \; |Ai| \Big/ \sum_{i=1}^{3}(1/\Delta Ai)^2 \pm \left[\sum_{i=1}^{3}(1/\Delta Ai)^2\right]^{-\frac{1}{2}} \qquad (41)$$

to find

$$|A| = (.93 \pm .06) \text{ Å}^4 \qquad (42)$$

It is this value that we will now compare with theoretical and other experimental results.

Let us first consider the various theoretical calculations for A . Before these results are presented several important points need to be considered. First these ab initio results are calculated for a fixed internuclear distance, usually the equilibrium geometry, while our results, as with most experimental results, are for the ground vibrational state. Only Amos[44] has given values which have been corrected for this. Second most calculations are done using a R_{CH} distance of 2.0665 a_o ,

while some recent theoretical and experimental studies[41] have shown that this distance is slightly shorter with a value of $R_{CH} = 2.052\, a_o$. Third these calculations were done for zero frequency, i.e. they are static values, while the experimental results are for the frequency of the laser line. In the case of α the static value is 2.57 $Å^3$ while the value at optical frequencies is 2.64 $Å^3$. This same order of increase is expected for the value of $|A|$. The table below presents the various theoretical results (in units of $Å^4$).

TABLE 4-2

GROUP	METHOD	$R_{CH}=2.0665\, a_o$	$R_{CH}=2.052\, a_o$	Vibrational Corr.
Buckingham[27]	as per A.2-A	.98	.97	
Amos[44]	SCF[42]	.79	.77	.82
	CI[43]	.71	.74	.79
John et al[45]	SCF	.81*		
Rivail et al (46)	SCF	.79+		

* $R_{CH} = 2.061\, a_o$

\+ R_{CH} used was not quoted

To estimate the error associated with these numbers consider the accuracy of the value of α that Amos has calculated at zero frequency, 2.46 $Å^3$, with the known value of α at optical frequencies, 2.64 $Å^3$, giving a discrepancy of approximately 7%. The values of $|A|$ given should be of the same order of accuracy. Considering the errors associated with these theoretical values our experimental value is in good agreement.

Let us now consider other experimental results. The values quoted

in the table below, except for the value of Shelton and Tabisz, have been derived from calculations which are based on the intermolecular potential between a methane molecule and an inert gas atom or more specifically based on the anisotropic interaction potential. It follows

TABLE 4-3

GROUP	METHOD	$\|A\|$ Å^4
Buck et al[20]	molecular beams scattering	2.67
Isnard et al[47]	second pressure virial coeff.	2.35
Rajan et al[48]	proton spin relaxation	2.71, .88, .89
Shelton and Tabisz[49]	collision induced scattering	1.00

that these values are only as accurate as the expression for the anisotropic interaction potential[50] which at the present is just a first order approximation. As is seen these values do not agree very well with the theoretical values (except for two of the values of Rajan et al).

In conclusion the value obtained by our set of experiments $(.93 \pm .06)$Å^4 is in excellent agreement with the theoretical values and is built on a stronger foundation than values which are dependent on the anisotropic potential.

4.3 Comparison of Theoretical and Experimental Spectra

To arrive at conclusions regarding the comparison of the experimental spectra and their associated theoretical spectra it is best to divide the spectra into three regions.

The first region is from 0 cm^{-1} to ~100 cm^{-1} and in this region the translational component dominates. Looking at figures 4-1 to 4-3 one finds good agreement for CH_4-CH_4 and CH_4-Ar and fair agreement for CH_4-Xe. Considering that the 3-body contribution is ignored one can certainly say that the experimental results give reasonable agreement with the theoretical model using equation (16) for $\beta(R)$. This is discussed in section 4-4.

The second region is from 100 cm^{-1} to ~250 cm^{-1}. It is in this region that the spectra make a transition from being translational to being rotational. The error associated with the theoretical spectra is greatest in this region for two basic reasons. First the translational spectrum at high frequencies is strongly dependent on the third term in the expression for $\beta(R)$ and this term is only a rough approximation based on experimental data for krypton. A small change in the value of the constant in the exponential will produce a large change in the translational spectrum in this region. The second reason is that in the calculation of the intensity of the rotational lines (equation (30)) we neglected the effect of nuclear spin[51]. Taking nuclear spin into account will effect the shape of the rotational envelopes with this change decreasing as the rotational state J increases. For this reason corrections resulting from factors which involve nuclear spin will have the greatest effect on the total spectrum in this second region. Considering these two effects the agreement we obtain in this region is very good.

The third region is from 250 cm^{-1} on. In this region the spectrum is almost completely due to rotational transitions. Comparing the theoretical spectra with the experimental spectra one finds excellent agreement with the slopes in this region. The obvious discrepancy

between theory and experiment in this region are the rotational line peaks.

Consider the CH_4-CH_4 spectrum first. Looking at figures 4-1 and 3-6 one could certainly say that rotational peaks are observed. The main discrepancy comes from the CH_4-Ar and CH_4-Xe spectra where no rotational peaks are observed though they should be stronger than those of the CH_4-CH_4 spectrum. It must be remembered though that these spectra are the result of taking the difference of one spectrum with two other spectra and the error associated with this process could neutralize or even override the small ripple in the spectrum. So though it is not possible to positively state that rotational lines were observed it must be realized that it is a relatively subtle feature and as such is extremely difficult to detect.

In addition to the agreement between each experimental and theoretical spectrum it is also of interest to compare the three experimental spectra in this region. On figure 4-4 the far tails of the three spectra have been plotted. They have been normalized to $\alpha^2\overline{R^{-8}}$ so as to give results which are only dependent on $|A|^2$. This is assuming that the translational spectrum in this region and the other rotational transition terms are negligible. These assumptions lead to errors of approximately ten to twenty per cent for each of the three spectra. However the consistency of the spectral shape for all three mixtures is the important feature on this plot. This is in excellent agreement with the theory where the spectral shape of the αA rotational transitions is identical for the three mixtures, that is its shape is determined principally by properties of the CH_4 molecule.

4.4 Pure Translational Spectra

To obtain the pure translational spectra for the three mixtures it is necessary to subtract the theoretical spectrum for the rotational transitions from the experimental results. This procedure is shown, for pure CH_4, on figure 4-5. The final translational spectra for CH_4-CH_4, CH_4-Ar, and CH_4-Xe are given on figures 4-6 to 4-8 along with the theoretical translational spectra that were used. As is seen reasonable agreement is given in all three cases.

4.5 Conclusions

Though the agreement between the theoretical spectra and the experimental spectra for the three gas mixtures gives general verification of the whole theoretical model there are three major points that should be mentioned.

1) The first is of course the value of A that we obtained. It is in excellent agreement with the ab initio calculations and in our opinion the best experimental value.
2) The translational spectra using equation (16) for $\beta(R)$ are in good agreement with the experimental spectra and it would be interesting to extend the use of equation (16) to other molecular pairs.
3) The terms in the pair polarizability expression, equation (6) appear to decrease rapidly to 0 (in terms of intensity contribution). If higher order terms,and additional contributions such as anisotropic overlap, did contribute a significant amount to the total intensity,differences would be

observed in the value of A obtained for CH_4-CH_4, where double transitions contribute, from the values obtained for CH_4-Ar and CH_4-Xe were only single transitions contribute.

Overall the theoretical model presented here has been handsomely verified by the experimental results.

FIGURES 4-1 TO 4-3

The following three figures are the best fitting theoretical spectra for the three experimental spectra. The values of |A| used for the theoretical spectra are .89 Å^4 for CH_4-CH_4, .90 Å^4 for CH_4-Ar, and 1.02 Å^4 for CH_4-Xe.

The intensity scale is given in units of cm^6.

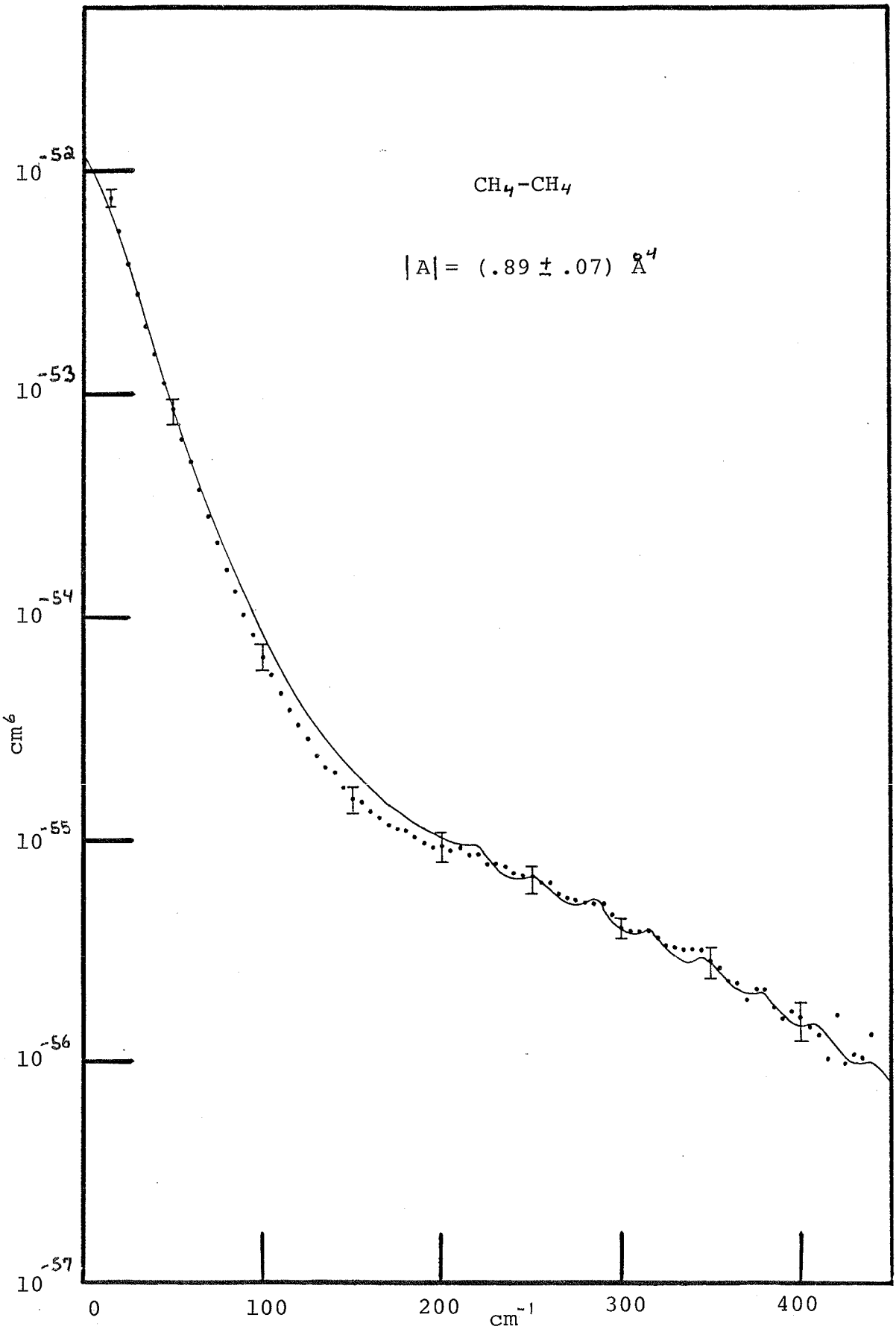
CH_4-CH_4
$|A| = (.89 \pm .07)$ Å^4
10^{-52}
10^{-53}
10^{-54}
10^{-55}
10^{-56}
10^{-57}
cm^6
0
100
200
300
400
cm^{-1}

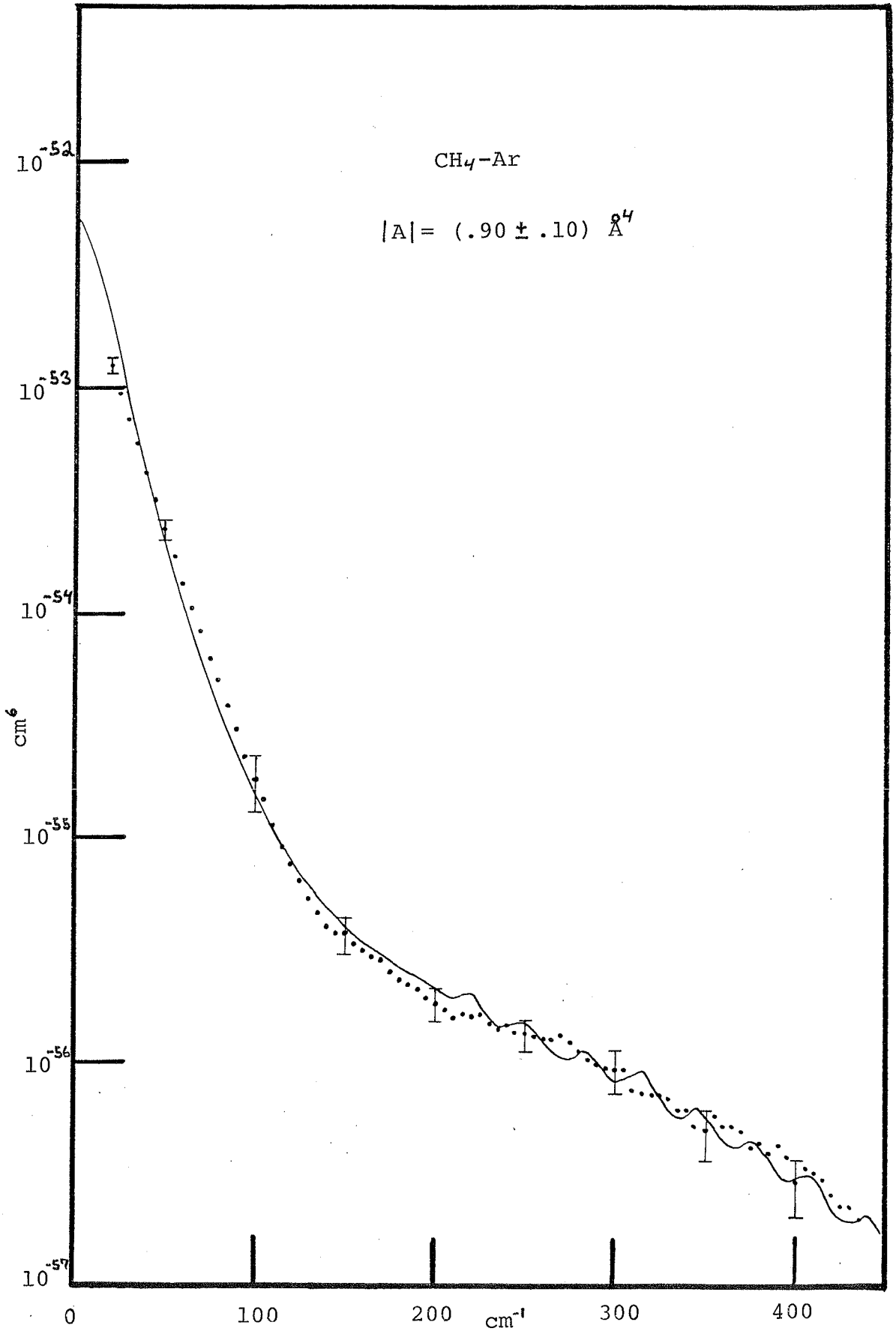
CH4-Ar
|A|= (.90 ± .10) Å4
10-52
10-53
10-54
10-55
10-56
10-57
cm6
0
100
200
300
400
cm-1

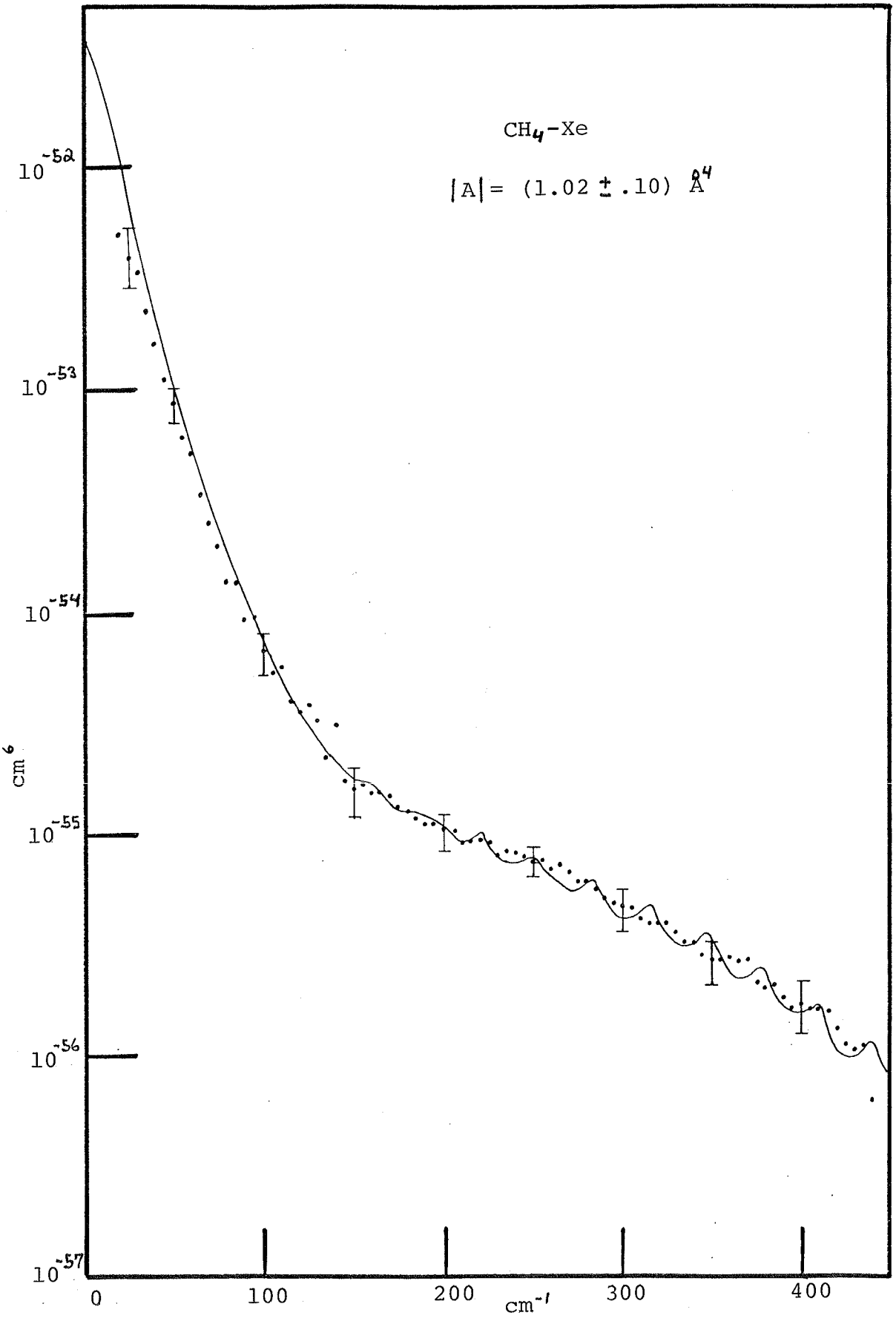
CH_4-Xe
$|A| = (1.02 \pm .10)$ Å^4
10^{-52}
10^{-53}
10^{-54}
10^{-55}
10^{-56}
10^{-57}
cm^6
0
100
200
300
400
cm^{-1}

FIGURE 4-4

The far tails of the experimental spectra, after being normalized with respect to $\alpha^2 \overline{R^{-8}}$. The spectral shape is the same for the three mixtures.

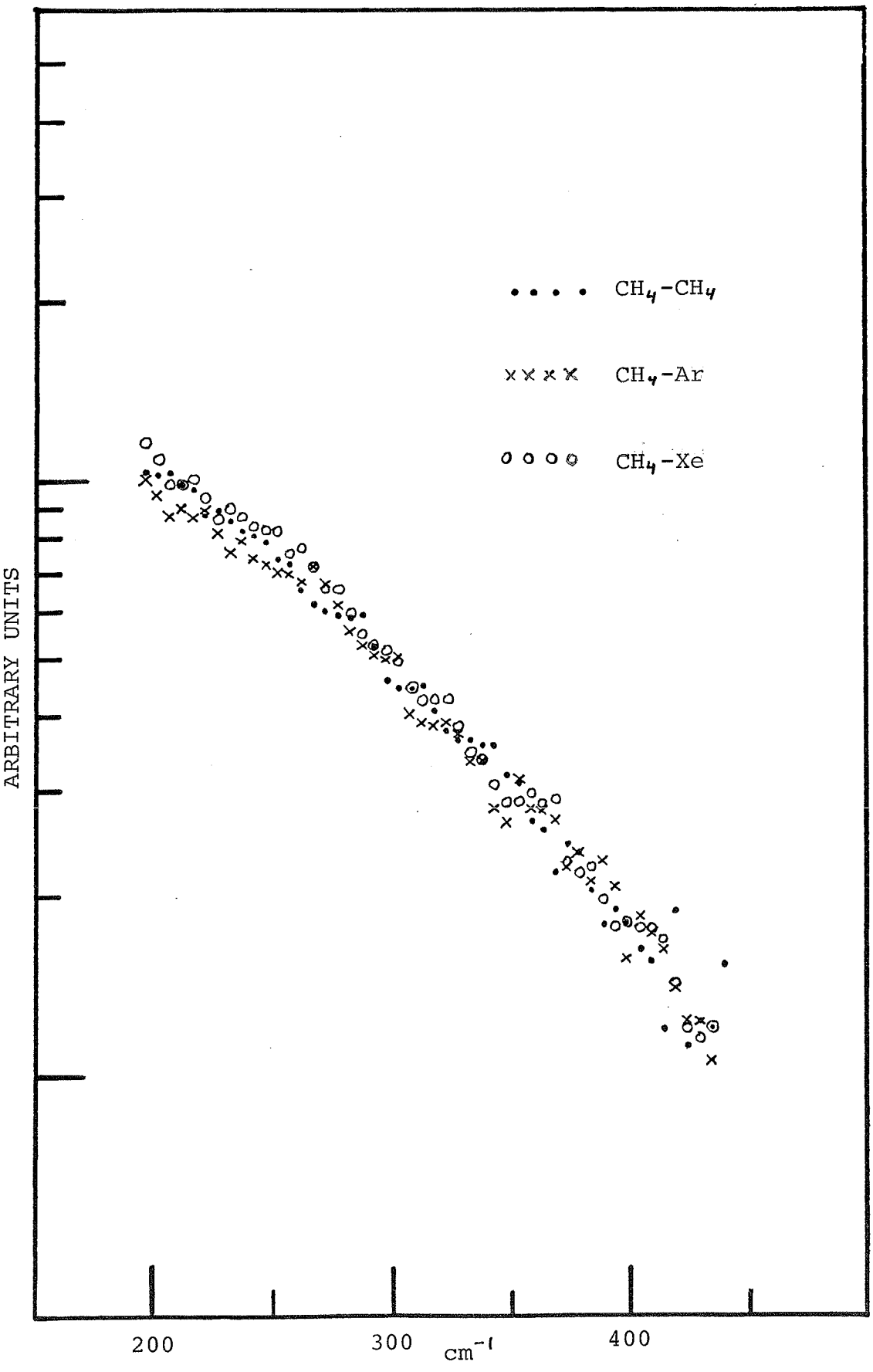
CH4-CH4
CH4-Ar
CH4-Xe
ARBITRARY UNITS
200
300
400
cm-1

FIGURE 4-5

The total experimental spectrum, the theoretical rotational component, and the difference, for the CH_4-CH_4 interaction.

The intensity scale is given in units of cm^6.

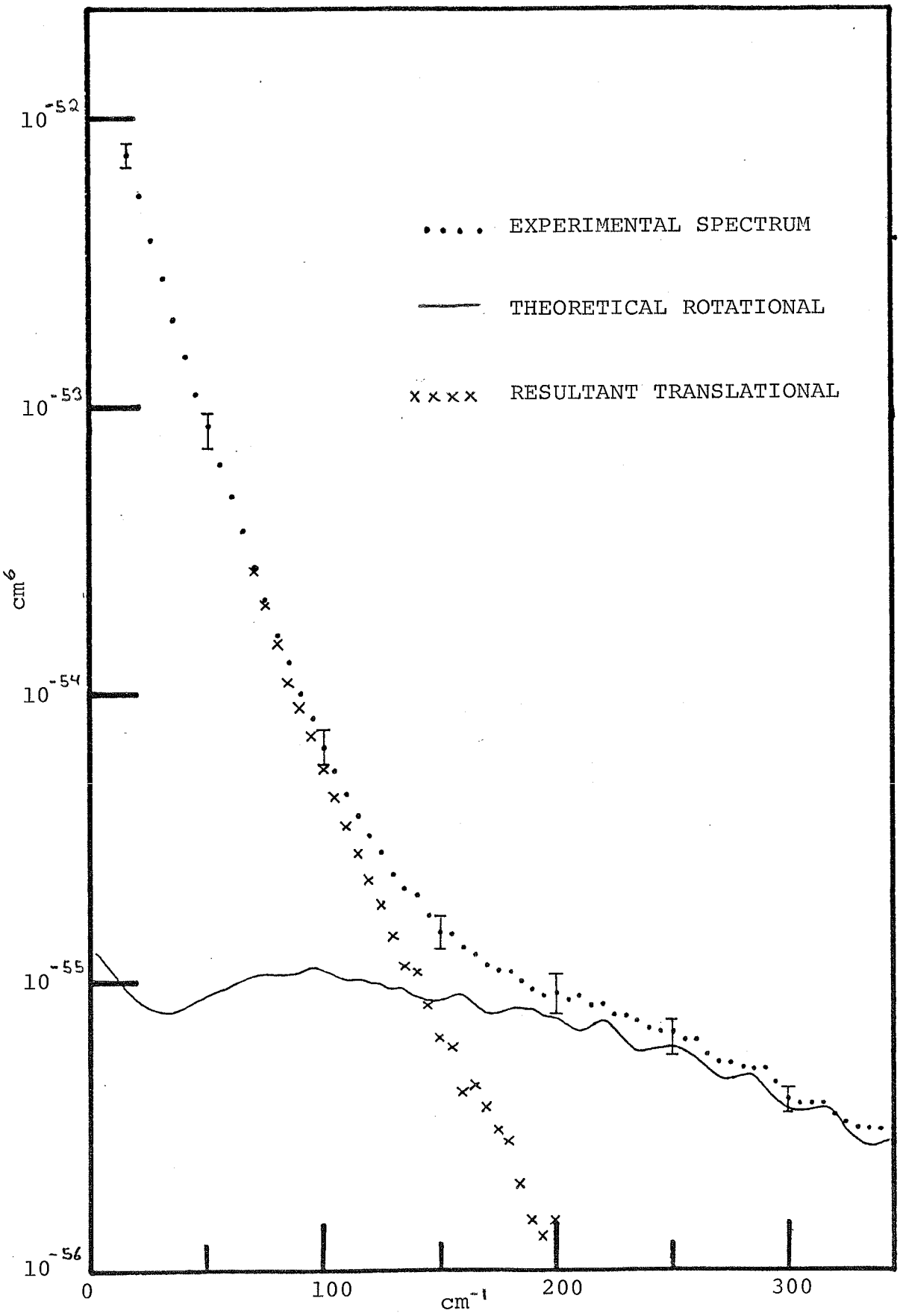
EXPERIMENTAL SPECTRUM
THEORETICAL ROTATIONAL
RESULTANT TRANSLATIONAL
10^{-52}
10^{-53}
10^{-54}
10^{-55}
10^{-56}
cm^6
0
100
200
300
cm^{-1}

FIGURES 4-6 TO 4-8

The final translational spectra for CH_4-CH_4, CH_4-Ar, and CH_4-Xe along with the theoretical translational spectra that were used.

The intensity scale is in units of cm^6.

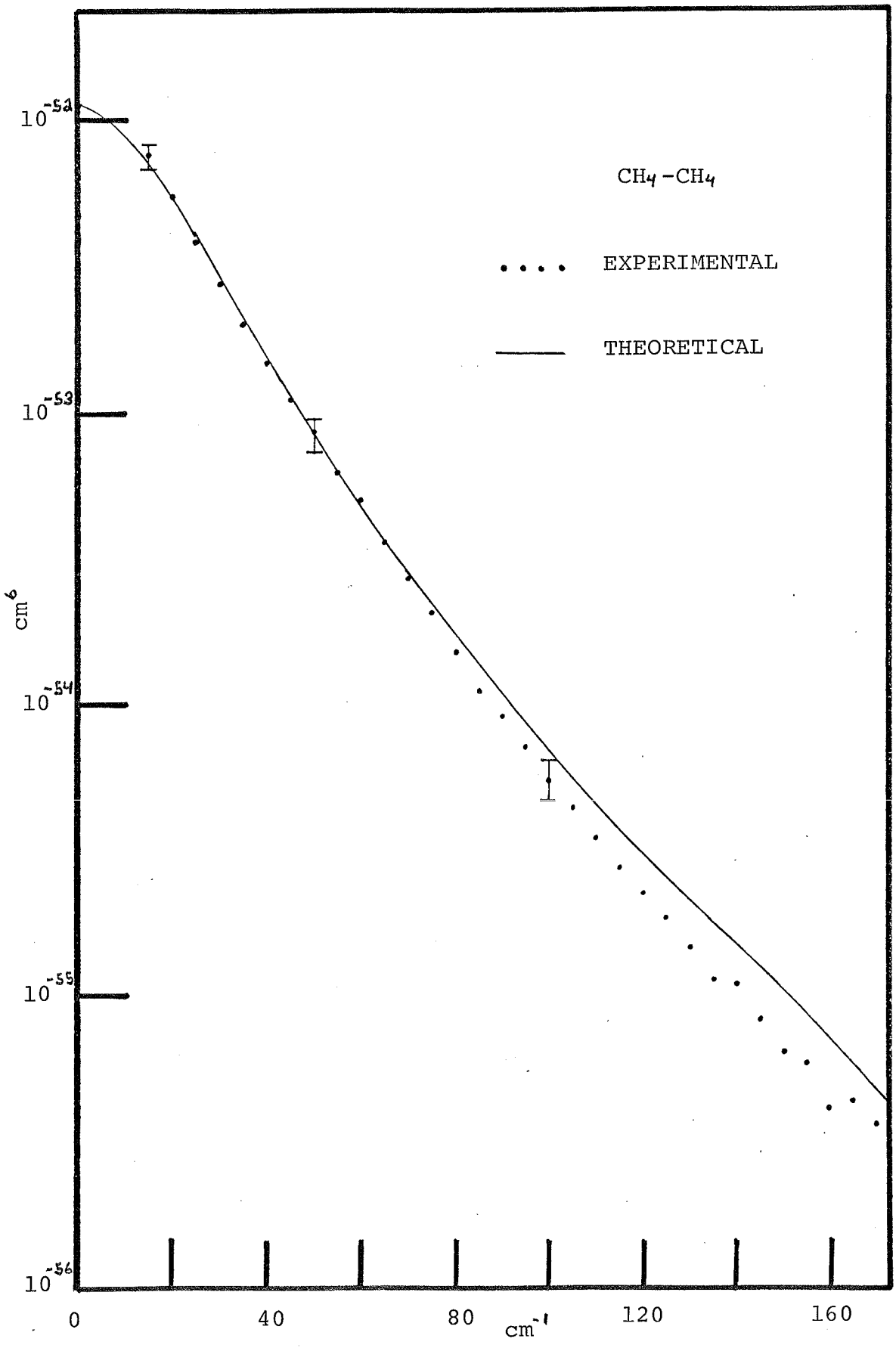
$CH_4 - CH_4$
EXPERIMENTAL
THEORETICAL
10^{-52}
10^{-53}
10^{-54}
10^{-55}
10^{-56}
cm^6
0
40
80
120
160
cm^{-1}

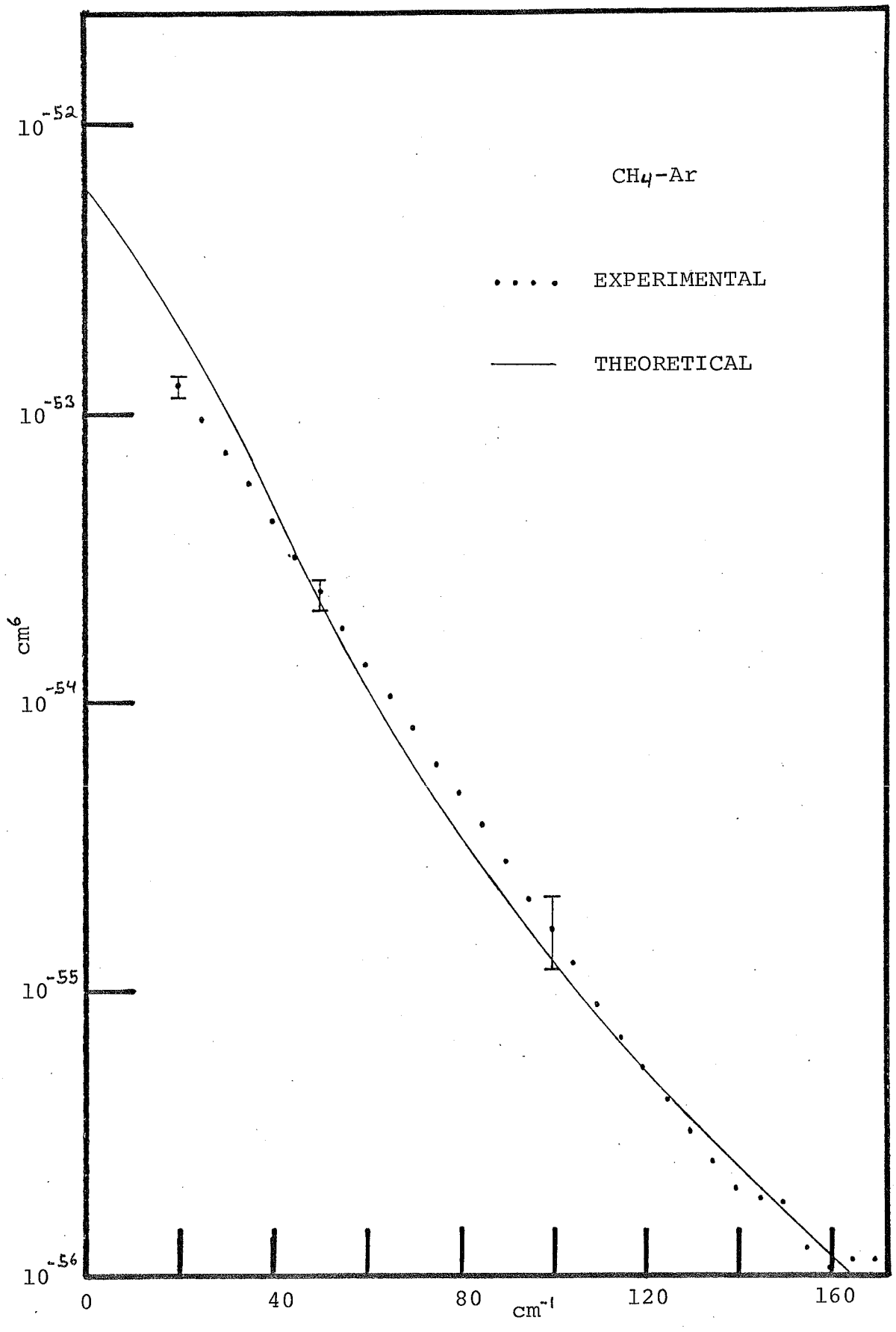
CH_4-Ar
EXPERIMENTAL
THEORETICAL
10^{-52}
10^{-53}
10^{-54}
10^{-55}
10^{-56}
cm^6
0
40
80
120
160
cm^{-1}

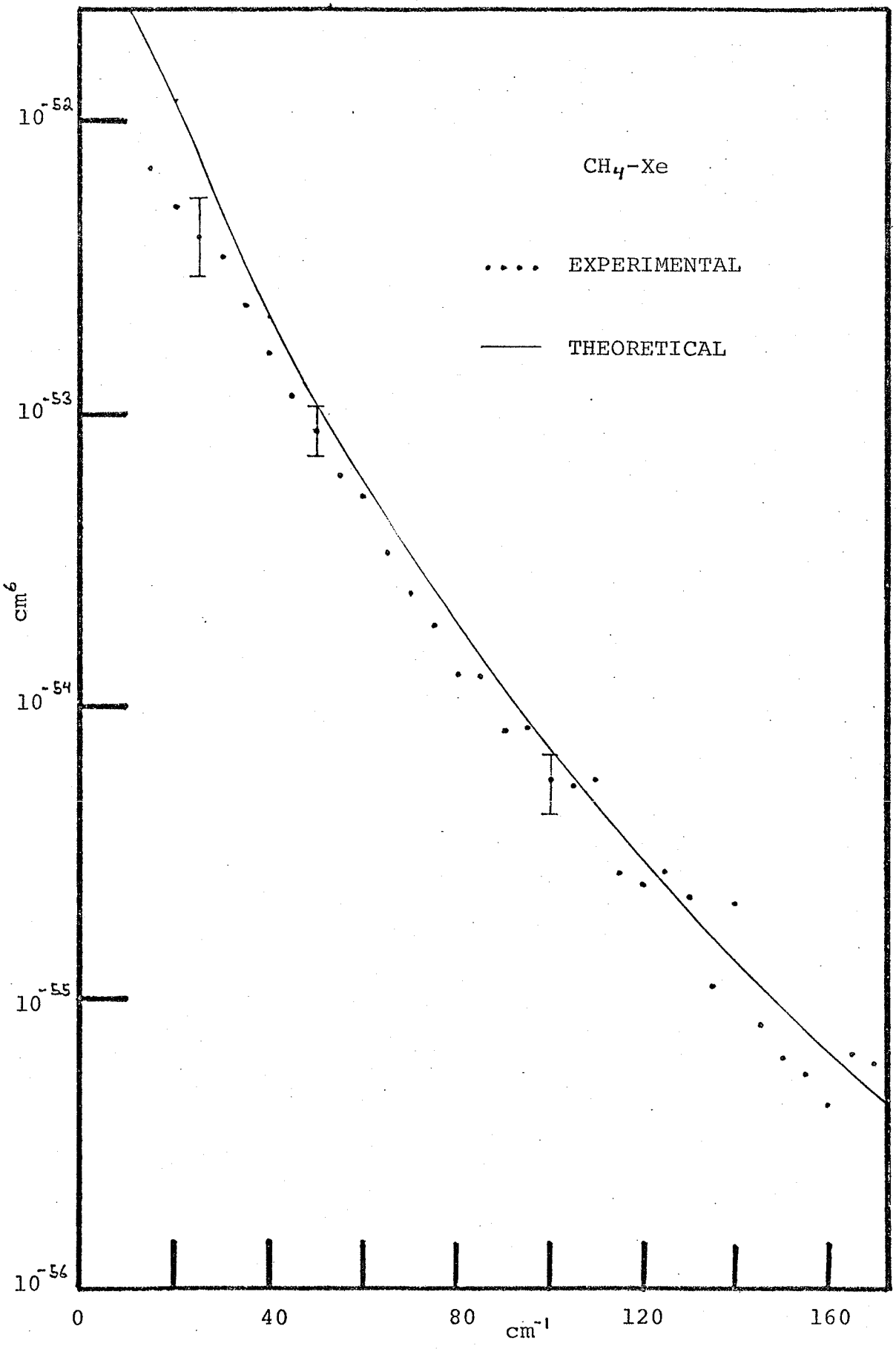
CH_4-Xe
EXPERIMENTAL
THEORETICAL
10^{-52}
10^{-53}
10^{-54}
10^{-55}
10^{-56}
cm^6
0
40
80
120
160
cm^{-1}

REFERENCES

1. G.C. Tabisz, Molecular spectroscopy (Chemical Society of London. Specialist periodical reports) vol.6, 136 (1979).

2. D.P. Shelton and G.C. Tabisz, Molecular Physics 40, 299 (1980).

3. A.D. Buckingham and G.C. Tabisz, Molecular Physics 36, 583 (1978).

4. D.P. Shelton, PhD thesis, University of Manitoba, (1979).

5. A.D. Buckingham and G.C. Tabisz, Optics Letters 1, 220 (1977).

6. A. Chave, PhD thesis, University of Angers, (1981).

7. S. Bhagavantan and D. Suryanarayana, Acta Cryst. 2, 21 (1949).

8. A.D. Buckingham, Adv. Chem. Phys. 12, 107 (1967).

9. P. Isnard, D. Robert and L. Galatry, Molec. Phys. 31, 1789 (1976).

10. G. Birnbaum and H. Sutter, Molec. Phys. 42, 21 (1981)

11. H.B. Levine, J. Chem. Phys. 56, 2455 (1972).

12. E.F. O'Brien, V.P. Gutschick, V. McKoy, and J.P. McTague, Phys. Rev. A8, 690 (1973).

13. P.J. Fortune and P.R. Certain, J. Chem. Phys. 61, 2620 (1974).

14. F. Barocchi, U. Bafile, R. Magli, M. Moraldi, M. Zoppi, Eighth International Conference on Raman Spectroscopy, Bordeaux, France, (1982).

15. R. Righini, K. Maki, and M.L. Klein, Chem. Phys. Lett. 80, 301 (1981).

16. The computer program was written by L. Frommhold. Gratitude is given to F. Barocchi who brought the program to our group.

17. L. Frommhold, Adv. Chem. Phys. 46, 1 (1981).

18. R.A. Aziz, Molecular Physics 38, 177 (1979).

19. J.K. Lee, D. Henderson, and J.A. Barker, Molecular Physics 29, 429 (1975).

20. U. Buck et al, J. Chem. Phys. 74, 1707 (1981).

21. The theoretical results are given as the cross section per unit bandwidth times the cell volume, hence cm^6. See L. Frommhold, K.H. Hong, and M.H. Proffitt, Molecular Physics 35, 665 (1978).

22. See, for example, Chapter 13 of:
G. Baym, Lectures on Quantum Mechanics, Benjamin, London (1973).

23. See, for example, Chapter 4 of:
M.E. Rose, Elementary Theory of Angular Momentum, Wiley, New York, (1957)

24. A.J.C. Ladd, CPGS thesis, Cambridge University, (1975).

25. A.J. Stone, Molecular Physics 29, 1461 (1975).

26. H.A. Posch, Molecular Physics 46, 1213 (1982).

27. A.D. Buckingham, Adv. Chem. Phys. 12, 107 (1967).

28. A.T. Amos and R.J. Criskin, J. Chem. Phys. 63, 1890 (1975).

29. M.N. Neuman, PhD thesis, University of Manitoba, (1981).

30. D.P. Shelton, M.Sc. thesis, (1975).

31. J.P. McTague, W.D. Ellenson, and L.H. Hall, J. Phys. (Paris) 33, 1 (1971).

32. F. Barocchi, M. Zoppi, D.P. Shelton, and G.C. Tabisz, Can. J. Phys. 55, 1962 (1977).

33. F. Barocchi, M. Neri, and M. Zoppi, Molec. Phys. 34, 1391 (1977).

34. D.P. Shelton and G.C. Tabisz, Molec. Phys. 46, 21 (1982).

35. J.H. Dymond, The Virial Coefficients of Gases, Clarendon, Oxford (1969).

36. A. Michels, T. Wassenaar, and P. Louverse, Physica 20, 99 (1954).

37. M. Zoppi, M. Moraldi, and F. Barocchi, Chem.Phys. Lett. 83, 294 (1981).

38. See, for example, Chapter 5 of:

K. Huang, Statistical Mechanics, Wiley, New York, (1963).

39. F. Barocchi, M. Zoppi, M. Proffit, and L. Frommhold, Can. J. Phys. 59, 1418 (1981).

40. See, for example, Chapter 4 of:

G.L. Squires, Practical Physics 2/e, McGraw Hill, London, (1968).

41. P. Pulay, W. Meyer, and J.E. Boggs, J. Chem. Phys. 68, 5077 (1978).

42. H.D. Cohen, and C.C. Roothaan, J. Chem. Phys. 43, S34 (1965).

43. B. Roos, Chem. Phys. Lett. 15, 153 (1972).

44. R.D. Amos, Molecular Physics 38, 33 (1979).

45. I.G. John, G.B. Bacskay, and N.S. Hush, Chem. Phys. 51, 49 (1980).

46. J.L. Rivail and A. Cartier, Chem. Phys. Lett. 61, 469 (1979).

47. P. Isnard, D. Robert, and L. Galatry, Molecular Physics 31, 1789 (1976).

48. S. Rajan, and K. Lalita, J. Mag. Resonance 16, 115 (1974).

49. D.P. Shelton, and G.C. Tabisz, Can. J. Phys. 59, 1430 (1981).

50. N. Meinander, private communication

51. I. Ozier, and K. Fox, J. Chem. Phys. 52, 1416 (1970).